UNIVERSIDAD
DE GRANADA

Ultralong-range polyatomic Rydberg molecules

Moléculas Rydberg poliatómicas de alcance ultra-largo

Tesis Doctoral

por

JAVIER AGUILERA FERNÁNDEZ

Programa de doctorado en Física y Matemáticas FisyMat

Universidad de Granada
2017

Editor: Universidad de Granada. Tesis Doctorales
Autor: Javier Aguilera Fernández
ISBN: 978-84-9163-745-5
URI: http://hdl.handle.net/10481/49168

Tesis Doctoral dirigida por

Dra. M. Rosario González Férez

Dña. M. Rosario González Férez, Doctora en Ciencias Físicas y Profesora Titular del Departamento de Física Atómica, Molecular y Nuclear de la Universidad de Granada

MANIFIESTA:

Que la presente Memoria titulada *Ultralong-range polyatomic Rydberg molecules*, y por su título en castellano, *Moléculas Rydberg poliatómicas de alcance ultra-largo*, presentada por Don Javier Aguilera Fernández para optar al Grado de Doctor en Física, ha sido realizada bajo mi dirección en el Departamento de Física Atómica, Molecular y Nuclear de la Universidad de Granada y el Instituto Carlos I de Física Teórica y Computacional de la Universidad de Granada.

Granada, 16 de Noviembre de 2017

Fdo.: M. Rosario González Férez

Memoria presentada por Don Javier Aguilera Fernández para optar al Grado de Doctor en Física por la Universidad de Granada.

Fdo.: Javier Aguilera Fernández

Compromiso de respeto de los derechos de autor

El doctorando D. Javier Aguilera Fernández y la directora de tesis Dra. M. Rosario González Férez garantizamos, al firmar esta tesis doctoral, que el trabajo ha sido realizado por el doctorando bajo la dirección de la directora de tesis y hasta donde nuestro conocimiento alcanza, en la realización del trabajo, se han respetado los derechos de otros autores a ser citados, cuando se han utilizado sus resultados o publicaciones.

Granada, 16 de Noviembre 2017

Directora de la Tesis	Doctorando
Fdo. M. Rosario González Férez	Fdo. Javier Aguilera Fernández

A mis padres, Yuris y Zulema

A mi hermana, Vivianna

A Ana

Agradecimientos

Esta tesis es el fruto de años de trabajo y paciencia. En el transcurso de la misma, he conocido gente maravillosa y especial de la cual he aprendido mucho en todas las esferas de la vida. Esta es una pequeña lista de las personas que más han resaltado en estos más de cuatro años.

En estan siempre en mi mente mis padres y mi hermana. Nada de esto hubiese sido posible sin sus esfuerzos y su sabiduría, que me han servido de guía en las noches más oscuras. A pesar de la distancia, he sentido durante este tiempo, su energía positiva, su amor y sus consejos. Gracias a ellos, he podido suavizar los momentos difíciles de esta tesis. En fin, no existen palabras de agradecimientos para estos pilares de mi vida.

Quisiera agradecer de todo corazón a Rosario la oportunidad que me ha brindado de colaborar y trabajar junto a ella. Gracias por la paciencia mostrada durante este tiempo, y por tener la puerta de su despacho en todo momento abierta. Le agradezco infinitamente todo lo que me ha enseñado, desde la física hasta aquellas herramientas que constituyen parte de la formación de un joven investigador. Aprecio mucho su rigor y su espíritu crítico, además de su visión perfeccionista del trabajo, valores inculcados que no olvidaré.

Extiendo este agradecimiento a todos los miembros del Departamento de Física Atómica, Molecular y Nuclear, y al grupo de investigación, por haberme tratado como uno más.

I would also like to thank Prof. Peter Schmelcher for the time I spent in Hamburg working at his group and to Markus Kurz and Christian Fey for fruitful discussions during my secondment in their group, and for the great collaboration we have since I started my PhD. I want extend my thanks to Prof. Hossein Sadeghpour, for the fruitful discussions, their effort and their time.

A mis compañeros de despacho, Juan, Rodrigo, Moy, Manuel, Conrado, que no solo me dieron la bienvenida al Departamento y a la Universidad de Granada, sino que hicieron que en esos primeros meses no se notara tanto la distancia y la ausencia. Creo que nadie se va a molestar si dentro de ellos, hago una mención especial a Juan; gracias a sus consejos, su ejemplo, y su ayuda desde el primer minuto que llegue a España.

A otros compañeros que se volvieron amigos y camaradas de noches, de comedores, de jugar al padel, de baile, de barbacoas, de cervezas y muchas cosas más. Entre ellos he de mencionar a Will, Peter, Luis, Kathe, Jordi, Rafa, Remi, Noelia, más que amigos, a los cuales he llegado a considerar una gran familia.

Fuera del ámbito de la Universidad, tengo que agradecer de una manera muy especial a Ana, por llegar en el momento justo. Le estoy enormemente agradecido, ya que su llegada arrojó luz sobre ciertas oscuridades. Gracias por su amor, su comprensión y sus acertados consejos.

Siguiendo esta línea, quisiera agradecer a Manolo, Conchi y Manuel Jesús, por haberme acogido como un hijo y como un hermano. Gracias nuevamente, de todo corazón.

Extiendo las gracias a esas personas que han hecho que Zagra se vuelva mi segunda casa. A Irene, Pilar, Alicia, Susana, Lola, Angustias, Raul, Antonio, Álvaro gracias por tratarme como a un zagreño más.

A mis amigos de Cuba, Sergio, Javier, Jorge, Roger porque en la distancia han mostrado su preocupacion por mi y por el trabajo que he estado realizando.

A mis compañeros del Departamento de Física Nuclear del Instituto Superior de Tecnologías Aplicadas de La Habana, por la formación, por los ánimos y por la confianza en todo momento.

Estoy convencido de que seguro se me queda alguien, pero desde lo más hondo de mi corazón, gracias y perdónenme.

Contents

Summary

In this thesis we have theoretically investigated the electronic structure and properties of two types of polyatomic Rydberg molecules, which differ on their binding mechanism.

We have first analyzed the impact of an external electric field on a triatomic Rydberg molecule formed by a Rydberg rubidium atom and two ground state rubidium atoms in three geometrical configurations: two collinear arrangements and a planar one. The binding mechanism is based on the low-energy collisions between the Rydberg electron and the ground state atoms. The electronic structure of these triatomic Rydberg molecules is described within the Born-Oppenheimer approximation, and we have used the s- and p-wave Fermi pseudo-potentials to describe the interaction between the Rydberg electron and each of the ground state perturbers. The adiabatic potential curves and surfaces present an oscillatory behaviour as the distance between the ground state atoms and the Rydberg ionic core increases, which is due to the highly oscillatory character of the Rydberg electron wave function. The potential wells of these electronic states are deep enough to accommodate several vibrational levels where the triatomic Rydberg molecule can exist. We have shown that the external electric field enhances the bound character of these adiabatic electronic states.

In the second part of this dissertation, we have investigated polyatomic Rydberg molecules formed by a rubidium Rydberg atom and one or two diatomic heteronuclear molecules, being KRb our prototype system. The binding mechanism is due to the anisotropic scattering of the Rydberg electron from the permanent electric dipole moment of the polar molecule. Within the Born-Oppenheimer approximation, we have performed a realistic treatment of the internal rotational motion of the diatomic molecules. For the triatomic Rydberg molecule, we have explored the adiabatic electronic states evolving from the Rydberg manifolds $\mathrm{Rb}(n, l \geq 3)$, with increasing principal quantum number n, and from the Rydberg states $\mathrm{Rb}(26d)$, $\mathrm{Rb}(28s)$ and $\mathrm{Rb}(27p)$. In all these cases, we have found oscillatory Born-Oppenheimer potentials, with stable configurations, which can accommodate several vibrational bound levels. For the pentaatomic Rydberg molecule, we have considered symmetric and asymmetric linear configurations and have studied the metamorphosis of the Born-Oppenheimer potential curves as the distances between the Rydberg core and the polar molecules increase. Our focus is on the pentaatomic Rydberg molecule formed from the degenerate manifold $\mathrm{Rb}(n = 20, l \geq 3)$ and the Rydberg state $\mathrm{Rb}(23s)$ with ground and rotationally excited KRb diatomic polar molecules, respectively. As in the triatomic Rydberg molecule, we have encountered stable electronic states with potential wells possessing rich vibrational spectra. Since the polar diatomic molecules are allowed to rotate within these polyatomic Rydberg molecules, we have also analyzed the impact of the Rydberg-atom-induced electric field on their rotational dynamics. We have shown that the directional properties of KRb strongly depend on the Rydberg state and on the initial rotational state of KRb forming the ultra-long range molecule. The polar molecule is significantly oriented and aligned if the Rydberg degenerate manifold is involved or if KRb was initially in its rotational ground state.

Resumen

En esta tesis doctoral, se han investigado la estructura electrónica y las propiedades de dos tipos de moléculas Rydberg poliatómicas que difieren en el mecanismo de enlace que las forma.

En primer lugar, se ha analizado el impacto de un campo eléctrico externo en una molécula Rydberg triatómica, formada por un átomo de rubidio en un estado Rydberg y dos átomos de la misma especie en el estado fundamental. Para ello, se han considerado tres configuraciones geométricas de la molécula Rydberg: dos lineales y una plana. En este sistema el mecanismo de enlace se debe a la colisión a baja energía entre el electrón Rydberg y los átomos en el estado fundamental. La estructura electrónica de estas moléculas Rydberg triatómicas se ha descrito dentro de la aproximación de Born-Oppenheimer, y la interacción entre el electrón Rydberg y los átomos en el estado fundamental en el marco de la teoría de colisiones a bajas energías usando los pseudo-potenciales de Fermi de onda-s y onda-p. Se ha mostrado que las curvas y superficies de potencial adiabáticas, presentan un comportamiento oscilatorio a medida que aumenta la distancia entre los átomos en estado fundamental y el core iónico, que refleja el carácter oscilatorio de la función de onda del electrón Rydberg. Los pozos de potencial de estos estados electrónicos adiabáticos son lo suficientemente profundos para albergar estados vibracionales donde esta molécula triatómica existiría. Se ha mostrado que el efecto principal del campo eléctrico externo es aumentar el carácter de enlace vibracional de estos estados electrónicos adiabáticos, ya que los pozos de potencial se hacen más profundos.

En la segunda parte de esta tesis doctoral, se ha investigado la estructura electrónica de moléculas Rydberg poliatómicas formadas por un átomo Rydberg y una o dos moléculas diatómicas heteronucleares. Se ha considerado como prototipo la molécula Rydberg poliatómica formada por un átomo de rubidio en un estado Rydberg y una o dos moléculas de KRb. En este sistema, el mecanismo de enlace se debe a la dispersión anisotrópica del electrón Rydberg con el momento dipolar eléctrico permanente de la molécula polar. Dentro de la aproximación Born-Oppenheimer, se ha descrito de manera realista el movimiento rotacional interno de la molécula diatómica usando la approximación de rotor rígido. Para la molécula Rydberg triatómica, se han explorado los estados electrónicos adiabáticos que surgen del multiplete Rydberg Rb($n, l \geq 3$), al variar el número cuántico principal n, y de los estados Rydberg Rb($26d$), Rb($28s$) y Rb($27p$). En todos estos casos los potenciales Born-Oppenheimer muestran un carácter oscilatorio con configuraciones estables, donde existen estados vibracionales ligados. Para la molécula Rydberg pentaatómica, se ha analizado una configuración lineal simétrica y otra asimétrica, y se han estudiado la metamorfosis de las curvas de potencial Born-Oppenheimer cuando la distancia entre las moléculas diatómicas y el core Rydberg aumenta. Para molécula Rydberg pentaatómica, nuestro estudio ha estado centrado en los niveles electrónicos que se forman a partir del multiplete degenerado Rydberg Rb($n = 20$, $l \geq 3$) y el estado Rydberg Rb($23s$), con las moléculas de KRb en los estados rotacionales fundamental y excitados respectivamente. Al igual que para molécula Rydberg triatómica, se han encontrado estados electrónicos estables con pozos de potencial que poseen varios estados vibracionales. Dado que las moléculas diatómicas pueden rotar dentro de estas

moléculas Rydberg poliatómicas, se ha analizado el impacto del campo eléctrico inducido por el átomo Rydberg en su dinámica rotacional. Se ha demostrado que las propiedades direccionales de la molécula KRb dependen en gran medida del estado Rydberg y del estado rotacional inicial de la molécula KRb que forman la molécula de alcance ultra-largo. Así, si el multiplete degenerado Rydberg forma la molécula Rydberg, la molécula de KRb está bastante orientada y alineada, y lo mismo sucede si inicialmente el KRb se encuentra en su estado rotacional fundamental.

Author's publications

Publications of the author upon which this Thesis are based. The numbers in brackets at the end of each reference indicate the chapter where it is located.

- J. Aguilera-Fernández, P. Schmelcher, and R. González-Férez, *Ultralong-Range Triatomic Rydberg Molecules in an Electric Field*, J. Phys. B **49**, (2016), [Chapter 3].
- J. Aguilera-Fernández, H. R. Sadeghpour, P. Schmelcher, and R. González-Férez, *Ultralong-Range Rb-KRb Rydberg Molecules: Selected Aspects of Electronic Structure, Orientation and Alignment*, J. of Phys. Conf. Ser. **635**, 012023 (2015), [Chapter 4].
- J. Aguilera-Fernández, H. R. Sadeghpour, P. Schmelcher, and R. González-Férez, *Electronic Structure of Ultralong-Range Rydberg Pentaatomic Molecules with Two Polar Diatomic Molecules*, arXiv:1710.01393, accepted for publication in Physical Review A (2017), [Chapter 5].

Chapter 1

Introduction

The success story of cold and ultracold quantum systems is based on the development of powerful experimental techniques to cool, trap and manipulate quantum gases, such as laser and evaporative cooling [1], magnetic and optical trapping [1], photoassociation [2], magnetoassociation [3], being the Bose-Einstein condensate [4] of alkali atoms its first breakthrough [5, 6]. These experimental techniques allow to routinely produce samples of ultracold atoms [7, 8], cold and ultracold molecules in their absolute ground state [9–11], and hybrid quantum systems formed by mixtures of atoms and atomic-ions [12, 13], atoms and molecules [14] or molecular-ions [15,16], or by Rydberg-atoms-based mixtures [17,21]. Indeed, the theoretical and experimental efforts undertaken to investigate the cold and ultracold regime are motivated by first principles, since these systems provide an ideal platform to explore fundamental questions in quantum mechanics, by modeling and analyzing complex few- and many-body systems under very clean and well-defined experimental conditions, which imply extremely high control on their interactions, and their internal as well as external degrees of freedom. But most important is the broad range of perspectives and potential applications of these ultracold quantum systems, including precision measurements [18–20], ultracold chemistry [22, 23], ultracold collisions [24], and quantum information [25–27]. Nowadays, we can affirm that modern atomic and molecular physics has become a very active, fruitful and promising research area with a plethora of intriguing physical phenomena to be explored.

In this modern ultracold atomic and molecular physics, Rydberg atoms have become a key ingredient in current experiments. Rydberg atoms have their valence electron in an excited orbital of high principal quantum number n [28]. Their long history goes back to the late nineteenth century, when the hydrogen spectrum was explored giving a mathematical interpretation to the Balmer series [29], this Balmer's formula was generalized by J. Rydberg to describe all levels and alkali atoms [30]. Along this substantial history, Rydberg physics was an active research area with the focus mainly on high resolution spectroscopy [31]. The renew interest on these highly excited and fragile atoms is motivated by their fascinating and extraordinary properties which allow to reach an experimentally high control of the interactions among them and with external fields. They also provide a broad range of applications in plasmas [32, 33], quantum optics and many-body physics of long-range interacting Rydberg systems [33], quantum simulators [34] as well as quantum information processing [35–37].

The alkali Rydberg atoms possess an ionic core of charge +1 and a valence electron orbiting around it, which allow us to theoretically describe them in a similar way as the hydrogenic Rydberg atom. Contrary to the point-like core, as can be considered the proton, in the

hydrogen atom, the closed-shell ionic core of the alkali Rydberg atom has internal structure which might significantly affect the wave functions of some Rydberg states. For high angular momentum Rydberg states with $l \gtrsim 4$, alkali Rydberg atoms are well described as a hydrogen atom because the valence electron does not resolve the inner core. In contrast, the Rydberg electron with low angular momentum $l \lesssim 3$ penetrates and polarizes the ionic core of the alkali atom, and the corresponding energy and wave function differ from the hydrogenic ones. The so-called quantum defects δ_{nl}, which depend on the principal and orbital quantum numbers, quantify the differences between both systems [28], and the energy of the Rydberg atom can be written as $E_{nl} = -\frac{R_y}{(n-\delta_{nl})^2}$, with $R_y = -13.6$ eV being the Rydberg constant. For these Rydberg states, $n^* = n - \delta_{nl}$ is defined as the effective principal quantum number. Due to these quantum defects, compared to the hydrogenic atom the energies of the low orbital angular momentum states ($l \lesssim 3$) are reduced, whereas the energy of the higher orbital angular momentum states coincides with the hydrogenic energy, and these states form a degenerate Rydberg manifold.

The valence electron in Rydberg atoms is located at large distances from the Rydberg core, and their orbital radius increases as $\langle r \rangle = \frac{1}{2}(3n^2 - l(l+1))$ [28], with l being the orbital quantum number. For instance, the orbital radius of Rb($35s$) is 1837.5 $a_0 \approx 97.2$ nm, i. e., the Rubidium atom in the Rydberg state $35s$ is several orders of magnitude larger than in its ground state. Their radiative lifetime increases as n^3 and n^5, for s-wave states and the circular ones with $l = n - 1$, respectively, giving rise to lifetimes of the order of milliseconds or even more, for instance, the lifetime for Rb in the $43s$ state is approximately 90 μs [28]. The large displacement of the Rydberg electron from the ionic core gives rise to huge electric dipole moments, increasing as n^2, and polarizabilities n^4 [28]. As a consequence, Rydberg atoms possess very high sensitivity to external fields, which play a crucial role to experimentally control and manipulate them. The interaction among Rydberg atoms is very strong, and they interact either via the dipole-dipole force, with the dipole-dipole coefficient $C_3 \propto n^4$, or van-der-Waals one, with the van-der-Waals coefficient increasing as $C_6 \propto n^{11}$. These strong interactions give rise to the Rydberg blockade mechanisms [38–40]: A Rydberg atom strongly inhibits excitation of a neighbouring atom. This is one of one of the most intriguing properties of two interacting Rydberg atoms, which creates coherent collective excitations, the so-called superatoms, in a dense gas [38–40]. A direct application of the Rydberg blockade is in quantum information processing, because it provides a state dependent interaction to devise two-qubit gates [35, 36]. Based on this blockade mechanism, a single Rydberg atom has been excited within a Bose-Einstein condensate [41], in such a way that the Rydberg electron interacts with the condensed atoms, exciting phonons and eventually provoking a collective oscillation of the condensate.

By standard two-photon excitation schemes, Rydberg atoms could be created in an ultracold atomic gas. Due to the Rydberg blockade mechanism, only a few Rydberg excitations could be created within the atomic cloud, whereas most of the atoms remain in their ground state. In such a hybrid system, ultralong-range molecules (ULRM) formed by a ground state and a Rydberg atom have theoretically been predicted to exist [42]. The well-known Rydberg molecules consist in a tightly bound positively charged core and an electron orbiting around [43, 44]. In contrast, these ultralong-range molecular species possess

very large internuclear distances between the Rydberg core and the ground state atom, which are of the order of the extension of the involved electronic Rydberg state. Since the Rydberg electron is distributed over a region that extends far from the Rydberg core, where the Coulomb potential is weak, and varies slowly as a function of the distance, it has a small energy, a low momentum and one could say that it occupies a "quasi-free" state. As a consequence, the interaction between a ground state and a Rydberg atom, which is a three-body problem, is approximately described as two independent two-body interactions: the scattering between the Rydberg electron and ground state perturber and between the Rydberg electron and core. The binding mechanism of these ULRM is then based on the low-energy collisions between the Rydberg electron and the ground state atom, which is described by s- and p-wave Fermi-type pseudo-potentials [45, 46]. A physical interpretation is that the ground state perturber locally probes the wave function of the Rydberg electron.

The adiabatic potential energy curves of these ULRM show an unusual oscillatory behaviour as a function of the internuclear distance reflecting the oscillating character of the Rydberg electron wave functions. Depending on the electronic orbital angular momentum of the Rydberg state involved, the ULRM could be classified in two different clases [42, 47]. The ULRM arising from the Rydberg electron in a degenerate manifold, i. e., from the high orbital angular momentum Rydberg states having negligible quantum defects, have vibrational binding energies in the GHz regime. They are known as trilobite states because their electron probability distribution resembling a trilobite fossil, and were initially described using pure s-wave electron-ground-state atom interaction. In addition, they have huge permanent electric dipole moments in the kilodebye range, e.g., the permanent electric dipole moment for the $n = 30$ $^3\Sigma$ trilobite state of Rb$(30, l \geq 3)$-Rb$(5S_{1/2})$ is $d = 0.3$ kD [42], and lifetimes on the order of tens or hundreds of microseconds. The ULRM formed from a Rydberg atom with low orbital angular momentum $l \leq 2$, possess shallow Born-Oppenheimer potential curves having wells with depths of few MHz [47]. The electron density of the ULRM from a p-wave Rydberg state resemble the shape of a butterfly, and they are known as butterfly states. These butterfly states also possess large electric dipole moments, e.g., the permanent electric dipole moment are approximately $d = 1.05$ kD and $d = -1.53$ kD for the Σ and Π symmetry states, respectively, from the Rydberg electron in the $n = 30$ state [47]. The ULRM involving quantum-defect split ns Rydberg states, were expected to be non-polar and to have a spherically symmetric, non-degenerate electronic wave function. However, it has been shown that the contribution of the nearly degenerate electronic manifold provokes the existence of relatively small electric dipole moments in these ns ULRM, e.g. approximately 1D for Rb$(35s)$-Rb$(5S_{1/2})$, which due to their small rotational constants give rise to large Stark effects [48].

Experimentally, the existence of these ULRMs was confirmed for Rb atoms in a s-wave Rydberg state [49]. Since this first experimental observation, these exotic Rydberg molecules have attracted quite interest in the field of ultracold Rydberg physics. For instance, the lifetimes of their ground and excited vibrational states were measured [50], their permanent electric dipole moments determined [48], their spectroscopic characterization of excited diatomic molecules bound by quantum reflection have been found [51], and URLMs formed by other atomic species such as Cs [52–54] and Sr [55–57] have been prepared and explored. The current experiment efforts are devoted to explore these ULRMs formed by Rydberg atoms in higher angular momentum [53, 54, 58–61]. The contribution of the spin through the

hyperfine interaction and the fine structure has been both experimentally and theoretically analyzed [54,59,64,65]. These exotic molecules show a high sensitivity to external fields, which become a experimental tool to control and manipulate their electronic structure, molecular geometry and binding properties [66–69]. The excitation of rovibrational molecular states with a variable degree of alignment has been demonstrated experimentally by using magnetic fields [60].

In an ultracold mixture of Rydberg and ground state atoms, it might occur, for high enough densities, that several ground-state atoms are immersed in the Rydberg cloud, so that polyatomic ULRMs could be created. The Born-Oppenheimer potentials for several configurations of polyatomic ULRM have been theoretically investigated [70–72]. If the interaction between the ground state atom and the electron is repulsive the ULRM could not support bound states, however, the triatomic ULRM exist and can accommodate vibrational bound states [71]. Recently Rydberg trimers and excited dimers bound by quantum reflection have been studied experimentally and theoretically [51]. By increasing the principal quantum number of the Rydberg state, the transition from a diatomic ULRM to a polyatomic one has been experimentally observed [73].

The experimental advances in ultracold atomic and molecular physics allow for the creation of quantum systems formed by ultracold atoms and ultracold polar molecules. If in such a hybrid system a Rydberg atom is created, a new kind of polyatomic Rydberg molecules are predicted to exist if a heteronuclear diatomic molecule is immersed into the wave function of the Rydberg electron [74–77]. The binding mechanism appears due to anisotropic scattering of the Rydberg electron from the permanent electric dipole moment of the polar molecule. Let us remark that for these polyatomic Rydberg molecules to exist, the heteronuclear diatomic molecule should have a subcritical permanent electric dipole moment, i. e., $d < 1.639$ D, to prevent binding of the Rydberg electron to the polar molecule [78–81]. The rotational spectra of open-shell diatomic molecules, such as OH, OD, LiO and NaO, is characterized by fine-structure interactions and the Λ-doubling effects, and can be described using a two state model [83, 84]. For these Λ-doublet molecules, the Rydberg electron is coupled to the two internal states of the polar ground state molecule [74]. In contrast, the Rydberg electron is coupled to several rotational states for closed-shell molecules, such as KRb or RbCs, provoking the hybridization of the rotational motion [77]. In both types of Rydberg molecules, we encounter a series of undulating Born-Oppenheimer potential curves (BOP), reflecting the oscillating character of the wave function of the Rydberg electron, and having well depths of a few GHz if they evolve from the Rydberg degenerate manifold with orbital quantum number $l > 2$ [74–77]. Analogously to the ULRM, these giant molecules also exhibit a high sensitivity to external fields, and could be easily manipulated by means of electric fields of a few V/cm [76, 77]. The Rydberg-electron-induced coupling gives rise to a strong hybridization of the rotational states and a strong orientation and alignment of the diatomic molecule. Since in the giant Rydberg molecule, the orientation of the diatomic molecule changes sign as the distance from the Rydberg core varies [74, 77], two internal rotational states of opposite orientation could be Raman coupled [74] to create a switchable dipole-dipole interaction needed to implement molecular qubits [85]. An important problem in ultracold molecular physics is the experimental detection of the internal molecular state, which normally implies the destruction of the molecule. There are have been theoretical

proposals to use the interaction between a Rydberg atom and a polar molecule, i. e., the basic interaction responsible for the existence of the polyatomic Rydberg molecules, to readout the internal state in a non-destructive way [86, 87].

Aim of this thesis

The aim of this thesis is to theoretically investigate the electronic structure and properties of polyatomic Rydberg molecules. We now describe in more detail this goal following the structure of this thesis.

We start by studying the impact of an external electric field on the electronic structure of a triatomic ULRM. We consider a triatomic ULRM formed by a Rubidium Rydberg atom and two Rubidium ground state atoms, and describe as point particles the Rydberg core and the ground state perturbers. We investigate three configurations of the atoms forming the triatomic ULRM: two collinear arrangements and a planar one. For the collinear configuration, we explore a symmetric arrangement where the two ground state perturbers are located at the same distance from the Rydberg core, but on different sides of it, and an asymmetric case with the Rb atoms being located on the same side of the Rb^+ core and at different distances. For the planar configuration, we assume that the ground state atoms are located at the same distance from the Rydberg core, but the two straight lines connecting their spatial positions and Rb^+ form an angle smaller than π. The interaction between the Rydberg electron and the two ground-state Rb atoms is approximated in the low-energy regime by the s- and p-wave Fermi-type pseudo-potentials [45, 46], which include the energy-dependent triplet s- and p-wave scattering lengths between the Rydberg electron and Rubidium in its ground state. These triatomic ULRM are analyzed within the Born-Oppenheimer approximation, assuming that the total wave function factorizes in two parts that describe the electronic and nuclear motions of the Rydberg triatomic molecule. The validity of the Born-Oppenheimer approximation is well justified to investigate the electronic structure of the ULRM due to the large difference between the energy scales associated to the Rydberg electron and to the vibrational states.

In chapter 2, we investigate within the Born-Oppenheimer approximation the adiabatic potential curves and surfaces for the collinear and planar geometries of the triatomic ULRM, respectively. We explore the impact of an additional electric field on these adiabatic potentials. For the molecular states with Σ and Π symmetry of the collinear configuration, our results show that the bound character of the molecular states increases as the electric field is increased, i. e., more vibrational bound states could be accommodated in the corresponding adiabatic potential. The adiabatic potential surfaces of the planar ULRM only show a significant dependence on the arrangement of the ground state atoms only when they approach each other. The interaction with the external electric field favours the symmetric linear configuration and increases the bound state character of molecular states, and vibrational states with the spatial extensions of a few hundreds Bohr radii could appear.

A selection of the results presented in Chapter 3 has been published in: J. Aguilera-Fernández, P. Schmelcher, and R. González-Férez, *Ultralong-range triatomic Rydberg molecules in an electric field*, J. Phys. B: At. Mol. Opt. Phys. **49** (2016) [88].

In chapter 3, we analyze the electronic structure of a triatomic Rydberg molecule,triatomic molecule formed by a Rydberg atom and a heteronuclear diatomic molecule. As prototype example, we consider the Rb-KRb triatomic Rydberg formed by a Rubidium Rydberg atom, and KRb diatomic molecule. Note that the KRb molecule is an ideal candidate for this triatomic molecule, since it has an electric dipole moment $d = 0.566$ D [89], which is smaller than the Fermi-Teller critical value 1.639 D [78, 79], and its rotational constant is $B = 1.114$ GHz [90]. The electronic structure of triatomic molecule is described within the Born-Oppenheimer approximation based on the different energy scales associated to the nuclei and electronic degrees of freedom. For the diatomic molecule, we perform a realistic treatment of its internal motion within the rigid-rotor approximation. This allows us to properly describe the dressing of the rotational motion of KRb provoked by the interaction of its permanent electric dipole moment with the electric fields due to the Rydberg core and electron. Note that we are taking into account the three spatial components of this electric field induced by the Rydberg atom.

We have first analyzed the adiabatic electronic states of the Rb($n; l \geq 3$)-KRb Rydberg molecule with varying principal quantum number n of the Rydberg electron. This study is an extension of the analysis previously done in Ref. [77]. With varying internuclear distance between the ionic core Rb^+ and the diatomic KRb, the BOPs show an oscillatory behaviour provoked by the shape of the Rydberg electron wave function. By increasing the principal quantum number n of the Rydberg manifold Rb($n; l \geq 3$), the depths of the outermost minima of lowest-lying BOPs evolving from Rb($n; l \geq 3$)-KRb($N = 0$) decrease, being still of a few GHz. This implies that these potential wells are deep enough to accommodate vibrational bound states, but the number of bound states decreases as n increases. In addition, we have explored the directional properties, i. e., orientation and alignment, of the diatomic molecule, and how does it change as the distance between KRb and Rb^+ increases.

In the laboratory, the Rydberg Rubidium atoms are routinely prepared by a two-photon excitation scheme, which implies that the Rydberg states Rb(ns) and Rb(nd) are easily accesible in Rydberg atom experiments. Thus, the possibility to experimentally observe these Rb-KRb triatomic molecule, requieres to investigate their electronic structure involving Rydberg states of Rubidium with low orbital angular momentum, i. e., $l \leq 2$, and to determine the existence the bound vibrational states in the corresponding adiabatic electronic states. This study has been performed also in Chapter 4, where we analyze the electronic structure of the following triatomic molecule: Rb($26d$)-KRb, Rb($27p$)-KRb and Rb($28s$)-KRb. We encounter that the BOPs evolving from Rb($26d$) Rb($27p$) and Rb($28s$) show a smooth oscillatory behaviour as the internuclear separation increases. If the diatomic molecule is in an excited rotational state, these BOPs present wells with depths of a few MHz, which support several vibrational bound states where these macroscopic Rydberg molecules could exist. Within these triatomic molecules, the orientation and alignment of the diatomic molecule are smaller, which can be explained in terms of the weaker electric fields induced by the Rydberg atom in these state with low angular momentum.

A selection of the results presented in Chapter 4 has been published in: J. Aguilera-Fernández, H.R. Sadeghpour, P. Schmelcher, and R. González-Férez, *Ultralong-Range Rb-KRb Rydberg Molecules: Selected Aspects of Electronic Structure, Orientation and Alignment*, J. of Phys. Conf. Ser. **635**, 012023 (2015) [91].

Motivated by the experimental results on polyatomic ULRM from the group of Prof. T. Pfau [51, 73], our next goal was to investigate more complex polyatomic Rydberg molecules formed by a Rydberg atom and two heteronuclear diatomic molecules. Experimentally, only a diatomic molecule could be found in the vicinity of a Rydberg atom in a dilute ultracold gas, or if the two species are located in the same potential well of an optical lattice, in both cases, the triatomic molecule could be created. However, in a mixture of ultracold atoms and molecules, it might occur that more than one diatomic molecule is immersed within the orbit of the Rydberg electron, and, therefore, it is possible to experimentally observe the spectroscopic signal of more complex polyatomic Rydberg molecules. In Chapter 5, we investigate the electronic structure of a pentaatomic molecule formed by a Rydberg atom and two ground state heteronuclear diatomic molecules. As in Chapter 4, we consider as prototype the pentaatomic molecule formed by Rubidium Rydberg atom and two KRb molecules. The diatomic molecules are described within the rigid rotor approximation taking into account their angular degrees of freedom, which provides a realistic analysis of the interaction between the Rydberg atom electric field and their permanent electric dipole moment and of the field-dressed directional properties.

Due to the numerical complexity associated to a complete description of an arbitrary configuration of the pentaatomic molecule, our study is restricted to two collinear configurations of the two polar diatomic molecules bound within the Rydberg orbit. We first analyze a symmetric arrangement with the two diatomic molecules located at the same distance from the Rydberg core, but at different sides of it. For this symmetric configuration, we investigate the adiabatic electronic states evolving from the Rydberg degenerate manifold Rb($n = 20, l \geq 3$) and the two diatomic molecules initially in the rotational ground state, i. e., the KRb-Rb($n = 20, l \geq 3$)-KRb pentaatomic molecule, and from the Rydberg state Rb($23s$) and the KRb molecules in the rotational excited states, i. e., the KRb-Rb($23s$)-KRb pentaatomic molecule. In addition, we analyze an asymmetric arrangement with the two diatomic molecules located at the same side of the Rydberg core, but at different distances. For the asymmetric pentaatomic molecule, we study the adiabatic electronic states evolving from the Rydberg degenerate manifold Rb($n = 20, l \geq 3$) and the two diatomic molecules initially in the rotational ground state, i. e., the Rb($n = 20, l \geq 3$)-KRb-KRb pentaatomic molecule, as the distance of one or two of the diatomic molecules from the Rydberg core increases. We equally explore the effects of the electric field due to the Rydberg atom on the rotational motion of diatomic molecules, by analyzing their orientation and alignment in both configurations of these pentaatomic molecules.

Our results show that the electronic structure strongly depends on the Rydberg state of Rb forming the corresponding pentaatomic molecule. The BOP evolving from the Rydberg degenerate manifold Rb($n = 20$, $l \geq 3$) presents potential wells with depths of a few GHz, which can accommodate several vibrational bound states. Thus, we can conclude that the pentaatomic molecules could be experimentally observed in both the linear symmetric and linear asymmetric configurations if the Rubidium atom is excited to the Rydberg state Rb($n = 20$, $l \geq 3$). For these configurations, the KRb molecules present a moderate orientation and alignment within these adiabatic electronic states. In contrast, the electronic structure of the symmetric pentaatomic molecule evolving from the Rydberg degenerate manifold Rb($23s$) presents unstable electronic states, but also stable ones having potential wells with depths of a few MHz. For this pentaatomic molecule to exist, the two KRb molecules should be initially

in excited rotational states, and we encounter binding vibrational energies a few MHz on these BOPs and a very small orientation for the KRb molecules.

A selection of the results presented in Chapter 5 has been submitted to publication to Physical Review A and accepted recently: J. Aguilera-Fernández, H.R. Sadeghpour, P. Schmelcher, and R. González-Férez, *Electronic structure of ultralong-range Rydberg pentaatomic molecules with two polar diatomic molecules*, arXiv:1710.01393, accepted for publication in Physical Review A (2017) [92].

Finally, the conclusions of this thesis are presented in Chapter 6 (English version) and Chapter 7 (Spanish version), where we also provide an outlook for future works, which might be considered a continuation of the studies performed in this thesis.

Chapter 2

Introducción

El éxito y popularidad de sistemas cuánticos fríos y ultrafríos se debe al desarrollo de técnicas experimentales de gran precisión que permiten enfriar, atrapar y manipular gases cuánticos. Entre ellas cabe destacar el enfríamiento por láser o por evaporación [1], trampas ópticas y magnéticas [1], la fotoasociación [2], la magnetoasociación [3]. La creacción experimental del condensado de Bose-Einstein [4] de átomos alcalinos en 1995 se puede considerar como uno de los grandes logros y avances de estas técnicas experimentales, proporcionando un gran empuje a este campo de investigación. En la actualidad, se producen de forma rutinaria gases de átomos ultrafríos [7,8], moléculas frías y ultrafrías en el estado fundamental [9–11], y sistemas cuánticos híbridos formados por una mezcla de átomos e iones átomicos [12, 13], átomos y moléculas [14] o moléculas e iones [15,16], o por una mezcla basada en átomos Rydberg [17,21]. De hecho, los grandes esfuerzos tanto experimentales como teóricos que se están llevado a cabo para investigar el régimen frío y ultrafrío están motivados por primeros principios, ya que estos sistemas proporcionan una plataforma ideal para estudiar cuestiones fundamentales de la mécanica cuántica. Así, se están modelando y analizando sistemas complejos de pocos y de muchos cuerpos, bajo condiciones experimentales limpias y bien definidas, de las que se tiene un gran control tanto de sus interacciones como de sus grados de libertad internos y externos. Aún más importante es la gran cantidad de posibles aplicaciones de estos sistemas cuánticos fríos y ultrafríos, que abarcan desde medidas de gran precisión [18–20], reacciones químicas en el régimen frío y ultrafrío [22, 23], colisiones ultrafrías [24], hasta información cuántica [25–27]. Hoy en día, se puede afirmar que la física atómica y molecular moderna se ha convertido en un campo de investigación muy activo, fructífero y prometedor compuesto por una gran cantidad de fenómenos físicos muy interesantes por investigar y explorar.

En este área de investigación de átomos y moléculas fríos y ultrafríos, los átomos Rydberg se han convertido en un ingrediente clave en los experimentos que se están llevando a cabo en la actualidad. Los átomos Rydberg tienen el electrón de valencia en un orbital excitado con un número cuántico principal n muy alto [28]. Su larga historia comienza a finales del siglo XIX, cuando fue explorado el espectro del átomo de Hidrógeno y se dio una interpretación matemática de la serie de Balmer [29], dicha fórmula de Balmer fue generalizada por J. Rydberg para describir todos los niveles de los átomos alcalinos [30]. Desde sus inicios, la física de átomos Rydberg ha sido una área de investigación enfocada principalmente en la espectroscopía de alta resolución [31]. En las últimas décadas, la comunidad de sistemas cuánticos fríos y ultrafríos ha mostrado un mayor interés en estos átomos frágiles y altamente excitados, que viene motivado por las propiedades extraordinarias y fascinantes de estos átomos Rydberg, que permiten obtener un gran control experimental de las interacciones entre ellos y también con campos externos. Estos sistemas Rydberg también tienen una gran cantidad de aplicaciones en física de plasmas [32, 33], óptica cuántica y física de

muchos cuerpos de sistemas Rydberg con interacciones de largo alcance [33], simuladores cuánticos [34], así como el procesamiento de información cuántica [35–37].

Los átomos alcalinos en un estado Rydberg, poseen un core iónico de carga +1 y un electrón de valencia orbitando alrededor de éste, lo que permite describirlos teóricamente como un átomo de hidrógeno bajo ciertas condiciones. El protón, i. e., el núcleo del átomo de hidrógeno, se puede considerar un núcleo puntual sin estructura, por el contrario el core, con las diferentes capas electrónicas cerradas de un átomo alcalino Rydberg, tiene una estructura interna que puede afectar de forma significativa a las funciones de onda de algunos estados Rydberg dependiendo de su momento angular orbital. Si el electrón Rydberg tiene un momento angular orbital alto, es decir, estados Rydberg con $l \gtrsim 4$, los átomos alcalinos Rydberg se pueden describir de forma precisa como un átomo de hidrógeno en un estado Rydberg porque el electrón de valencia no penetra el core y no es capaz de distinguir su estructura interna. Por el contrario, un electrón de Rydberg con momento angular bajo $l \lesssim 3$, penetra y polariza el core del átomo alcalino, y tanto la energía como la función de onda difieren de las correspondientes del átomo de hidrógeno. Los llamados defectos cuánticos δ_{nl}, que dependen de los números cuánticos principal y orbital, cuantifican las diferencias entre ambos sistemas [28], y la energía del átomo de Rydberg puede ser escrita como $E_{nl} = -\frac{R_y}{(n-\delta_{nl})^2}$, donde $R_y = -13.6eV$ es la constante de Rydberg. Para estos estados Rydberg, $n^* = n - \delta_{nl}$ define un número cuántico principal efectivo. Debido a estos defectos cuánticos, en comparación con el átomo hidrogenoide, las energías de los estados con bajo momento angular orbital ($l \lesssim 3$) disminuyen, mientras que la energía de los estados con altos momentos angulares orbitales coinciden con la energía de los átomos hidrogenoides, y están degenerados formando un multiplete de estados Rydberg (degenerados) con número cuántico principal n y momento angular orbital $l \gtrsim 3$.

El electrón de valencia en los átomos Rydberg está muy alejado del core iónico, y el valor esperado de radio orbital viene dado por $\langle r \rangle = \frac{1}{2}(3n^2 - l(l+1))$ [28], siendo l el número cuántico orbital. Por ejemplo, el radio orbital de Rb($35s$) es 1837.5 $a_0 \approx 97.2$ nm, es decir, el átomo de rubidio en el estado Rydberg $35s$ es varios órdenes de magnitud más grande que en el estado fundamental. Su vida media incrementa según la ley de potencias n^3 y n^5, para estados en onda-s y estados circulares con $l = n - 1$, respectivamente, dando lugar a vidas medias del orden de los milisegundos o incluso mayores. Por ejemplo, la vida media del Rb en el estado $43s$ es aproximadamente 90 μs [28]. En estos átomos, la gran distancia que separa el electrón Rydberg del core iónico da lugar a momentos dipolares eléctricos muy grandes, que aumenta como n^2, y a polarizabilidades como n^4 [28]. Como consecuencia, los átomos Rydberg son muy sensibles a campos externos, los cuales proporcionan una herramienta esencial para el control y la manipulación experimental de estos sistemas.

Dos átomos Rydberg interaccionan entre sí por medio de la fuerza dipolo-dipolo, con el coeficiente dipolo-dipolo que aumenta con el número cuántico principal como $C_3 \propto n^4$, o a través de la fuerza de van-der-Waals, con un coeficiente de van-der-Waals que aumenta como $C_6 \propto n^{11}$. Estas fuertes interacciones dan lugar a un mecanismo de bloqueo Rydberg [38–40]: la creación de un átomo de Rydberg inhibe fuertemente la excitación de un átomo vecino. Ésta es una de las propiedades más intrigantes e interesantes de la interacción entre dos átomos Rydberg, ya que crea excitaciones colectivas coherentes en un gas atómico denso, los llamados superátomos [38–40]. Una aplicación directa del bloqueo Rydberg es el procesamiento de información cuántica, debido a que proporciona una interacción

dependiente del estado que permite diseñar puertas lógicas de dos qubits [35, 36]. Debido a este mecanismo de bloqueo Rydberg, se ha podido excitar un único un átomo Rydberg en de un condensado de Bose-Einstein [41], de tal manera que el electrón de Rydberg interactúa con los átomos condensados, excitando fonones, y eventualmente, provocando una oscilación colectiva del condensado.

La ténica experimental más usada para crear átomos Rydberg en un gas ultrafrío es por medio de una doble excitación usando dos campos láseres de frequencias diferentes. Debido al mencionado mecanismo de bloqueo Rydberg, sólo unas pocas excitaciones pueden ser creadas dentro la nube atómica y la mayor parte de los átomos permanecen en el estado fundamental. En un sistema híbrido de este tipo, se predijo teóricamente la existencia de las moléculas de alcance ultra-largo (ULRM de sus siglas en inglés) formadas por un átomo en el estado fundamental y un átomo Rydberg [42]. Las moléculas Rydberg más conocidas consisten en dos átomos fuertemente unidos, que están caracterizados por dos núcleos y una nube electrónica a su alrededor en la que un electrón está en un estado excitado orbitando alrededor [43, 44]. Por el contrario, estas especies moleculares de alcance ultra-largo están caracterizadas por distancias internucleares entre el core Rydberg y el átomo en el estado fundamental muy grandes, que son del orden de la extensión del estado electrónico Rydberg que crea esta molécula. Dado que la órbita del electrón Rydberg se distribuye sobre una región que se extiende más allá del core Rydberg, donde el potencial de Coulomb es débil, y varía lentamente como función de la distancia, el electrón de valencia tiene una energía muy pequeña, un momento bajo y se puede decir que ocupa un estado cuasi-libre. Como consecuencia, la interacción entre el átomo en el estado fundamental y el átomo Rydberg, que es un problema de tres cuerpos, se puede describir aproximadamente como dos interacciones independientes de dos cuerpos: la colisión entre el electrón Rydberg y el átomo en el estado fundamental, y entre el electrón de Rydberg y el propio core iónico. El mecanismo de enlace de estas ULRM está basado en la colisión a bajas energías entre el electrón Rydberg y el átomo en el estado fundamental, que se describe por los pseudo-potenciales de Fermi para onda-s y onda-p [45,46]. Una posible interpretación física es que el átomo que perturba muestrea localmente la función de onda del electrón Rydberg. Las curvas de energía potencial adiabáticas de estas ULRM muestran un inusual comportamiento oscilatorio como función de la distancia internuclear, que refleja el carácter oscilatorio de las funciones de ondas del electrón Rydberg.

Dependiendo del momento angular orbital del estado Rydberg que crea estas moléculas, las ULRMs se clasifican en dos clases distintas [42,47]. Si la ULRM surge a partir de electrón de Rydberg en un multiplete degenerado, i. e., con un momento angular orbital alto $l \geq 3$ con defectos cuánticos muy pequeños; esta molécula tiene energías de enlace vibracional del orden de los GHz. Estos sistemas se conocen como trilobites ya que su distribución de probabilidad electrónica se asemeja a un fósil de trilobite. Al principio, estos estados se describieron usando solo la contribución en onda s de la interacción electrón Rydberg y átomo en el estado fundamental. Dichos estados tienen un enorme momento dipolar eléctrico permanente en el rango de los kilodeybe, por ejemplo, el momento dipolar eléctrico permanente para el estado trilobite $n = 30$ $^3\Sigma$ del Rb$(30, l \geq 3)$- Rb$(5S_{1/2})$ es $d = 0.3$ kD [42], y las vidas medias están en el rango de los 10 y 100 microsegundos. La ULRM formada por un átomo Rydberg con bajo momento angular orbital $l \leq 2$, posee curvas de energía potencial Born-Oppenheimer con pozos potenciales poco profundos, de unos pocos MHz, [47]. La densidad electrónica de

la ULRM formada con estado Rydberg en onda-p se parece a una mariposa, y se les conoce como estados butterfly. Estos estados de butterfly también poseen un momento dipolar eléctrico muy grande, por ejemplo, los valores del momento dipolar eléctrico permanente para los estados de simetría Σ y Π son $d = 1.05$ kD y $d = -1.53$ kD, respectivamente, para un electrón de Rydberg en el estado $n = 30$ [47]. Se esperaría entonces que la ULRM, que se forma a partir de los estados de Rydberg en onda s, i. e., de un estado Rydberg ns, fuera no polar y que tuviera una función de onda electrónica no degenerada, esférica, y simétrica. Sin embargo se ha demostrado que la contribución del estado electrónico principal cuasi-degenerado, provoca la existencia de momentos dipolares eléctricos pequeños en estas ULRM en onda s, por ejemplo, aproximadamente 1D, para Rb($35s$)-Rb($5S_{1/2}$), que debido a sus pequeñas constantes rotacionales dan lugar a grandes desplazamientos de energía debido al efecto Stark [48].

Experimentalmente, la existencia de estas ULRM fue confirmada para átomos de Rb en estados Rydberg en onda-s [49]. Desde esta primera observación experimental, estas exóticas moléculas Rydberg han atraído un gran interés en el campo de la física de sistemas Rydberg ultrafríos. Por ejemplo, se midieron la vida media de sus estados fundamentales y de sus estados vibracionales excitados [50], se ha determinado su momento dipolar eléctrico permanente [48], se han caracterizado espectroscópicamente moléculas diatómicas excitadas [51], y se han preparado y explorado las ULRMs formadas por otros átomos tales como Cs [52–54] y Sr [55–57]. En la actualidad, los esfuerzos experimentales están enfocados a explorar estas ULRMs formadas por átomos Rydberg con momento angular orbital altos [53, 54, 58–61]. La contribución del espín a través de la interacción hiperfina y la estructura fina ha sido analizada tanto teórica como experimentalmente [54, 59, 64, 65]. Estas moléculas exóticas muestran una alta sensibilidad a campos externos, que se convierten en una herramienta experimental ideal para controlar y manipular su estructura electrónica, su geometría molecular y sus propiedades de enlace [66–69]. Se ha demostrado experimentalmente que la excitación usando campos magnéticos de estados moleculares rovibracionales con diferentes grados de alineación [60].

En un gas de átomos ultrafríos en el estado fundamental y en un estado Rydberg, si la densidad es lo suficientemente alta, es posible que más de un átomo en el estado fundamental este localizado dentro de la órbital del átomo Rydberg. Así, se podrían crear ULRMs poliatómicas. Los potenciales de Born-Oppenheimer para algunas configuraciones de ULRMs poliatómicas han sido investigados teóricamente [70–72]. Si la interacción entre el átomo en el estado fundamental y el electrón Rydberg es repulsiva, es decir la longitud de colisión entre el electrón y el átomo es positiva, la ULRM diatómica no puede soportar estados ligados, sin embargo, la ULRM triatómica existe y tiene estados ligados vibracionales [71]. Recientemente han sido estudiados tanto teórico como experimentalmente dímeros excitados y trímeros Rydberg ligados mediante la reflexión cuántica [51]. Al aumentar el número cuántico principal del estado de Rydberg, se ha observado experimentalmente la transición de una ULRM diatómica a una poliatómica [73].

Los avances experimentales en la física atómica y molecular de sistemas ultrafríos permiten la creación de sistemas cuánticos híbridos formados por átomos ultrafríos y por moléculas polares ultrafrías. Si en tales sistemas híbridos se crea un átomo Rydberg se ha demostrado teóricamente la existencia de un nuevo tipo de moléculas Rydberg si una molécula diatómica

heteronuclear está dentro de la órbita de la función de onda del electrón Rydberg [74–77]. El mecanismo de enlace aparece debido a la colisión anisotrópica entre el electrón Rydberg con el momento dipolar eléctrico de la molécula polar. Para que estas moléculas Rydberg poliatómicas existan, la molécula diatómica heteronuclear debe tener un momento dipolar eléctrico permanente subcrítico, es decir, $d < 1.639$ D, para evitar que el electrón Rydberg se una a la molécula diatómica polar y el átomo Rydberg se ionice [78–81]. El espectro rotacional de moléculas diatómicas de capa abierta, tales como OH, OD, LiO y NaO, está caracterizado por la estructura fina y el efecto del desdoblamiento Λ, y puede ser descritas como un sistema de dos estados [82–84]. Para estas moléculas de doblete-Λ, el campo eléctrico debido al átomo Rydberg acopla los dos estados internos de la molécula polar, el estado excitado y el fundamental [74]. Por el contrario, el electrón de Rydberg está acoplado a varios estados rotacionales para un molécula de capa cerrada, tal como KRb o RbCs, provocando la hibridización del movimiento rotacional [77]. En ambos tipos de moléculas Rydberg, encontramos una serie de curvas potenciales de Born-Oppenheimer (BOP de sus siglas en inglés) con un comportamiento ondulatorio, reflejando así el carácter oscilatorio de la función de onda del electrón Rydberg. Estos potenciales de Born-Oppenheimer presentan pozos con profundidades de unos pocos GHz, si se crean a partir del estados Rydberg degenerados con $l > 2$ [74–77]. Al igual que las ULRM, estas moléculas Rydberg gigantes también son muy sensibles al campo externo, y pueden manipular muy fácilmente con campos eléctricos de unos pocos V/cm [76, 77]. El acoplamiento creado por el electrón Rydberg da lugar a una fuerte hibridización de los estados rotacionales de la molécula diatómica y a una fuerte orientación y alineación de la misma. Dado que en estas moléculas Rydberg gigantes, la orientación de la molécula diatómica cambia de signo al variar la distancia al core iónico [74, 77], dos estados rotacionales internos de orientación opuesta pueden acoplarse por Raman [74] para crear una interacción dipolo-dipolo modificable que se necesita para implementar un qubits molecular [85]. Un problema importante en física molecular ultrafría es la detección experimental del estado interno, que normalmente implica la destrucción de la molécula via, por ejemplo, la ionización de la misma. Se ha propuesto teóricamente utilizar la interacción entre un átomo Rydberg y una molécula polar, es decir, la interacción básica responsable de la existencia de las moléculas Rydberg poliatómicas, para detectar el estado interno de la molécula diatómica de forma no destructiva [86, 87].

Objetivo de esta tesis

El objetivo de esta tesis es investigar teóricamente la estructura electrónica y las propiedades de las moléculas Rydberg poliatómicas. A continuación, se describe en detalle este objetivo siguiendo la estructura de esta tesis.

Se ha comenzado estudiando el impacto de un campo eléctrico externo en la estructura electrónica de una molécula Rydberg triatómica. Consideraremos una ULRM triatómica formada por un átomo de rubidio en un estado Rydberg y dos átomos de rubidio en el estado fundamental. Éstos, al igual, que el core Rydberg, serán descritos como partículas puntuales. Se han investigado tres configuraciones de los átomos que forman la ULRM: dos lineales y una plana. Para las configuraciones lineales, se ha explorado una disposición simétrica donde los dos átomos en el estado fundamental están situados a la misma distancia del core iónico, pero

en diferentes lados del mismo, y un caso asimétrico con los átomos de Rb localizados al mismo lado del Rb^+ y a diferentes distancias. Para la configuración plana, hemos asumido que los átomos en el estado fundamental están localizados a la misma distancia del core Rydberg, pero las dos líneas rectas que conectan sus posiciones espaciales y el Rb^+ forman un ángulo más pequeño que π. La interacción entre el electrón Rydberg y los dos átomos de Rb en el estado fundamental se aproxima en el régimen de bajas energías por los pseudo-potenciales de Fermi para onda-s y onda-p, los cuales incluyen la longitud de dispersión de triplete de onda-s y onda-p, dependientes de la energía, entre el electrón Rydberg y los átomos de rubidio en el estado fundamental. Estas ULRM triatómicas son analizadas dentro de la aproximación de Born-Oppenheimer, asumiendo que la función de onda total se divide en dos partes que describen los movimientos electrónicos y nucleares de la molécula Rydberg triatómica. La validez de la aproximación de Born-Oppenheimer para investigar la estructura electrónica de la ULRM está justificada debido a la gran diferencia entre las escalas de energías asociadas a la estructura electrónica y los estados vibracionales.

En el Capítulo 3, investigaremos dentro de esta aproximación de Born-Oppenheimer, las curvas y superficies de energía potencial adiabáticas, para las geometrías lineal y plana de la ULRM triatómica, respectivamente. También analizaremos el impacto de un campo eléctrico adicional en estos potenciales electrónicos adiabáticos. Para estados moleculares con simetría Σ y Π de la configuración colineal nuestros resultados muestran que el carácter de ligadura de los estados electrónicos aumenta al incrementar el campo eléctrico, es decir, que existen más estados ligados en el potencial adiabático correspondiente. Las superfices de energía potencial adiabática de la ULRM plana dependen débilmente de la disposición de los átomos en el estado fundamental solo cuando se aproximan entre ellos. La interacción con el campo eléctrico externo favorece la configuración lineal simétrica y aumenta el número de estados vibracionales algunos de ellos tienen extensiones espaciales de unos pocos cientos de radio de Bohr.

Una selección de los resultados presentados en el Capítulo 3 han sido publicados en: J. Aguilera-Fernández, P. Schmelcher, and R. González-Férez, *Ultralong-range triatomic Rydberg molecules in an electric field*, J. Phys. B: At. Mol. Opt. Phys. **49** (2016) [88].

En el Capítulo 4, analizaremos la estructura electrónica de una molécula Rydberg triatómica, formada por un átomo Rydberg y una molécula diatómica heteronuclear. Como ejemplo prototipo hemos considerado la molécula Rydberg triatómica Rb-KRb, formada por un átomo de rubidio en un estado Rydberg, y una molécula diatómica de KRb. La molécula de KRb puede formar estas moléculas Rydberg porque tiene un momento dipolar eléctrico $d = 0.566$ D [89], que es más pequeño que el valor crítico de Fermi-Teller 1.639 D [78, 79], y su constante rotacional es $B = 1.114$ GHz [90]. La estructura electrónica de esta molécula Rydberg triatómica se describe dentro de la aproximación de Born-Oppenheimer en función de las diferentes escalas de energías asociadas al núcleo y a los grados de libertad electrónicos. Para la molécula diatómica, hemos realizado una descripción realista de su movimiento interno dentro de la aproximación del rotor rígido. Esto nos permite describir adecuadamente la hibridación del movimiento rotacional de KRb, provocado por la interacción de su momento dipolar eléctrico permanente con el campo eléctrico debido al átomo Rydberg.

Hemos analizado primero los estados electrónicos adiabáticos de la molécula Rydberg $Rb(n; l \geq 3)$-KRb, al variar el número cuántico principal n del electrón Rydberg. Este

estudio es una extensión del análisis previamente realizado en la Ref. [77]. Al aumentar la distancia internuclear entre el Rb^+ y la molécula de KRb la curvas de energía potencial muestran un carácter oscilatorio provocado por la función de onda del electrón Rydberg. Con el incremento del número cuántico principal n del Rb($n; l \geq 3$), la profundidad de los pozos del estado electrónico más bajo que proviene de Rb($n; l \geq 3$)-KRb($N = 0$), disminuye pero se mantiene en el rango de unos pocos GHz. De hecho, estos pozos potenciales son lo suficientemente profundos tener estados ligados vibracionales, pero el número de estados ligados disminuye a medida que n aumenta. Además, hemos analizado la orientación y la alineación de la molécula diatómica, y su evolución al aumentar la distancia entre KRb y Rb^+.

En el laboratorio, los átomos de rubidio en estados de Rydberg se preparan rutinariamente mediante un esquema de excitación de dos fotones. Esto significa que los estados Rydberg en onda s u onda d, i. e., Rb(ns) o Rb(nd), son fácilmente accesibles en los experimentos con átomos Rydberg. Por lo tanto la posibilidad de observar experimentalmente estas moléculas Rydberg Rb-KRb, requiere investigar su estructura electrónica cuando son creadas a partir de estados Rydberg con un momento angular orbital bajo, es decir, $l \leq 2$ y determinar la existencia de estados ligados vibracionales en los correspondientes estados electrónicos adiabáticos. Este estudio se ha llevado a cabo también el Capítulo 4, donde hemos analizado la estructura electrónica de las moléculas Rydberg Rb($26d$)-KRb, Rb($27p$)-KRb and Rb($28s$)-KRb. Hemos encontrado que los correspondientes estados electrónicos muestran un carácter oscilatorio suave al aumentar la separación internuclear. Si la molécula diatómica está en un estado rotacional excitado, estos estados electrónicos presentan pozos con profundidades de unos pocos MHz, que tiene varios estados ligados vibracionales donde estas moléculas macroscópias podrían existir. Por último, también hemos mostrado que la orientación y alineación de la molécula diatómica son más pequeñas porque el campo eléctrico creado por el átomo Rydberg en este estados con bajo momento angular orbital es más débil.

Una selección de los resultados presentados en el Capítulo 4 han sido publicados en: J. Aguilera-Fernández, H.R. Sadeghpour, P. Schmelcher, and R. González-Férez, *Ultralong-Range Rb-KRb Rydberg Molecules: Selected Aspects of Electronic Structure, Orientation and Alignment*, J. of Phys. Conf. Ser. **635**, 012023 (2015) [91].

Motivados por los resultados experimentales en la ULRM poliatómica, del grupo del Prof. T. Pfau [51, 73], nuestro próximo objetivo ha sido investigar moléculas Rydberg poliatómicas más complejas, formadas por un átomo Rydberg y dos moléculas diatómicas heteronucleares. Experimentalmente, sólo en un gas ultrafrío diluido, sería posible encontrar una sola molécula diatómica en las proximidades de un átomo Rydberg o si las dos especies están localizadas en el mismo pozo potencial en una red óptica, en ambos casos, se podría crear la molécula Rydberg triatómica. Sin embargo, en una mezcla de átomos y moléculas ultrafrías, podría ocurrir que más de una molécula diatómica se encuentren dentro de la órbita del electrón Rydberg, y siendo posible observar experimentalmente la señal espectroscópica de moléculas Rydberg poliatómicas más complejas. En el Capítulo 5, hemos investigado la estructura electrónica de un molécula Rydberg pentaatómica, formada por un átomo de Rydberg y dos moléculas diatómicas heteronucleares en el estado fundamental. Igual que se hizo en el Capítulo 4, hemos considerado como prototipo la molécula Rydberg pentaatómica formada por un átomo de rubidio en un estado Rydberg y dos moléculas de KRb. Las moléculas

diatómicas se describen dentro de la aproximación del rotor rígido teniendo en cuenta sus grados de libertad angulares, haciendo así un análisis realista de la interacción entre el campo eléctrico del átomo Rydberg y su momento dipolar eléctrico permanente y las propiedades direccionales de las moléculas diatómicas.

Debido a la complejidad numérica asociada a la descripción completa de una configuración arbitraria de la molécula Rydberg pentaatómica, nuestro estudio está restringido a dos configuraciones lineales. Primero analizamos una disposición simétrica en la que las dos moléculas diatómicas se encuentran localizadas a la misma distancia del ión Rb^+, pero a diferentes lados del mismo. Para esta configuración simétrica, hemos investigado los estados electrónicos adiabáticos que evolucionan a partir del multiplete degenerado Rydberg Rb($n = 20, l \geq 3$) y las dos moléculas diatómicas inicialmente se encuentran en un estado fundamental rotacional, es decir, la molécula Rydberg pentaatómica KRb($N = 0$)-Rb($n = 20, l \geq 3$)-KRb($N = 0$), y del Rb($23s$) con las dos moléculas de KRb en un estado rotacional excitado, es decir, la KRb($N > 0$)-Rb($23s$)-KRb($N > 0$). Además analizamos una configuración asimétrica con las dos moléculas diatómicas localizadas al mismo lado del ión Rb^+, pero a diferentes distancias del mismo. Para esta configuración asimétrica, hemos estudiado los estados electrónicos adiabáticos que surgen a partir del Rb($n = 20, l \geq 3$), donde las dos moléculas diatómicas se encuentran inicialmente en un estado fundamental rotacional, es decir, la molécula Rydberg pentaatómica Rb($n = 20, l \geq 3$)-KRb($N = 0$)-KRb($N = 0$), a medida que la distancia entre una o las dos moléculas diatómicas, y el core iónico aumenta. Exploramos igualmente los efectos del campo eléctrico debido al átomo Rydberg en el movimiento de las molécula diatómicas analizando su orientación y alineación en ambas configuraciones de esta molécula Rydberg pentaatómica.

Nuestros resultados demuestran que la estructura electrónica depende en gran medida del estado Rydberg del átomo Rb formando la molécula Rydberg pentaatómica correspondiente. Los estados electrónicos muestran pozos con profundidades de unos pocos GHz o MHz si el estado del electrón Rydberg es Rb($n = 20$, $l \geq 3$) o Rb($23s$), respectivamente. En ambos casos pueden tener varios estados vibracionales ligados, y podemos concluir que las molécula Rydberg pentaatómicas pueden ser observadas experimentalmente en las configuraciones lineales tanto simétrica como la asimétrica. Para estas configuraciones, las moléculas de KRb presentan una orientación y alineación moderada dentro de estos estados electrónicos adiabáticos. La estructura electrónica de la moléculas simétricas y asimétricas que involucran al Rb($23s$) además presentan estados electrónicos inestables. Nótese que para que esta molécula Rydberg pentaatómica exista, las dos moléculas de KRb deberían estar inicialmente en estados rotacionales excitados, y encontramos energías vibracionales de enlace a unos pocos MHz en estas BOPs y una pequeña orientación para estas moléculas de KRb.

Una selección de los resultados presentados en el Capítulo 5 están incluidos en la siguiente publicación: J. Aguilera-Fernández, H.R. Sadeghpour, P. Schmelcher, and R. González-Férez, *Electronic structure of ultralong-range Rydberg pentaatomic molecules with two polar diatomic molecules*, aceptada en la revista Physical Review A (2017) [92].

Finalmente, las conclusiones de esta tesis serán presentadas en los Capítulos 6 (versión en inglés) y 7 (versión en español), donde también se indican posibles trabajos de investigación sobre esto sistemas Rydberg que se podrían llevar a cabo en el futuro, y que pueden considerarse una continuación naturaal de los estudios realizados en esta tesis doctoral.

Chapter 3

Triatomic Rydberg Molecules in an Electric Field

3.1 Introduction

In this chapter, we consider a triatomic ultralong-range molecule formed by a Rydberg atom and two neutral ground state atoms, and explore, to our knowledge for the first time, the impact of an external electric field on its electronic structure. This study is motivated by the high sensitivity of Rydberg atoms and Rydberg molecules to external fields. For diatomic Rydberg molecules, it has been analyzed the impact of electric and magnetic fields on the their electronic structure, molecular geometry and binding properties [66–69]. These studies show that electric and magnetic fields provide experimental knobs to control and manipulate these systems, as it is the case for Rydberg atoms.

The two ground state atoms and the Rydberg core are described as point particles, and we restrict this study to the low-energy regime approximating the interaction between the Rydberg electron and each neutral atom by the Fermi pseudopotential [45, 46]. Compared to previous studies about the electronic structure of these triatomic Rydberg molecules [70, 71], we include both the s-wave and p-wave interactions of the Rydberg electron and the ground state atoms. Our focus is on three different configurations: two collinear arrangements of the atoms and planar one, which are shown in Fig. 3.1. For the collinear configurations, we consider the symmetric case where the two ground state atoms are located on different sides of the positively charged Rydberg core and at the same distance from it, see Fig. 3.1 (a), and an asymmetric case with the atoms being located on the same side of the Rb^+ core and at different distances, see Fig. 3.1 (b). We also analyze a planar configuration where the two straight lines connecting the spatial positions of each ground state atom and the Rydberg core form an angle smaller than π, thereby assuming that the distances of the two ground state atoms from the Rydberg core are the same, see Fig. 3.1 (c).

We investigate the molecular states of collinear and planar geometries by analyzing their adiabatic potential curves (APC) and surfaces (APS) within the Born-Oppenheimer approximation, respectively. For the above-mentioned three configurations, we encounter a variety of different molecular states with deep potential wells leading to bound ULRMs. We explore in particular the impact of an additional electric field on these adiabatic potentials and show that the bound character of the molecular states increases in case of the linear configuration.

This chapter is organized as follows. The Hamiltonian of the triatomic Rydberg molecule in an external electric field is described in Sec. 3.2. We analyze the electronic structure of the linear and planar configurations in Sec. 3.3 and Sec. 3.4, respectively, where we also explore the impact of a static electric field on the corresponding molecular states.

Part of the contents of this chapter is adapted from the reference: J. Aguilera-Fernández,

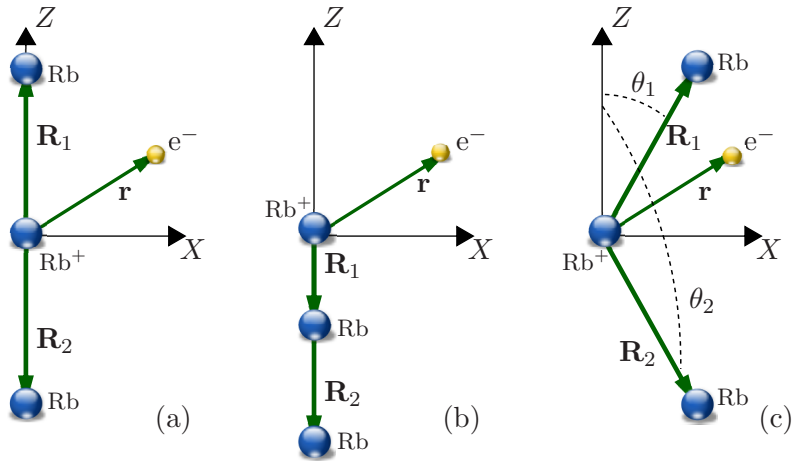

Figure 3.1: Sketches (not to scale) of three different configurations of the triatomic molecule formed by a Rydberg atom and two ground state atoms in the XZ-plane.

P. Schmelcher, and R. González-Férez, *Ultralong-Range Triatomic Rydberg Molecules in an Electric Field*, J. Phys. B: At. Mol. Opt. Phys. **49** (2016) [88].

3.2 The molecular Hamiltonian

We consider a triatomic Rydberg molecule formed by a Rydberg atom and two ground state neutral atoms in a static electric field. It is assumed that the two ground state atoms and the Rydberg core can be described as point particles and we fix the center of the laboratory fixed frame (LFF) at the position of the ionic core. Our study focuses on the low-energy regime and the interaction between the Rydberg electron and a neutral atom is described by the Fermi pseudopotential [45, 46]:

$$V(\mathbf{r},\mathbf{R}_i) = \; 2\pi A_s[k(R_i)]\delta(\mathbf{r}-\mathbf{R}_i) + 6\pi A_p^3[k(R_i)]\overleftarrow{\nabla}\delta(\mathbf{r}-\mathbf{R}_i)\overrightarrow{\nabla}\,, \tag{3.1}$$

where $\mathbf{r}$ and $\mathbf{R}_i = (R_i, \theta_i, \phi_i)$ are the positions of the Rydberg electron and neutral atoms with respect to the Rydberg core, respectively, with $i = 1, 2$. Note that in expression (3.1), the symbols $\overleftarrow{\nabla}$ and $\overrightarrow{\nabla}$ mean differentiation operator, acting on the function on the left and right side of the Hamiltonian operator, respectively. The energy-dependent triplet s- and p-wave scattering lengths are given by

$$A_s(k) \;=\; -\frac{\tan[\delta_0(k)]}{k}\,, \tag{3.2}$$

$$A_p^3(k) \;=\; -\frac{\tan[\delta_1(k)]}{k^3}\,, \tag{3.3}$$

with $\delta_l(k)$, $l = 0, 1$ being the corresponding phase shifts. The kinetic energy of the Rydberg electron at the collision point with the neutral atom, R_i, can be approximated by the semiclassical expression $E_{kin} = k^2/2 = 1/R_i - 1/2n^2$, with n being the principal quantum number of the Rydberg electron. The energy-dependent phase shifts $\delta_l(k)$ versus

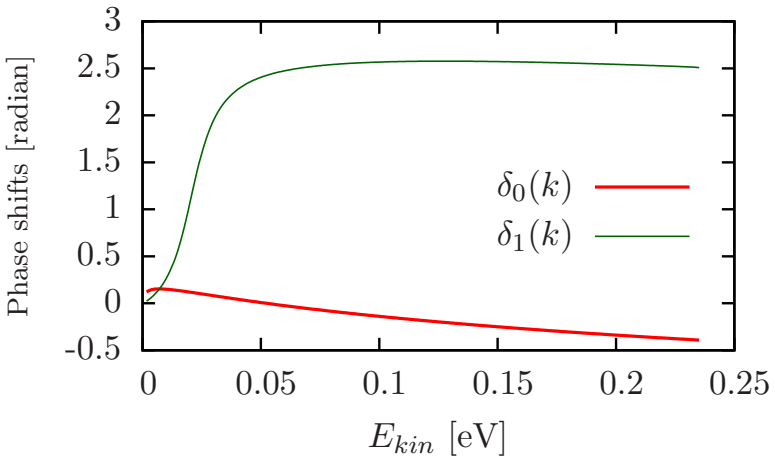

Figure 3.2: Energy-dependent triplet phase shifts, δ_0 (k) and $\delta_1(k)$, for the s- and p-wave scattering of an electron from the ground state Rb atom as a function of the electron kinetic energy E_{kin}.

the kinetic energy E_{kin} of the electron are presented in Fig. 3.2. In case the energy-dependent phase shifts $\delta_l(k)$ are not numerically known, they can be approximated by their low-energy dependence [46]:

$$A_s(k) \approx a_T + \frac{\pi}{3}\alpha_n k + \mathcal{O}(k^2)\,, \tag{3.4}$$

$$A_p^3(k) \approx -\frac{\pi\alpha_n}{15k}\,, \tag{3.5}$$

where α_n is the ground state polarizability of the neutral ground state atom, and a_T is the scattering length of the collision between the electron and the ground state perturber. The ground state atom ^{87}Rb has a negative triplet scattering length for the collision with the electron $a_T = -16.05\ a_0$ [96].

The Hamiltonian of this triatomic Rydberg molecule reads

$$H = T_n + H_{el} + V(\mathbf{r}, \mathbf{R}_1) + V(\mathbf{r}, \mathbf{R}_2), \tag{3.6}$$

where T_n is the nuclear kinetic energy operator for all relative nuclear motions. The second term stands for the Hamiltonian of the Rydberg electron in an external electric field

$$H_{el} = H_0 + \mathbf{F}\cdot\mathbf{r} = \frac{\mathbf{p}^2}{2m_e} + V_l(r) + \mathbf{F}\cdot\mathbf{r}, \tag{3.7}$$

with m_e being the electron mass, $\mathbf{p}$ its relative momentum, and $V_l(r)$ the angular momentum l-dependent model potential

$$V_l(r) = -\frac{Z_l(r)}{r} - \frac{\alpha_c}{r^4}\left[1 - e^{(r/r_c)^6}\right], \tag{3.8}$$

where $Z_l(r)$ is an effective charge, α_c the static dipole polarizability of the positive-ion core and r_c is a cutoff radius [97].

The last term in the Hamiltonian of the Rydberg electron (3.7) is the interaction with the external electric field, which is taken parallel to the LFF Z-axis $\mathbf{F} = F\mathbf{Z}$, with F being the field strength.

Within the framework of the Born-Oppenheimer approximation, whose validity is well justified for the ULRM given the typical energy scales of the Rydberg electron as compared to the vibrational states, the total wave function factorizes in two parts that describe the electronic and nuclear motions of the Rydberg trimer. The total wave function can then be written as $\Psi(\mathbf{r}, \mathbf{R}_1, \mathbf{R}_2) = \psi(\mathbf{r}; \mathbf{R}_1, \mathbf{R}_2)\phi(\mathbf{R}_1, \mathbf{R}_2)$, where $\psi(\mathbf{r}; \mathbf{R}_1, \mathbf{R}_2)$ and $\phi(\mathbf{R}_1, \mathbf{R}_2)$ are the adiabatic electronic and nuclear wave functions, respectively. Note that within this chapter we focus on the electronic structure of the triatomic ULRM in particular in the presence of an electric field. Thus, the Schrödinger equation for the electronic motion for fixed positions of the nuclei is given by

$$[\, H_0 + \mathbf{F}\cdot\mathbf{r} + V(\mathbf{r}, \mathbf{R}_1) + V(\mathbf{r}, \mathbf{R}_2)\,]\,\psi_i(\mathbf{r}; \mathbf{R}_1, \mathbf{R}_2) = \epsilon_i(\mathbf{R}_1, \mathbf{R}_2)\psi_i(\mathbf{r}; \mathbf{R}_1, \mathbf{R}_2),$$

with $\epsilon_i(\mathbf{R}_1, \mathbf{R}_2)$ being the adiabatic potential energy surface which depends on the position of the two atoms $\mathbf{R}_1$ and $\mathbf{R}_2$. For fixed positions of the ground state atoms, we solve the adiabatic electronic Schrödinger equation (3.9) expanding the electronic wave function $\psi(\mathbf{r}; \mathbf{R}_1, \mathbf{R}_2)$ in the basis formed by the field-free Rydberg electron wave functions $\chi_{nlm}(\mathbf{r}) = R_{nl}(r)Y_{lm}(\vartheta, \varphi)$, where $R_{nl}(r)$ is the radial wave function and $Y_{lm}(\vartheta, \varphi)$ the spherical harmonics, and n, l and m are the principal, orbital and magnetic quantum numbers, respectively. Note that $H_0\chi_{nlm}(\mathbf{r}) = E_{nl}\chi_{nlm}(\mathbf{r})$ with E_{nl} being the Rydberg electron field-free eigenenergy. This field-free energy of the Rydberg electron $E_{n,l}$ is given by

$$E_{n,l} = \begin{cases} -\frac{1}{2(n-\delta_{n,l,j})^2} & \text{if} \quad l \leq 3, \\ -\frac{1}{2n^2} & \text{if} \quad l \geq 4, \end{cases} \tag{3.9}$$

where $\delta_{n,l,j}$ is the quantum defect of the Rydberg states with low rotational angular momentum. As it was mentioned in the Introduction, we can distinguish between the low and high angular momentum states of alkali atoms. The probability of finding the Rydberg electron of a high angular momentum state near the ionic core is negligible. As a consequence, the ionic core is not resolved, and an alkali Rydberg atom in a high angular momentum state can be described as a hydrogen atom considering the ionic core as a point-like charge. In contrast, the former ones penetrate the ionic core, and significantly differ from the hydrogenic states due to core penetration, scattering, and polarization effects. The quantum defect distinguishes between the high and low angular momentum Rydberg states of an alkali atom by taking into account these core-scattering and polarization effects of the Rydberg electron. Indeed, the quantum defect $\delta_{n,l,j}$ quantifies these differences, and depends on the quantum numbers n, and l, and total angular momentum $\mathbf{j} = \mathbf{l} + \mathbf{s}$, $\mathbf{s}$ being the spin, of the Rydberg atom. The quantum defect are determined via the modified Rydberg-Ritz expression [98]

$$\delta_{n,l,j} = \delta_0 + \frac{\delta_2}{(n-\delta_0)^2} + \frac{\delta_4}{(n-\delta_0)^4} + \frac{\delta_6}{(n-\delta_0)^6} + \ldots \tag{3.10}$$

The values of the parameters δ_i with $i = 0, 2, 6$, and 8 are presented in Table 3.1. In this

State	δ_0	δ_2	δ_4	δ_6	δ_8
$nS_{1/2}$	3.1311804	0.1784	−1.8	–	–
$nP_{1/2}$	2.6548849	0.2900	−7.9040	116.4373	−405.907
$nP_{3/2}$	2.6416737	0.2950	−0.97495	14.6001	−44.7265
$nD_{3/2}$	1.34809171	−0.60286	−1.50517	−2.4206	19.736
$nD_{5/2}$	1.34646572	−0.59600	−1.50517	−2.4206	19.736
nF_j	0.016312	−0.064007	−0.36005	3.2390	–

Table 3.1: For the rubidium atom, modified Rydberg-Ritz parameters for the calculation of the quantum defect (3.10). See Ref. [99], for the $l \leq 2$, δ_0 and δ_2, and Ref. [98] the other parameters.

thesis, we do not take into account the spin of the Rydberg atom, so for those states with two values of the total quantum number j, i. e., $j = l \pm 1/2$ with $l = 1$, and 2, the quantum defect is defined as the average value. For p-wave Rydberg states, the quantum defect is $\delta_{n,1} = \frac{\delta_{n,1,1/2}+\delta_{n,1,3/2}}{2}$, whereas for the d-wave Rydberg states, $\delta_{n,2} = \frac{\delta_{n,2,3/2}+\delta_{n,2,5/2}}{2}$. For the sake of simplicity, in this dissertation, we use the following notation $\delta_{n,l}$ for the quantum defect, and do not specify the total angular momentum of the Rydberg atom as subindex. In addition, through this thesis we have neglected the quantum defect of the nf Rydberg states. For the high angular momentum Rydberg states, the core penetration and polarization effects are very small and give rise to zero quantum defects, the corresponding wave functions are mathematically identical to their hydrogenic counterparts.

In the basis set expansion, the electronic wave function is then written as

$$\psi_i(\mathbf{r};\mathbf{R}_1,\mathbf{R}_2) = \sum_{n,l,m} C_{n,l,m}(\mathbf{R}_1,\mathbf{R}_2)\chi_{nlm}(\mathbf{r}), \tag{3.11}$$

where we have explicitly indicated that the coefficients of the expansion $C_{n,l,m}(\mathbf{R}_1,\mathbf{R}_2)$ depend on the fixed positions of the two ground state atoms $\mathbf{R}_1$ and $\mathbf{R}_2$. This basis set expansion combined with the linear variational principle allows us to transform the Schrödinger equation in an eigenvalue problem, see Appendix C. The Hamiltonian matrix is given by

$$\langle\chi_{n_1l_1m_1}|H|\chi_{n_2l_2m_2}\rangle = \langle\chi_{n_1l_1m_1}|H_0 + \mathbf{F}\cdot\mathbf{r} + V(\mathbf{r},\mathbf{R}_1) + V(\mathbf{r},\mathbf{R}_2)|\chi_{n_1l_2m_2}\rangle. \tag{3.12}$$

The Hamiltonian matrix is diagonalized using the restarted Lanczos procedure [93] implemented in the Arnoldi Package (ARPACK) [94, 95].

We now provide all the matrix elements appearing in the Hamiltonian matrix. For the field-free Hamiltonian of the Rydberg electron, the matrix elements read

$$\langle\chi_{n_1l_1m_1}|H_0|\chi_{n_2l_2m_2}\rangle = \langle\chi_{n_1l_1m_1}|\frac{\mathbf{p}^2}{2m_e} + V_l(r)|\chi_{n_1l_2m_2}\rangle = E_{n_1,l_1}\delta_{n_1,n_2}\delta_{l_1,l_2}\delta_{m_1,m_2}, \tag{3.13}$$

with $\delta_{i,j}$ being the Kronecker delta.

The matrix element of the interaction with the external electric field reads

$$\langle \chi_{n_1 l_1 m_1} | \mathbf{F} \cdot \mathbf{r} | \chi_{n_2 l_2 m_2} \rangle = F \langle R_{n_1 l_1} | r | R_{n_2 l_2} \rangle \langle Y_{l_1 m_1} | \cos\theta | Y_{l_2 m_2} \rangle, \tag{3.14}$$

where we have taken into account that the electric field is parallel to the LFF Z-axis.

Finally, the matrix element of the Fermi pseduo-potentials of one of the ground state atoms is given by

$$\begin{aligned} \langle \chi_{n_1 l_1 m_1} | V(\mathbf{r}, \mathbf{R}_1) | \chi_{n_2 l_2 m_2} \rangle &= 2\pi A_s[k(R_i)] \chi^*_{n_1 l_1 m_1}(\mathbf{R}_i) \chi_{n_2 l_2 m_2}(\mathbf{R}_i) \\ &+ 6\pi A_p^3[k(R_i)] \overrightarrow{\nabla} \chi^*_{n_1 l_1 m_1}(\mathbf{R}_i) \cdot \overrightarrow{\nabla} \chi_{n_2 l_2 m_2}(\mathbf{R}_i), \end{aligned} \tag{3.15}$$

with $i = 1, 2$. Note that in the second term of this expression, we have to take the partial derivatives with respect to R_i, θ_i and ϕ_i.

In this chapter, we consider a triatomic Rydberg molecule formed by three rubidium atoms, Rb_3, two of them in the ground state and the third one in a Rydberg excited state. Our analysis focuses on the molecular electronic states evolving from the Rydberg degenerate manifold Rb($n = 35$, $l \geq 3$). Thus, in the basis set expansion of the Rydberg wave function (3.11), we include in the basis set the degenerate manifold Rb($n = 35$, $l \geq 3$) and the energetically closest neighboring Rydberg levels $38s$, $37p$ and $36d$. Let us mention again that in this chapter we neglect the quantum defect of the $35f$ Rydberg state. The approximation of including only these Rydberg levels is based in the energy structure presented in Table 3.2. In the next section, we show that due to the interaction with the two ground state atoms, the BOP evolving from the field-free Rydberg degenerate manifold Rb($n = 35$, $l \geq 3$) are shifted less than ~ 35GHz. This indicates that the largest coupling of the Rydberg states from this manifold takes palce with the neighbouring level Rb($38s$).

3.3 The linear triatomic Rydberg molecule

In this section, we consider the linear symmetric and asymmetric configurations of the ULRM, with the two ground state perturbers located along the LFF Z-axis. For the linear symmetric ULRM, we investigate the Born-Oppenheimer potential curves with Σ and Π molecular symmetry, as the distance of two ground state atoms from the ionic core Rb^+ increases, whereas for the asymmetric arrangement the position of one of the perturbers is fixed and the distance of the second one from Rb^+ increases. We also explore the metamorphosis of the BOP curves of these two ULRMs with varying electric field strengths.

3.3.1 The symmetric linear configuration

We start by considering the symmetric linear triatomic ULRM presented in Fig. 3.1 (a), with the neutral atoms located along the LFF Z-axis at different sides of the Rydberg core and at the same distance, i. e., $R_1 = R_2 = R$ and $\theta_1 = 0$, $\theta_2 = \pi$. This Rydberg molecule has been previously investigated in field-free space by modeling the interaction between the Rydberg electron and the neutral atoms via the s-wave scattering pseudopotential and neglecting the contribution of the p-wave scattering [70, 71]. For this triatomic system, the APCs with Σ molecular symmetry (and s-wave interaction only) are presented in Fig. 3.3 (a), where the

n	l	$E_{n,l}$(THz)	$\Delta E_{n,l}$(GHz)
36	3	−2.5384	147.12
39	0	−2.5570	128.50
37	2	−2.6314	97.62
38	1	−2.5879	54.12
35	3	−2.6855	0
38	0	−2.7058	−20.26
36	2	−2.7394	−53.89
37	1	−2.7868	−101.28
34	3	−2.8458	−160.29
37	0	−2.8679	−182.41
35	2	−2.9046	−219.10
36	1	−2.9564	−270.88

Table 3.2: For the rubidium atom, energies and energies differences $\Delta E_{n,l} = E_{n,l} - E_{35,3}$ of the Rydberg levels close to the degenerate Rydberg manifold $n = 35$ and $l \geq 3$.

APC of a diatomic ULRM with the ground state atom located on the LFF Z-axis is also shown. For the triatomic ULRM, we observe that two adiabatic potential curves with gerade and ungerade symmetry split away from the Rb($n = 35$, $l \geq 3$) degenerate manifold. In Ref. [70], it is shown that the gerade (ungerade) APC can be written as a sum in terms of the probability densities of Rydberg electronic states with even (odd) angular momentum $l \geq 3$. These two APC oscillate around the adiabatic electronic curve of the diatomic ULRM, and, in particular, exhibit deeper potential wells, which indicates a higher degree of stability. At large separations between the atoms and Rb^+, these potential curves converge to the APC of a diatomic Rydberg molecule with only one ground state atom, see Fig. 3.3 (a), because the sums of even-l and odd-l probability densities that contribute to the gerade and ungerade molecular states, respectively, are very similar as R increases [70]. Based on previous studies which show that the p-wave scattering pseudopotential plays a crucial role on the electronic structure of diatomic ULRMs [47, 68, 100], we present here the electronic structure of this triatomic ULRM including both the s and p-wave interactions of the Rydberg electron and the ground state atoms. The molecular electronic potentials with Σ and Π symmetry of the triatomic ULRM are shown in Figures. 3.3 (b) and (c), respectively. For the sake of comparison, the APCs of a diatomic ULRM with the ground state atom located on the LFF Z-axis are also presented.

Let us first analyze the Σ molecular levels. For the triatomic ULRM, the p-wave interaction provokes that two additional potentials with Σ molecular symmetry are shifted away from the Rb($n = 35$, $l \geq 3$) degenerate manifold. The resonance of the p-wave scattering length at $R \approx 750\ a_0$ significantly affects the APC and their slope becomes pronounced for $R \lesssim 1200\ a_0$. Indeed, two of these APCs suffer avoided crossings with the adiabatic state evolving from the

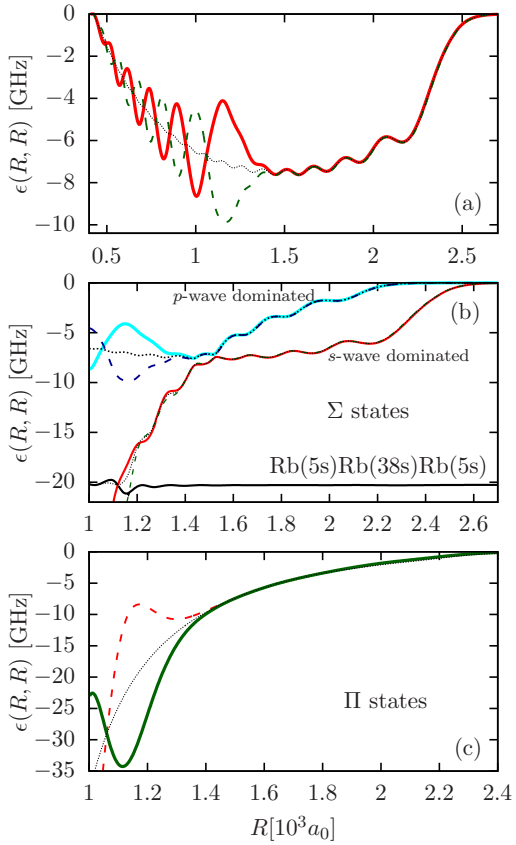

Figure 3.3: Symmetric linear triatomic ULRM with the ground state atoms located along the LFF Z-axis with $\theta_1 = 0$ and $\theta_2 = \pi$, and at equal separations from the Rb^+ core, i. e., $R_1 = R_2 = R$. Adiabatic electronic potentials as a function of the distance R between the Rydberg core and theneutral atoms: (a) obtained including only the s-wave interaction, (b) and (c) taking into account the s- and p-wave interactions and for Σ and Π molecular symmetry, respectively. The gerade and ungerade symmetry curves are plotted with solid and dashed lines, respectively. In panel (b), the APC evolving from the Rb($38s$) Rydberg state is also shown. For the sake of completeness, we plot the APC of the diatomic ULRM (dotted lines) obtained including (a) only the s-wave interaction, (b) and (c) both the s- and p-wave interactions and for Σ and Π molecular symmetry, respectively. The zero energy has been set to the energy of the field-free Rb($n = 35, l \geq 3$) degenerate manifold.

non-degenerate Rydberg level Rb($38s$), whose energy, on the scale of the figure, remains approximately constant for larger values of R. The p-wave and s-wave dominated Σ-APCs suffer several avoided crossings close to the internuclear distance $R \approx 1500\ a_0$. The oscillatory behavior of these adiabatic potentials is due to the highly oscillatory character of the Rydberg electron wave function in the Rb($n = 35$, $l \geqslant 3$) state. The ground state atoms, considered to a good approximation as point particles, probe locally in space the electronic wave function of the highly excited Rydberg atom. At large separations between the Rydberg core and the ground state atoms, the s-wave (p-wave) dominated Σ molecular states become degenerate and converge to the s-wave (p-wave) Σ-APC of the diatomic ULRM. For these large values of R, the electronic structure of the triatomic ULRM is composed of the molecular states of two diatomic ULRMs that share the same Rydberg core and one has the ground state atom at $\theta = 0$ whereas the other one has it at $\theta = \pi$.

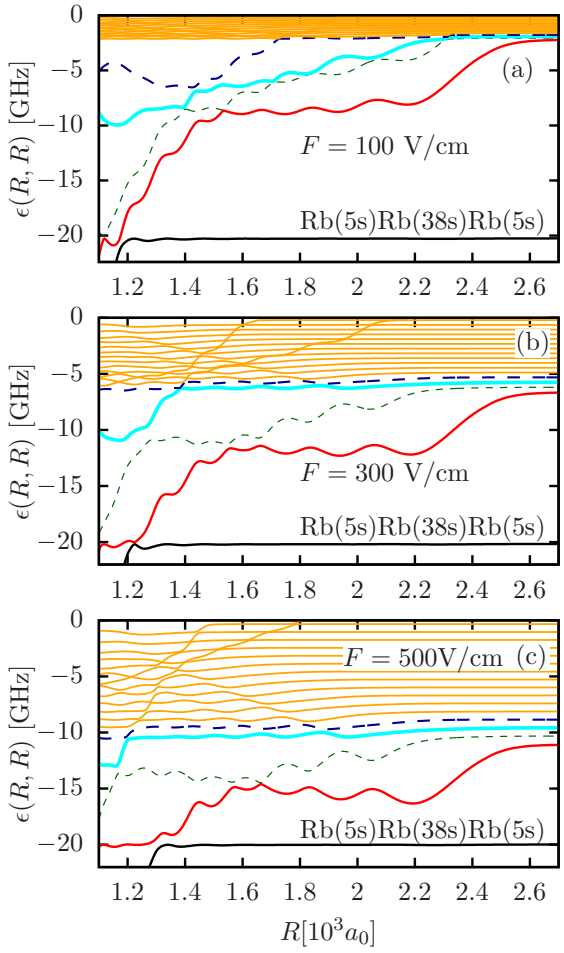

Figure 3.4: For the symmetric linear ULRM: molecular states with Σ symmetry evolving from the degenerate manifold Rb($n = 35$, $l \geq 3$) versus the interatomic distance R of the ground state atoms from the Rydberg core in an external electric field of strength (a) $F = 100$ V/m, (b) $F = 300$ V/m, and (c) $F = 500$ V/m. The APCs have been derived including both the s-wave and p-wave interaction. The zero energy has been set to the energy of the field-free Rb($n = 35$, $l \geq 3$) degenerate manifold.

We focus now on the APCs with Π molecular symmetry. The p-wave interaction is responsible for the adiabatic potentials with Π molecular symmetry, cf. Fig. 3.3 (c). In contrast to the Π molecular levels of the diatomic ULRM, these two APCs show potential wells that could accommodate several vibrational bound states. For large internuclear distances, these two adiabatic electronic potentials become degenerate and equal to the corresponding potentials of a diatomic ULRM.

Due to their large dipole moments, Rydberg atoms are extremely sensitive to weak static electric fields, and, as consequence, the level structure of the ULRM is also significantly affected. In Fig. 3.4 (a), (b) and (c), we present the APCs with Σ molecular symmetry in a static electric field of strength $F = 100$ V/m, 300 V/m, and 500 V/m, respectively. Due to the interaction with the dc field, additional molecular states are shifted from the field-free Rb($n = 35$, $l \geq 3$) Rydberg manifold, which reflects that the Stark interaction

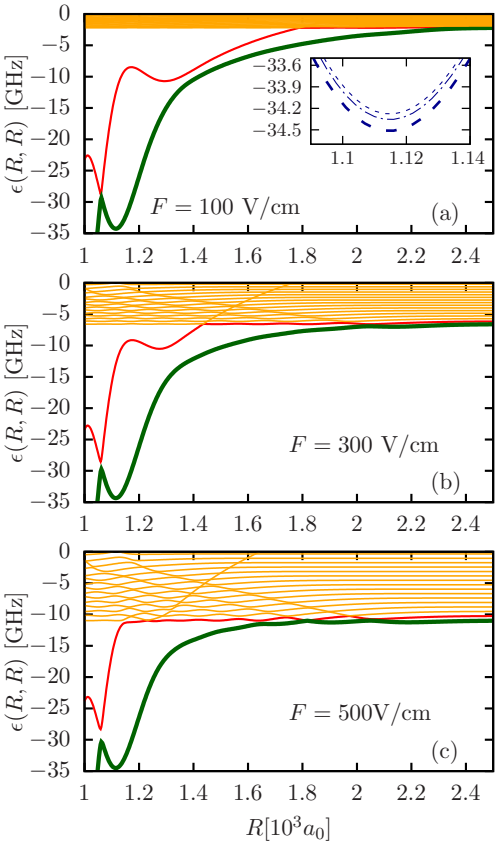

Figure 3.5: For the symmetric linear ULRM: electronic states with Π molecular symmetry evolving from the degenerate manifold Rb($n = 35, l \geq 3$) versus the interatomic distance R of the ground state atoms from the Rydberg core in an electric field of strength (a) $F = 100$ V/m, (b) $F = 300$ V/m, and (c) $F = 500$ V/m. The APCs have been derived including both the s-wave and p-wave interaction. The zero energy has been set to the field-free energy of the Rb($n = 35$, $l \geq 3$) degenerate manifold.

couples states with field-free orbital numbers l and $l \pm 1$. The electric field couples the adiabatic electronic states with gerade and ungerade symmetry and the degeneracy at large internuclear distances of these APCs is lifted. For $F = 100$ V/m, the overall energy of one of the states with s-wave (p-wave) dominated character decreases, whereas the energy of the second one increases approaching the adiabatic electronic states from the Rb($n = 35$, $l \geq 3$) manifold. By further increasing F, the energies of all APCs show a decreasing behaviour. For $F = 500$ V/m, two of the APCs are merged with the field-dressed adiabatic electronic potentials that are split from the field-free Rb($n = 35$, $l \geq 3$) Rydberg manifold, and we encounter several avoided crossings, see Fig. 3.4 (c). Thus, only two molecular states remain energetically well separated from the field-dressed levels evolving from the Rb($n = 35$, $l \geq 3$) Rydberg manifold. The avoided crossing between the lowest-lying APCs from the Rydberg trimer Rb($5s$)Rb($n = 35$, $l \geq 3$)Rb($5s$) and the molecular state from Rb($5s$)Rb($38s$)Rb($5s$) becomes broader as F is increased. Note that due to the quadratic Stark shift of the $38s$ Rydberg state, the APC of Rb($5s$)Rb($38s$)Rb($5s$) is very weakly affected by the electric field. Due to the interplay between the interaction of the Rydberg atom with the two neutral

atoms and with the external electric field, the change in energy of the APCs depends on the internuclear separation between the Rydberg core and the two ground state atoms. At large internuclear distances, when the interaction with the two ground state atoms becomes negligible, all the APCs from the Rb($n = 35, l \geq 3$) Rydberg manifold are shifted linearly in energy with the dc field strength, which corresponds with the Stark shift of the ($n = 35, l \geq 3$) Rydberg manifold of an isolated Rb atom.

Analogous results are found for the field-dressed molecular states with Π molecular symmetry, see Fig. 3.5. For large internuclear separations $R \gtrsim 1400\ a_0$, the degeneracy of the two Π adiabatic electronic states is lifted. For $F = 100$ V/m, one of the APCs increases in energy compared to its field-free value, whereas the other one decreases, see Fig. 3.5 (a), whereas for $F = 300$ V/m and $F = 500$ V/m the energies of all APCs are reduced. In addition, the crossing of the field-free APCs at $R \approx 1060\ a_0$ becomes an avoided crossing in the presence of the dc field. These Π molecular states are weakly affected by the external field for $1000\ a_0 \lesssim R \lesssim 1250\ a_0$, their Stark shifts depend quadratically on the field strength and are hardly visible on the scale of Fig. 3.5. For instance, the energy of the minimum appearing at $R \approx 1115\ a_0$ for the lowest lying Π-APC is shifted 0.3 GHz from its field-free value for $F = 500$ V/m. As F is increased, the field-free highest-lying APC gets mixed with the additional field-dressed APCs evolving from the Rb($n = 35, l \geq 3$) manifold suffering several avoided crossings with them. Again, at large internuclear distances, the Stark shifts of all the APCs from the Rb($n = 35, l \geq 3$) Rydberg manifold depend linearly on F.

3.3.2 The non-symmetric linear configuration

We consider now a linear triatomic Rydberg molecule with the two ground state atoms located along the LFF Z-axis and at the same side of the Rydberg core, i. e., $\theta_1 = \theta_2 = \pi$. A sketch of this configuration is presented in Fig. 3.1 (b). The position of one of the atoms is fixed at $R_1 = 1200\ a_0$, whereas the distance of the second one from the Rb^+ core, R_2, varies for $R_2 > R_1$. This condition allows us to neglect the interaction between both ground state atoms because their vibrational wave functions do not overlap in space. Note that the distance of the first atom from the Rb^+ core has been arbitrarily fixed to $R_1 = 1200\ a_0$, and that qualitatively similar results are obtained for other values of R_1. The Σ and Π molecular states are plotted versus the internuclear separation R_2 in Fig. 3.6 and Fig. 3.7, respectively.

For the electronic structure with Σ molecular symmetry, the presence of the second atom provokes that two extra adiabatic electronic states are split away from the Rb($n = 35$ and $l \geq 3$) degenerate manifold. These two APCs show an oscillatory behaviour superimposed to a broad potential well over the regions $1400\ a_0 \lesssim R_2 \lesssim 2350\ a_0$ and $1300\ a_0 \lesssim R_2 \lesssim 2700\ a_0$ for the p-wave and s-wave dominated states, respectively. These APCs can accommodate many vibrational levels, with spacing ~ 150MHz approximately, some of them having spatial extensions of a few hundreds Bohr radii. Several avoided crossings are encountered between these two adiabatic electronic states, and also between the s-wave dominated state and the p-wave dominated state evolving from the Rydberg diatomic molecule. For large values of R_2, the interaction with the second atom becomes negligible and the triatomic Rydberg molecule becomes an effective diatomic system. In this case, the two energetically lowest Σ-symmetry APCs have the energies of the corresponding electronic states of the diatomic Rydberg molecule with the ground state atom located at $R_1 = 1200\ a_0$; whereas the other

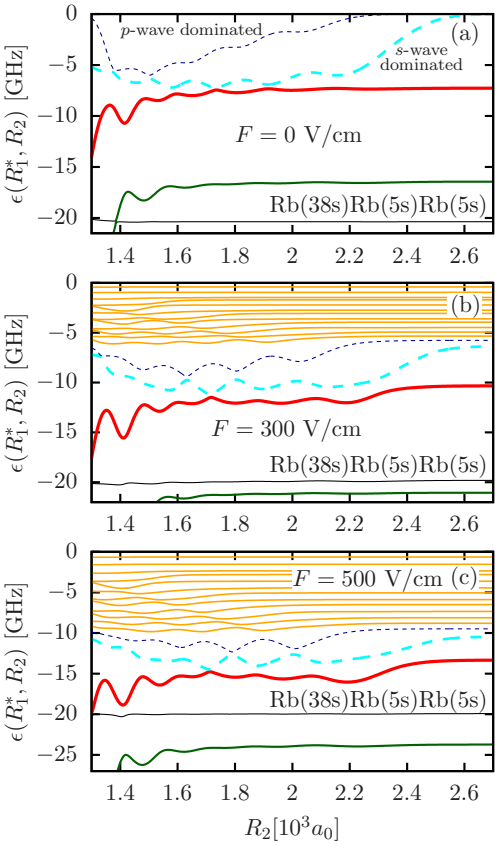

Figure 3.6: Asymmetric linear ULRM with the two ground state atoms located at the same side of the Rydberg core, i. e., $\theta_1 = \theta_2 = \pi$ and one fixed at $R_1^* = 1200\ a_0$. APCs with Σ molecular symmetry evolving from the degenerate manifold Rb($n = 35$, $l \geq 3$) versus the separation R_2 between the second atom and Rb^+, for an electric field of strength (a) $F = 0$ V/m, (b) $F = 300$ V/m, and (c) $F = 500$ V/m. The APCs have been derived including both the s-wave and p-wave interaction. The zero energy has been set to the field-free energy of the Rb($n = 35$, $l \geq 3$) degenerate manifold.

two APCs approach zero energy.

Due to the second atom, an extra Π molecular state is shifted from the Rb($n = 35$ and $l \geq 3$) Rydberg manifold, see Fig. 3.7 (a), which shows a deep well with a minimum at $R \approx 1345\ a_0$. This APC is deep enough to accommodate several vibrational bound states, where the triatomic molecule would exist. The lowest-lying molecular state of this symmetry has a shallow potential well of approximately 150 MHz deep at $R_2 \approx 1410\ a_0$. For $R \gtrsim 1500\ a_0$, the lowest lying Π-APC shows a constant behaviour with the energy of the corresponding APC of the diatomic ULRM.

In the presence of an external electric field, the energy of the APCs with Σ and Π molecular symmetries decreases as F is increased, see Fig. 3.6 and Fig. 3.7. We start analyzing the results for the electronic states with Σ molecular symmetry. The APC of the Rb($38s$)Rb($5s$)Rb($5s$) trimer is weakly affected by the electric field due to the quadratic Stark effect of the Rb($38s$) Rydberg state. The lowest-lying APC evolving from the Rb($n = 35, l \geq 3$) manifold has an energy smaller than the Rb($38s$)Rb($5s$)Rb($5s$) electronic

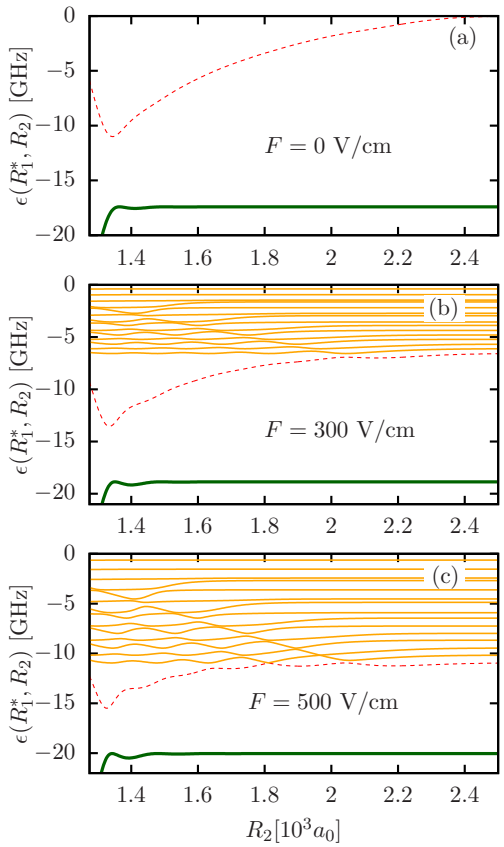

Figure 3.7: Asymmetric linear ULRM, with the two ground state atoms located at the same side of the Rydberg core, i. e., $\theta_1 = \theta_2 = \pi$ and one fixed at $R_1^* = 1200\ a_0$. APCs with Π molecular symmetry evolving from the degenerate manifold Rb($n = 35$, $l \geq 3$) as a function of distance R_2 between the Rydberg core and the second atom for an electric field of strengths (a) $F = 0$ V/m, (b) $F = 300$ V/m, and (c) $F = 500$ V/m. The APCs have been derived including both the s-wave and p-wave interaction. The zero energy has been set to the field-free energy of the Rb($n = 35$, $l \geq 3$) degenerate manifold.

state for $F = 300$ V/cm and 500 V/cm. The second-lowest-lying APC evolving from the Rb($n = 35, l \geq 3$) manifold also decreases in energy and its outermost well becomes more pronounced and shows an increasing depth as F is increased. For the two extra adiabatic electronic states with Σ symmetry, which appear due to the second atom, the electric field provokes that their broad wells become less deep whereas the superimposed oscillatory behaviour remains, see Figures 3.6 (b) and (c). The Stark effect breaks the degeneracy of the field-free degenerate adiabatic electronic states and extra APCs are shifted from the field-free degenerate manifold Rb($n = 35, l \geq 3$). These extra molecular levels show an oscillatory behavior for $R_2 \lesssim 2000\ a_0$, which provokes many avoided crossings among them, and for larger values of R_2, they possess a constant energy approximately. Similar results are observed for the adiabatic energies with Π molecular symmetry, see Fig. 3.7. The lowest-lying molecular state evolving from the Rb($n = 35, l \geq 3$) Rydberg manifold suffers a quadratic Stark effect and, therefore, is weakly affected by the weak electric field. The second lowest-lying potential decreases in energy as F increases and the depth of the pronounced wells is significantly

reduced, but remains a few GHz deep and can accommodate vibrational bound states. An increasing number of avoided crossings for large values of R_2 with increasing field strength is encountered.

3.4 The planar triatomic Rydberg molecule

In this section, we consider a planar ULRM with the neutral atoms located in the LFF XZ-plane, i. e., $\phi_1 = \phi_2 = 0$, and $\theta_2 = \pi - \theta_1$ with $0 \leq \theta_1 < \pi/2$, see Fig. 3.1 (c). For the sake of simplicity, we restrict this study to the configuration with the ground state atoms located at the same distance from the Rydberg core, i. e., $R_1 = R_2 = R$. Note that we impose the conditions $0 \leq \theta_1 < \pi/2$ and $\pi/2 < \theta_2 \leq \pi$ to avoid the spatial overlap of the vibrational states of the two ground state atoms, such that the interaction between them can be neglected. The energetically lowest-lying APS evolving from the Rb($n = 35, l \geq 3$) Rydberg manifold are shown as a function of R and θ_1 in Fig. 3.8.

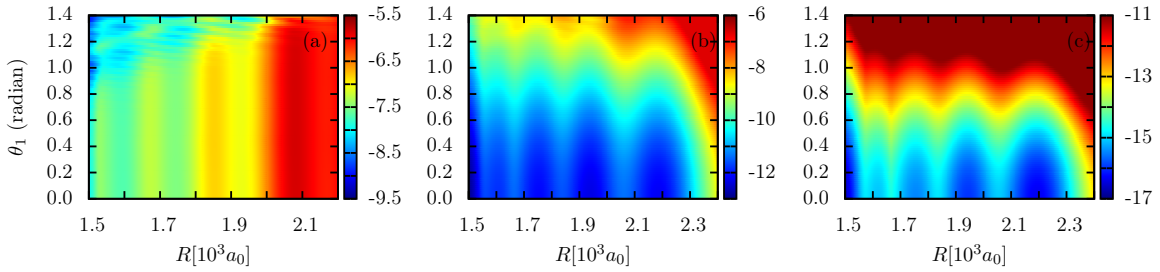

Figure 3.8: For the planar ULRM: The lowest lying APS evolving from the Rb($n = 35, l \geq 3$) Rydberg manifold in an external electric field parallel to the LFF Z axis and field strength (a) $F = 0$ V/m, (b) $F = 300$ V/m, and (c) $F = 500$ V/m. The APSs have been derived including both the s-wave and p-wave interaction. The zero energy has been set to the field-free energy of the Rb($n = 35$, $l \geq 3$) degenerate manifold.

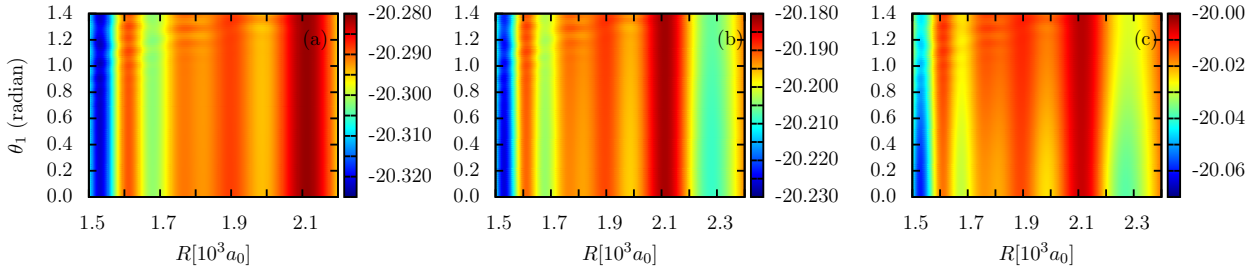

Figure 3.9: For the planar ULRM: The lowest lying APS evolving from the Rb($n = 38$, $l = 0$) Rydberg manifold in an external electric field parallel to the LFF Z axis and field strength (a) $F = 0$ V/m, (b) $F = 300$ V/m, and (c) $F = 500$ V/m. The APSs have been derived including both the s-wave and p-wave interaction.

The field-free APS shows a weak dependence on the polar angle θ_1 for different values of R, cf. Fig. 3.8 (a). For $R \gtrsim 2000\ a_0$, these field-free APSs are almost independent of the

angle θ_1, whereas for smaller internuclear separations, we encounter a smooth dependence on θ_1 for $\theta_1 \gtrsim 0.8$. This is due to the spatial proximity of the two ground state atoms. By adding an electric field, the APS strongly depends on the polar angle θ_1. The electric field parallel to the Z axis favours the linear configuration of the ULRM with both ground state atoms located along the Z axis, see Figures 3.8 (b) and (c). For this APS, the deepest well is shifted towards larger values of R as F is increased, and it is located at $R \approx 2200\ a_0$, $\theta_1 = 0$ and $\theta_2 = \pi$ for $F = 500$ V/m. This molecular curve approaches to a constant energy, given by the corresponding Rydberg state of the field-dressed Rb for large internuclear separations and large values of θ_1. For $F = 500$ V/m, this effect is observed for $\theta_1 \gtrsim 1.1$, and its limit is the energy the lowest-lying field-dressed state of the Rydberg manifold ($n = 35, l \geq 3$) of an isolated Rb atom in an electric field.

In Fig. 3.9, we present the APS evolving from the Rydberg state Rb($n = 38$, $l = 0$). The field free APS shows an oscillatory behaviour as R is increased, and a weak dependence on the angle θ_1, which increases as the two ground state atoms are closer, i. e., as θ_1 approach $\pi/2$. Compared to the APS presented in 3.8 (b), the depths of potential wells are significantly smaller, and are on the range of a few tens MHz. The main properties of the APS do not change on the presence of the external electric field. As indicated above, the impact of the electric field on the APS of Rb($5s$)Rb($38s$)Rb($5s$) is very weak, which can be explained in terms of the quadratic Stark shift of the $38s$ Rydberg state. The asymptotic limit of the APS for $R \gtrsim 2400\ a_0$ is shifted to larger energies as the electric field strength is increased. We also observe that the depths increase a few MHz as the field strength is increased up $F = 500$ V/m.

Chapter 4

Ultralong-range Rydberg Rydberg Molecules

4.1 Introduction

Recently, our research group has investigated electronic properties of the polyatomic Rydberg molecule composed of a Rb Rydberg atom and the KRb diatomic molecule [77]. Compared to previous studies [74, 75] in which the diatomic molecule was described as a two level model, our theoretical description includes an explicit treatment of the angular degrees of freedom of the diatomic molecule within the rigid-rotor approximation. Here, we consider the triatomic Rydberg molecule presented in Fig. 4.1, and extend our previous study by analyzing how the adiabatic electronic structure changes as the Rydberg excitation is increased and by analyzing electronic states evolving from Rydberg states with low angular momentum. We investigate the molecule and obtain Born-Oppenheimer potential (BOP) curves of the $\mathrm{Rb}(n, l \geq 3)$-KRb Rydberg molecule with varying principal quantum number n of the Rydberg electron and varying internuclear distance between the ionic core Rb^+ and the diatomic KRb. The lowest-lying BOPs evolving from $\mathrm{Rb}(n, l \geq 3)$ and $\mathrm{KRb}(N = 0)$ present potential wells with depths of a few GHz, and we have investigated their vibrational bound states. We also explore the adiabatic potentials of the Rydberg molecule formed by the KRb being in a rotational excited state, and the Rydberg states $\mathrm{Rb}(26d)$, $\mathrm{Rb}(27p)$ and $\mathrm{Rb}(28s)$. These BOPs evolving from these quantum-defect Rydberg states present wells with depths of a few MHz that support several vibrational bound states. This opens the possibility of creating these macroscopic Rydberg molecules by two-photon excitation of ground-state Rb in an ultracold mixture of Rb and KRb. The orientation and alignment of the diatomic molecule within the Rydberg molecule are also analyzed in terms of the contributions to the electric field due to the Rydberg electron and ionic core. For completeness, we provide in Appendix B a description of the impact of an external static electric field on the rotational dynamics of KRb. In particular, we present the field-dressed eigenstates, their hybridization of the angular motion, and their orientation as the electric field strength increases.

This chapter is organized as follows. In Sec. 4.2 we describe the adiabatic Hamiltonian of the triatomic Rydberg molecule. The electronic structure of a Rb-KRb Rydberg molecule is analyzed in detail in Sec. 4.3: We analyze the Born-Oppenheimer potentials evolving from the degenerate Rydberg manifolds $\mathrm{Rb}(n, l \geq 3)$ and and the Rydberg states $\mathrm{Rb}(26d)$, $\mathrm{Rb}(27p)$ and $\mathrm{Rb}(28s)$, and the directional properties of the KRb diatomic molecule within the Rb-KRb Rydberg trimer.

Part of the contents of this chapter is adapted from the reference: J. Aguilera-Fernández, H.R. Sadeghpour, P. Schmelcher, and R. González-Férez, *Ultralong-Range Rb-KRb Rydberg Molecules: Selected Aspects of Electronic Structure, Orientation and Alignment*, J. of Phys. Conf. Ser. **635**, 012023 (2015).

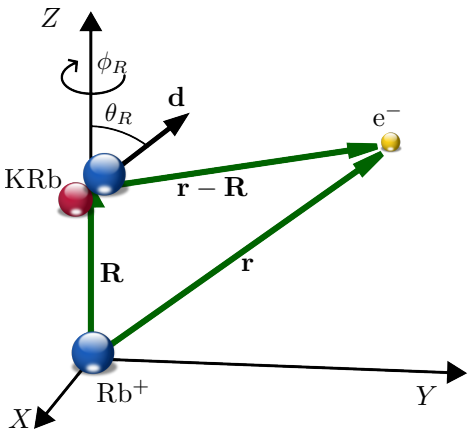

Figure 4.1: A sketch (not to scale) of the triatomic molecule formed by the Rydberg atom and diatomic polar molecule Rb-KRb. The center of the LFF is fixed at the ionic core Rb^+, and the diatomic polar molecule is located on the Z-axis. The permanent electric dipole moment of the KRb $\mathbf{d}$ is parallel to its internuclear axis. The Euler angles (θ_R, ϕ_R) relate the molecular fixed frame with the laboratory fixed, and describe the rotational motion of the diatomic molecule.

4.2 The adiabatic Hamiltonian of the triatomic Rydberg molecule

We consider a triatomic Rydberg molecule formed by a Rydberg atom and a diatomic heteronuclear molecule, with its center of mass located on the Z axis in the laboratory fixed frame (LFF) at a distance R from the ionic core, the latter being placed at the origin of the LFF. The Born-Oppenheimer Hamiltonian reads

$$H_{ad} = H_A + H_{mol}, \tag{4.1}$$

where H_A is the single electron Hamiltonian describing the Rydberg atom

$$H_A = -\frac{\hbar^2}{2m_e}\nabla_r^2 + V_l(r), \tag{4.2}$$

with $V_l(r)$ being the l-dependent model potential [97], and l the angular quantum number of the Rydberg electron.

Within the rigid-rotor approximation, the term H_{mol} is the Hamiltonian of the rotational motion of the diatomic molecule in the electric field due to the Rydberg electron and ionic core

$$H_{mol} = B\mathbf{N}^2 - \mathbf{d}\cdot\mathbf{F}_{ryd}(\mathbf{R},\mathbf{r}), \tag{4.3}$$

with $\mathbf{N}$ being the molecular angular momentum operator, B the rotational constant, and $\mathbf{d}$

the permanent electric dipole moment, which has spatial components

$$d_x = \sin\theta\cos\phi, \tag{4.4}$$
$$d_y = \sin\theta\sin\phi, \tag{4.5}$$
$$d_z = \cos\theta, \tag{4.6}$$

with $\Omega = (\theta, \phi)$ being the Euler angles describing the rotational motion of the diatomic molecule in the laboratory fixed frame. To facilitate the numerical resolution of the Schrödinger equation, we express the components of the electric dipole moment in terms of the spherical harmonics as

$$d_x = \sqrt{\frac{2\pi}{3}}\left[Y_{1-1}(\theta,\phi) - Y_{11}(\theta,\phi)\right], \tag{4.7}$$
$$d_y = \sqrt{\frac{2\pi}{3}}\left[Y_{1-1}(\theta,\phi) + Y_{11}(\theta,\phi)\right], \tag{4.8}$$
$$d_z = \sqrt{\frac{4\pi}{3}}Y_{10}(\theta,\phi). \tag{4.9}$$

The interaction of the Rydberg electron and the core with the dipole moment of the molecule is long-range (R^{-2}) and in the case of the former, anisotropic. The electric fields are internal ones and due to the presence of charged particles. The electric field created by the ionic core and Rydberg electron at position $\mathbf{R}$ reads [74, 75]

$$F_{ryd}(\mathbf{R},\mathbf{r}) = e\frac{\mathbf{R}}{R^3} + e\frac{\mathbf{r}-\mathbf{R}}{|\mathbf{r}-\mathbf{R}|^3}, \tag{4.10}$$

due to the spatial configuration of the Rydberg molecule analyzed in this thesis, we take $\mathbf{R} = R\hat{Z}$. We consider all three spatial components of this electric field taking into account that the position of the polar molecule is fixed along the LFF Z-axis. The detailed expression of the electric field of the Rydberg electron is given in Appendix A.

The orbital angular momentum of the Rydberg electron $\mathbf{l}$ and the rotational angular momentum of the diatomic molecule $\mathbf{N}$ are coupled to the total angular momentum of the Rydberg molecule (excluding an overall rotation) $\mathbf{J} = \mathbf{N} + \mathbf{l}$. For the considered configuration of the Rydberg molecule, the total angular momentum $\mathbf{J}$ is not conserved, but its projection onto the LFF Z-axis M_J is a good quantum number.

The Schrödinger equation associated with the Hamiltonian (4.1) is

$$\left[H_A + H_{mol}\right]\Psi(\mathbf{r},\Omega;R) = E(R)\Psi(\mathbf{r},\Omega;R), \tag{4.11}$$

where $\Psi(\mathbf{r},\Omega;R)$ is the wave function, and $E(R)$ is the Born-Oppenheimer potentials of the adiabatic electronic state. By using the expressions (4.2) and (4.3) for the Rydberg electron and diatomic molecule Hamiltonian, this equation reads

$$\left[-\frac{\hbar^2}{2m_e}\nabla_r^2 + V_l(r) + B\mathbf{N}^2 - \mathbf{d}\cdot\mathbf{F}_{ryd}(R,\mathbf{r})\right]\Psi(\mathbf{r},\Omega;R) = E(R)\Psi(\mathbf{r},\Omega;R). \tag{4.12}$$

Table 4.1: For the rubidium atom, energies and energies differences $\Delta E_{n,l} = E_{n,l} - E_{25,3}$ of the Rydberg levels close to the degenerate Rydberg manifold $n = 25$ and $l \geq 3$.

n	l	$E_{n,l}$(THz)	$\Delta E_{n,l}$(GHz)
26	3	−4.8666	397.11
29	0	−4.9164	347.29
27	2	−4.9989	264.81
28	1	−5.1188	144.85
25	3	−5.2637	0
28	0	−5.3198	−56.06
26	2	−5.4126	−148.91
27	1	−5.5479	−284.21
24	3	−5.7115	−447.78
27	0	−5.7749	−511.18
25	2	−5.8799	−616.20
26	1	−6.0333	−769.58

Note that in the Rydberg electron and core electric field $\mathbf{F}_{ryd}(R, \mathbf{r})$ (4.10), we have used that the spatial position of the diatomic molecule is fixed in the Z-axis of the laboratory fixed frame, i. e., $\mathbf{R} = R\hat{Z}$.

To solve this Schrödinger equation, we make a basis set expansion of the wave function $\Psi(\mathbf{r}, \Omega; R)$ in terms of the coupled basis

$$\psi_{nlNJM_J}(\mathbf{r}, \Omega_d) = \sum_{m_l=-l}^{m_l=l} \sum_{M_N=-N}^{M_N=N} \langle lm_l NM_N | JM_J \rangle \, \psi_{nlm}(\mathbf{r}) \, Y_{NM_N}(\Omega_d), \tag{4.13}$$

where $\psi_{nlm}(\mathbf{r})$ is the Rydberg electron wave function, $Y_{NM_N}(\Omega)$ the spherical harmonics representing the field-free rotational wave function of the diatomic molecule with the rotational and magnetic quantum numbers N and M_N, respectively, Ω_d the internal coordinates of the diatomic molecule, and $\langle lm_l NM_N | JM_J \rangle$ the Clebsch-Gordan coefficient. Taking into account the azimuthal symmetry of the Rydberg molecule, the basis set expansion of the wave function reads

$$\Psi(\mathbf{r}, \Omega; R) = \sum_{n,l,N,J} C_{nlNJ}(R) \psi_{nlNJM_J}(\mathbf{r}, \Omega), \tag{4.14}$$

where we have explicitly indicated the dependence of the wave function and expansion coefficients $C_{nlNJ}(R)$ on the internuclear distance R between the diatomic molecule and the ionic core. For computational reasons, of course, we have to cut the infinite series (4.14) to a finite one. In this work, we have included the rotational excitations with $N \leq 6$ for KRb, and

for Rb, the $(n, l \geq 3)$ degenerate manifold, and the energetically neighboring levels $(n+1)d$, $(n+2)p$, and $(n+3)s$. The quantum defect of the Rb(nf) Rydberg state has been neglected. In Table 4.1, we show the energies and energy differences of the quantum defect states and the Rydberg manifolds close to Rb$(n = 25, l \geq 3)$. These large energy difference justify our approximation in reducing the number of Rydberg states used to solve the Schrödinger equation.

Applying the linear principle the Schrödinger equation, which is a partial differential equation, is transformed in a eigenvalue problem We provide now all the matrix elements of the terms appearing Hamiltonian matrix. The matrix element of H_A the single electron Hamiltonian describing the Rydberg atom is given by

$$\langle \psi_{n_1 l_1 N_1 J_1 M_J} | H_A | \psi_{n_2 l_2 N_2 J_2 M_J} \rangle = E_{n_1,l_1} \delta n_1, n_2 \delta l_1, l_2 \delta N_1, N_2 \delta J_1, J_2, \tag{4.15}$$

where E_{n_1,l_1} is the energy of the Rydberg electron

$$E_{n,l} = \begin{cases} \frac{-1}{2(n-\delta_{n,l})^2} & l \leq 3, \\ \frac{-1}{2n^2} & l \geq 4, \end{cases} \tag{4.16}$$

being n the principal quantum number and $\delta_{n,l}$ the quantum defects, see Sec. 3.2 in the previous chapter. For the rotational kinetic energy of the diatomic polar molecule, the matrix element is

$$\langle \psi_{n_1 l_1 N_1 J_1 M_J} | B\mathbf{N}^2 | \psi_{n_2 l_2 N_2 J_2 M_J} \rangle = B N_1(N_1+1) \delta_{n_1,n_2} \delta_{l_1,l_2} \delta_{N_1,N_2} \delta_{J_1,J_2}. \tag{4.17}$$

The matrix element of the interaction between the permanent electric dipole moment of the diatomic molecule and the electric field due to the Rydberg core and electron reads

$$\begin{aligned} &\langle \psi_{n_1 l_1 N_1 J_1 M_J} | -\mathbf{d} \cdot \mathbf{F}_{ryd}(R, \mathbf{r}) | \psi_{n_2 l_2 N_2 J_2 M_J} \rangle = - \sum_{m_{l_1}=-l_1}^{m_{l_1}=l_1} \sum_{M_{N_1}=-N_1}^{M_{N_1}=N_1} \sum_{m_{l_2}=-l_2}^{m_{l_2}=l_2} \sum_{M_{N_2}=-N_2}^{M_{N_2}=N_2} \\ &\langle l_1 m_{l_1} N_1 M_{N_1} | J_1 M_J \rangle \langle l_2 m_{l_2} N_2 M_{N_2} | J_2 M_J \rangle \\ [\quad &\langle N_1 M_{N_1} | d_x | N_2 M_{N_2} \rangle \langle n_1 l_1 m_{l_1} | F^x_{ryd}(R, \mathbf{r}) | n_2 l_2 m_{l_2} \rangle \\ +\quad &\langle N_1 M_{N_1} | d_y | N_2 M_{N_2} \rangle \langle n_1 l_1 m_{l_1} | F^y_{ryd}(R, \mathbf{r}) | n_2 l_2 m_{l_2} \rangle \\ +\quad &\langle N_1 M_{N_1} | d_z | N_2 M_{N_2} \rangle \langle n_1 l_1 m_{l_1} | F^z_{ryd}(R, \mathbf{r}) | n_2 l_2 m_{l_2} \rangle \\ +\quad &\langle N_1 M_{N_1} | d_z | N_2 M_{N_2} \rangle \langle n_1 l_1 m_{l_1} | \frac{1}{R^2} | n_2 l_2 m_{l_2} \rangle \,]\,. \end{aligned} \tag{4.18}$$

The expressions of these matrix elements are provided in Appendix A and Appendix D.

4.2.1 The rovibrational Hamiltonian of the triatomic Rydberg molecule

The existence of these triatomic Rydberg molecules depends on the potential wells of the adiabatic electronic states, and, in particular, if they are deep enough to accommodate bound levels. This is determined by the binding energies of the rovibrational levels, which are characteristic of each electronic state. In the framework of the Born-Oppenheimer

approximation, the rovibrational Hamiltonian reads

$$H = T_R + \frac{\hbar^2 \mathcal{J}^2(\vartheta, \varphi)}{2\mu R^2} + E(R), \tag{4.19}$$

where R is the internuclear distance between the Rydberg core and the diatomic molecule. (ϑ, φ) are the Euler angles, which determine the rotation of the whole Rydberg molecule in the laboratory fixed frame. Note that we are using the molecule fixed frame with the coordinate origin at the Rydberg core Rb^+. $\hbar\mathcal{J}(\vartheta, \varphi)$ is the orbital angular momentum of the Rydberg triatomic molecule. The vibrational kinetic energy T_R is given by

$$T_R = -\frac{\hbar^2}{2\mu R^2} \frac{\partial}{\partial R} \left(R^2 \frac{\partial}{\partial R} \right), \tag{4.20}$$

where the reduced mass of the Rydberg molecule μ is approximated by $\mu = m_{Rb} m_{KRb}/(m_{Rb} + m_{KRb})$, with $m_{KRb} = m_{Rb} + m_K$, m_{Rb} and m_K being the mas of the rubidium and potassium atoms, respectively. The adiabatic electronic potential energy curve $E(R)$ is the solution of the Schrödinger equation associated to Hamiltonian (4.1) of the Rydberg molecule.

In the absence of external electric or laser fields, the vibrational and rotational degrees of freedom of the Rydberg molecule are not coupled in the rovibrational Hamiltonian (4.19). The total rovibrational wave function can be written as product of a rotational and a vibrational part, which can be numerically computed independently. In this thesis, we are interested in the existence of vibrational bound levels, and not on the rotational excitations associated to each vibrational band. Thus, we fix the rotation of the whole Rydberg molecule to zero, i. e., the quantum number $\mathcal{J} = 0$, and solve the radial part of the rovibrational Schrödinger equation, which is given by

$$\left[-\frac{\hbar^2}{2\mu R^2} \frac{\partial}{\partial R} \left(R^2 \frac{\partial}{\partial R} \right) + E(R) \right] \chi(R) = \varepsilon \chi(R), \tag{4.21}$$

where $\chi(R)$ and ε are the vibrational eigenfunctions and eigenvalues, respectively. To solve this vibrational Schrödinger equation we use the discrete variable representation, which represent the vibrational wave function by its value in a certain radial grid. In this case, the radial grid is equidistant due to the large spatial extensions of the vibrational wave functions. In Appendix C, we provide a short description of this numerical method.

4.3 The electronic structure of the Rb-KRb Rydberg molecule

Now we explore the electronic structure of the Rydberg molecule formed by a Rb atom and the heteronuclear molecule KRb with rotational constant $B = 1.114$ GHz [90], and electric dipole moment $d = 0.566$ D [89]. The interaction between the electric field created by the ionic core and Rydberg electron and the permanent electric dipole moment of KRb is responsible for the binding mechanism of Rb-KRb. The electric field (4.10) decreases as the distance between Rb^+ and KRb is increased, and, therefore, the coupling between the subsystems Rb and KRb also decreases. For large enough values of R, the adiabatic electronic potentials approach the energies of the uncoupled system $E_{nl} + BN(N+1)$,with E_{nl} being the energy

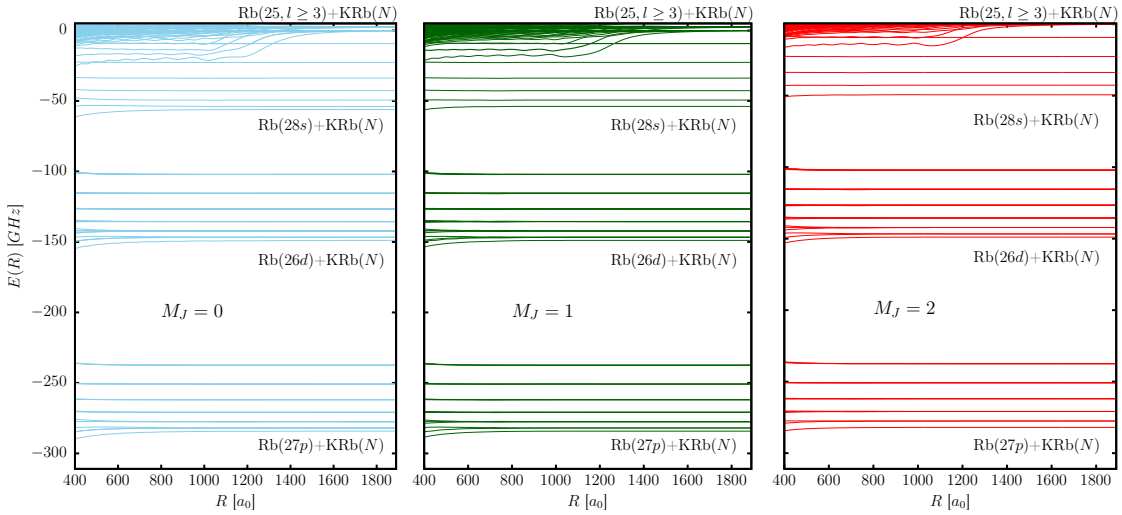

Figure 4.2: For the Rb-KRb Rydberg molecule, the Born-Oppenheimer potentials as a function of the distance between KRb and Rb^+ for (a) $M_J = 0$ and (b) $M_J = 1$ are shown, specifically the BOP evolving from Rb(28s) and KRb in a rotational excited state, and from the Rb($n = 25, l \geq 3$) manifold and the rotational ground state of KRb. The energetically lowest-lying adiabatic potentials evolving from the Rb($n = 25, l \geq 3$) manifold are shown with thicker lines. The zero energy has been set to the energy of the Rb($n = 25, l \geq 3$) degenerate manifold and the KRb($N = 0$) state.

of Rb(n, l), and $BN(N + 1)$ the rotational energy of KRb in an eigenstate with rotational quantum number N.

The BOPs of the Rb-KRb molecule evolving from the Rydberg degenerate manifold Rb($n = 25, l \geq 3$) and with magnetic quantum numbers $M_J = 0$, $M_J = 1$ and $M_J = 2$ are presented in Fig. 4.2 (a), Fig. 4.2 (b), and Fig. 4.2 (c) respectively. Where the zero energy has been set to the energy of the Rb($n = 25, l \geq 3$) manifold and the KRb diatomic molecule being in their rotational ground state $N = 0$. Additionally, in this figure we observe the adiabatic states evolving from Rb(28s), Rb(26d) and Rb(27p) and KRb in a rotational excited states. It is important remark that these BOPs also show an oscillatory behaviour, having potential wells of many several MHz, which are not appreciated on the Fig. 4.2, due to scale of this figures, but we will discuss their main properties later.

4.3.1 The Born-Oppenheimer potentials evolving from the Rydberg degenerate manifold Rb($n, l \geq 3$)

As mentioned above, in this section we focus our attention in the BOPs from evolving from the Rydberg degenerate manifold Rb($n = 25, l \geq 3$) and with magnetic quantum numbers $M_J = 0$, $M_J = 1$ and $M_J = 2$ to Rb(28s) are presented in Fig. 4.2 (a), Fig. 4.2 (b), and Fig. 4.2 (c) respectively. For the considered configuration of the Rydberg molecule, the Born-Oppenheimer potentials only depend on the distance between Rb^+ and KRb, by rotating the position of KRb in the ZX-plane these adiabatic curves become surfaces with a dependence on the rotation angle. In this region of the spectrum, we encounter adiabatic states evolving from Rb(28s) and KRb in a rotationally excited state, which show a very

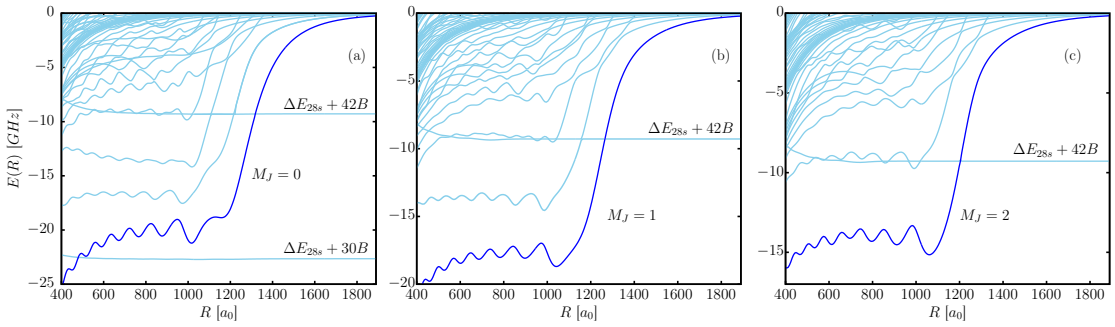

Figure 4.3: For the Rb-KRb Rydberg molecule, the Born-Oppenheimer potentials as a function of the distance between KRb and Rb^+ for (a) $M_J = 0$ and (b) $M_J = 1$ are shown, specifically the BOP evolving from Rb($28s$) and KRb in a rotational excited state, and from the Rb($n = 25, l \geq 3$) manifold and the rotational ground state of KRb. The energetically lowest-lying adiabatic potentials evolving from the Rb($n = 25, l \geq 3$) manifold are shown with thicker lines. The zero energy has been set to the energy of the Rb($n = 25, l \geq 3$) degenerate manifold and the KRb($N = 0$) state.

weak dependence on the internuclear distance. This behavior is due to the small impact of the Rydberg electric field on the $N = 6$ excited state of KRb, which possesses a large field-free rotational energy. The electronic states evolving from the Rb($n = 25, l \geq 3$) manifold are shifted in energy from the uncoupled-system energy $E_{nl} + BN(N + 1)$. These energy shifts strongly depend on the internuclear separation of Rb-KRb due to the interplay between the electric fields created by the Rydberg electron and the ionic core. They are of the range from a few to tens of GHz. The BOPs oscillate as a function of R, and numerous avoided crossings among neighboring electronic states characterize the spectrum. For $R \sim 1000\, a_0$, the energetically lowest-lying BOPs present potential wells of a few GHz depths, which support several vibrational states [77]. By further increasing R, the coupling between the Rydberg atom and KRb decreases, and the BOPs approach the asymptotic limit of the uncoupled system. As indicated above, in these figures the zero energy has been set at $E_{n=25,l\geq 3}$, i. e., for the uncoupled system KRb($N = 0$) and Rb($n = 25, l \geq 3$).

We focus now on the evolution of the electronic structure as the principal quantum number of the Rydberg degenerate manifold Rb($n, l \geq 3$) is increased. In Fig. 4.4, we present the energetically lowest-lying adiabatic electronic states with $M_J = 0$ and $M_J = 1$ evolving from the Rb($n, l \geq 3$) manifolds for $n = 21, 23, 25, 26, 27, 29, 31$, and 33. These BOPs show a qualitatively similar oscillatory behavior as a function of R. By increasing the principal quantum number of the Rydberg manifold, some differences are observed.

First, the energy shift of these BOPs from the degenerate manifold of the Rydberg atom decreases as n is increased. Second, the location of the potential wells is shifted towards larger values of the internuclear separation between Rb^+ and KRb. This is due to the radial extension of the electronic Rydberg wave function of Rb($n, l \geq 3$) which increases as n is enhanced. Third, the depth of the wells decreases with increasing n. The outermost potential well of the $M_J = 0$ BOPs is very shallow and do not support vibrational bound states. In contrast, the potential well with $M_J = 0$ located at the left of this outermost one is the deepest one supporting several bound states and with depths of several GHz for

all the Rb$(n, l \geq 3)$-KRb$(N = 0)$ molecules investigated here. The vibrational states and the square of their wave functions are presented in Fig. 4.5. For instance, we have found 7 and 6 vibrational bound states in these potential wells of these energetically lowest-lying Rb$(n = 25, l \geq 3)$ and Rb$(n = 31, l \geq 3)$ BOPs with $M_J = 0$, respectively.

4.3.2 The Born-Oppenheimer potentials evolving from the Rb($26d$) Rydberg state

In the absence of an external electric field, the Rydberg atoms are created via standard two-photon excitation process in an nd or an ns Rydberg state. Thus, in an ultracold mixture of Rb and KRb, the ultralong-range Rydberg molecule could be experimentally created involving one of these two Rydberg states. In this subsection, we investigate the adiabatic electronic states of the triatomic Rydberg molecule formed from Rb($26d$).

The BOPs for $M_J = 0$ evolving from the Rb($26d$) Rydberg states and the diatomic molecule in the rotational excitations up to $N \leq 5$ are presented in Fig. 4.6. Note that these adiabatic potentials have been computed using $N \leq 8$ to ensure the convergence of the results evolving from KRb in a field-free rotational states $N = 4$ and $N = 5$. The total angular momentum in the uncoupled system is $J = |2 - N|, \ldots N + 2$. Thus, there are 5 adiabatic electronic states for $M_J = 0$ and the diatomic molecule having field-free rotational quantum number $N = 2, 3, 4$ and 5, whereas there is one BOP for $N = 0$, and 3 BOPs for $N = 1$.

We encounter stable and unstable adiabatic electronic states showing a decreasing and increasing behaviour, respectively, as the separation between KRb and the ionic core Rb^+ decreases. At large separations, when the interaction due to the Rydberg electric field becomes negligible, these BOPs approach the energetical limit $\Delta E_{26d} + BN(N + 1)$, with $N = 0$, 1, 2, 3, 4 and 5, and $\Delta E_{26d} = E_{24,3} - E_{26d} = -148.91$ GHz. In each panel of Fig. 4.6, we indicate the asymptotic limit by Rb($26d$)-KRb(N). These BOPs show either a strong or a weak dependence on R. The BOPs with oscillatory behavior possess potential wells having depths of a few to a few tens of MHz. We have computed the vibrational spectra of these BOPs by solving the vibrational Schrödinger equation (4.21) of this Rydberg molecule. These

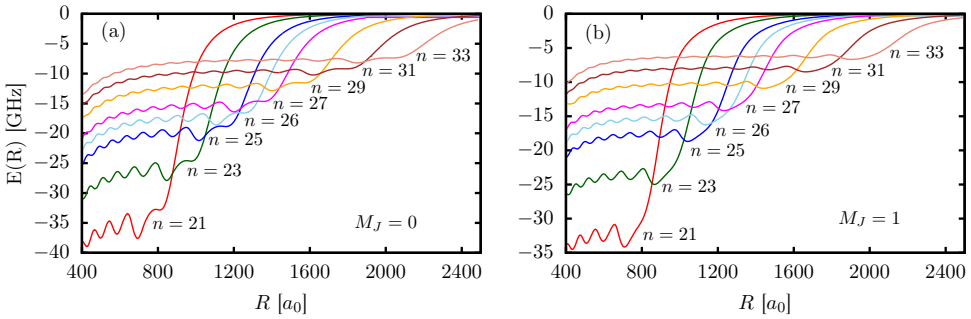

Figure 4.4: For the Rb-KRb molecule, the energetically lowest-lying BOPs with $M_J = 0$ and $M_J = 1$ evolving from the Rb$(n, l \geq 3)$ Rydberg manifold, for $n = 21, 23, 25, 26, 27, 29, 31$, and 33, and KRb in the rotational ground state $N = 0$ are shown. To facilitate the comparison, the zero energy has been set to the energy of the Rb$(n, l \geq 3)$ manifold and the KRb$(N = 0)$ level.

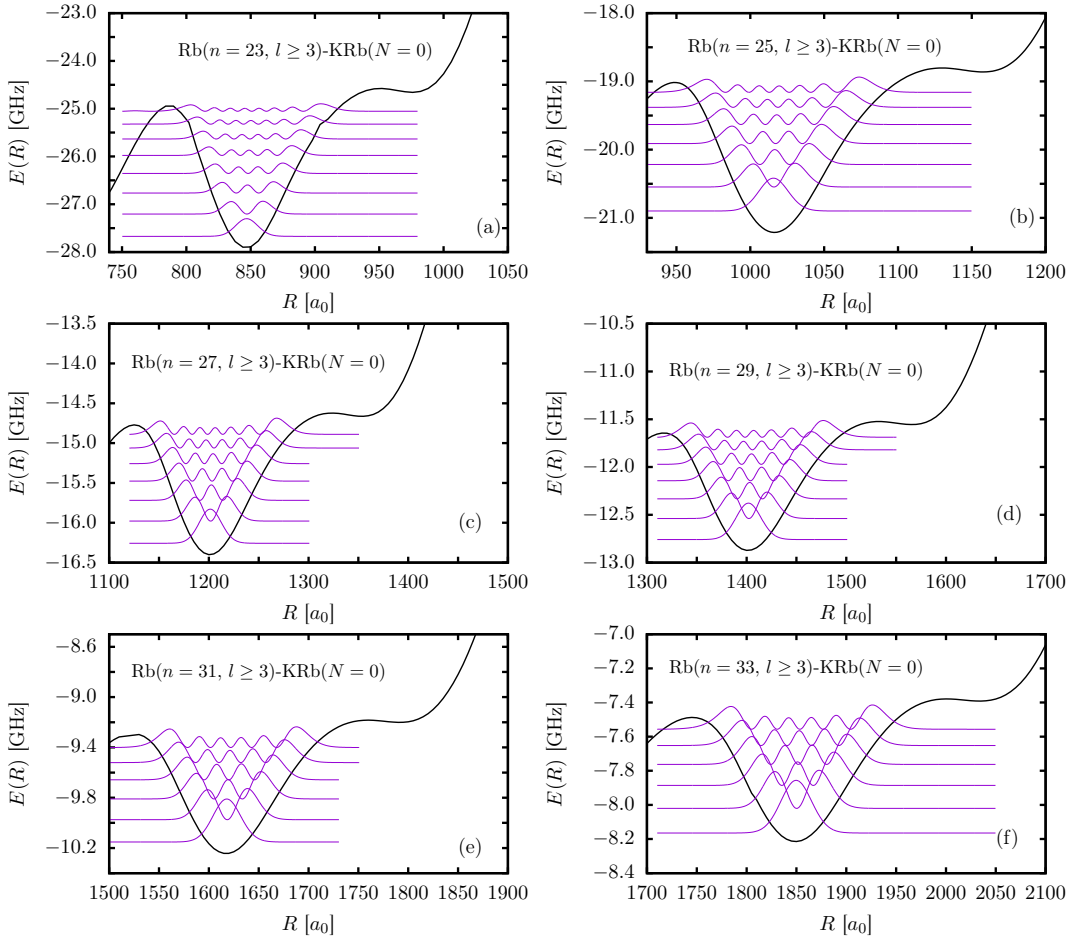

Figure 4.5: For the Rb-KRb molecule, the vibrational levels for the energetically lowest-lying BOPs with $M_J = 0$ evolving from the Rb$(n, l \geq 3)$ Rydberg manifold, for $n = 23, 25, 27, 29, 31$, and 33, and KRb in the rotational ground state $N = 0$ are shown.

potential wells are deep enough to accommodate at least one vibrational level in which the triatomic Rydberg molecule would exist. For a few vibrational levels, the square of the vibrational wave functions are shown in the potential wells in Fig. 4.6. The lowest-lying BOPs evolving from the rotational excitation $N = 2, \ldots, 5$ of KRb have several vibrational bound states with vibrational wave functions extending over several potential wells, and some of them with spatial extensions of a few hundreds Bohr radii.

4.3.3 The Born-Oppenheimer potentials evolving from the Rb($28s$) Rydberg state

As we have indicated in the previous section, the Rydberg atom in a ns states could be created by a two-photon exicitation process. We analyze here the adiabatic electronic states electronic states evolving from the Rydberg state Rb($28s$) and the diatomic polar molecule in

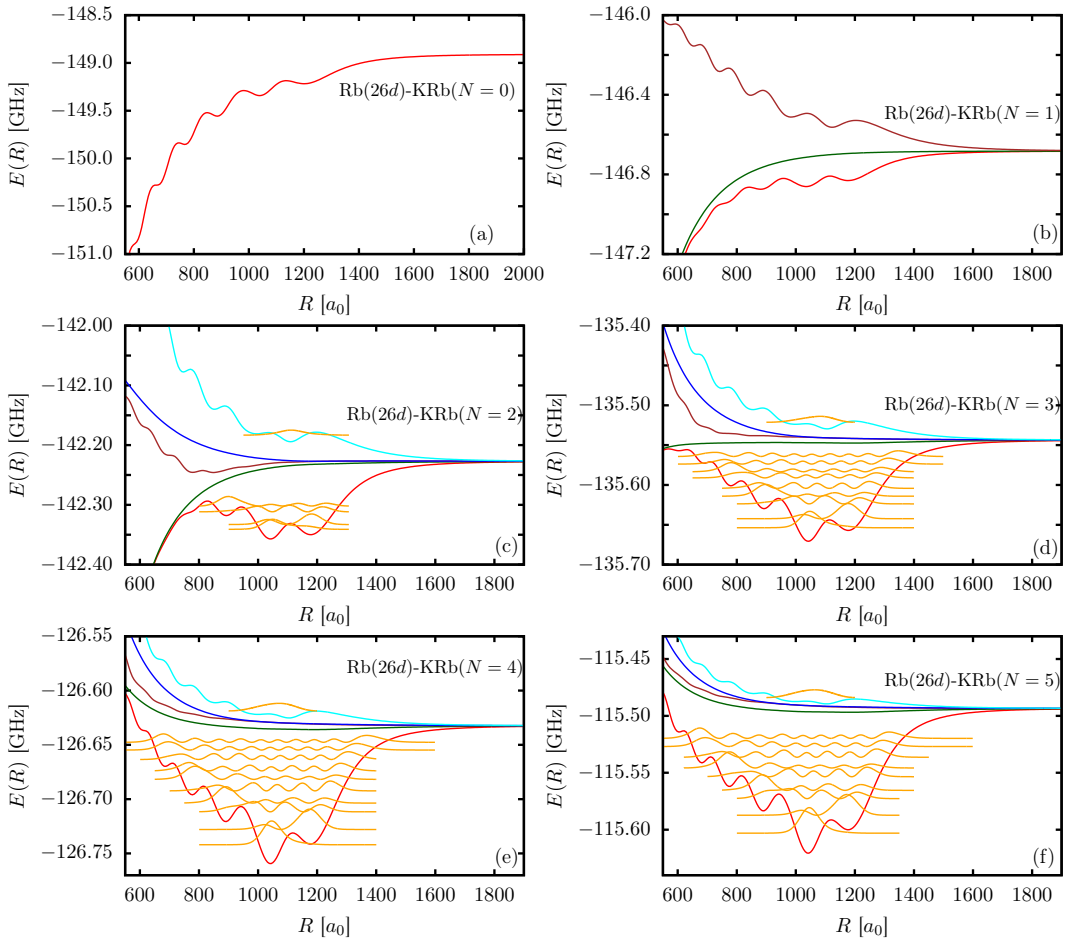

Figure 4.6: For the Rb-KRb Rydberg molecule, Born-Oppenheimer potentials with $M_J = 0$ evolving from the Rb(26d) state and KRb in the rotational levels (a) $N = 0$, (b) $N = 1$, (c) $N = 2$, (d) $N = 3$, (e) $N = 4$ and (f) $N = 5$. The asymptotic limit Rb(26d)-KRb(N) is indicated in each panel. In the potentials wells of some BOPs, the square of the vibrational wave functions are shown in arbitrary units. The zero energy has been set to the energy of the Rb($n = 25, l \geq 3$) degenerate manifold and the KRb in its ground state, i. e., Rb($n = 25, l \geq 3$)-KRb($N = 0$).

a rotational state with $N \leq 5$. The corresponding BOPs for $M_J = 0$ are presented in Fig. 4.7.

The total angular momentum of these BOP is $J = N$, because $l = 0$ for Rb(28s). For each rotational excitation of KRb, there is only one adiabatic electronic state, which approaches in the asymptotic limit the energy $\Delta E_{28s} + BN(N + 1)$, with $N = 0, \ldots, 5$, and $\Delta E_{28s} = E_{24,3} - E_{28s} = -56.06$ GHz. These BOPs show an oscillatory behaviour as R, although these oscillations are very smooth for the Rydberg molecule Rb(28s)-KRb(N=0) in Fig. 4.7 (a). The BOPs evolving from KRb in a rotational excited states possess potential wells having depths up to a few tens of MHz, which are are deep enough to accommodate several vibrational levels. We have also computed the vibrational wave function of this triatomic Rydberg molecule, and the square of the wave functions are shown in the potential wells in Fig. 4.7. As in the previous

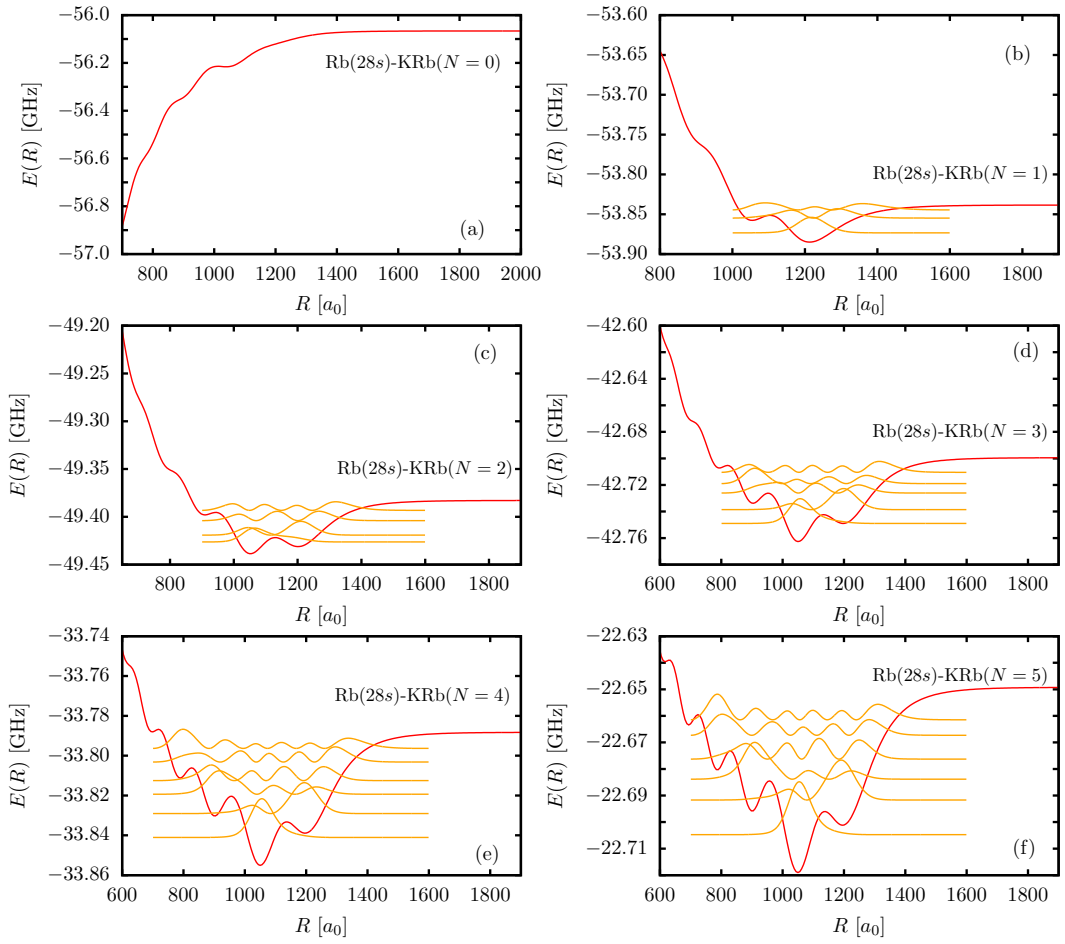

Figure 4.7: For the Rb-KRb Rydberg molecule, Born-Oppenheimer potentials with $M_J = 0$ evolving from the Rb($28s$) state and KRb in the rotational levels (a) $N = 0$, (b) $N = 1$, (c) $N = 2$, (d) $N = 3$, (e) $N = 4$ and (f) $N = 5$. The asymptotic limit Rb($28s$)-KRb(N) is indicated in each panel. In the potentials wells, the square of the vibrational wave functions are shown in arbitrary units. The zero energy has been set to the energy of the Rb($n = 25, l \geq 3$) degenerate manifold and the KRb in its ground state, i. e., Rb($n = 25, l \geq 3$)-KRb($N = 0$).

case, there are vibrational bound states with wave functions extending over several potential wells. Our conclusion is that the Rydberg molecule Rb($28s$)-KRb(N) could be experimentally created and observed only if KRb is in a rotational excited state with $N \geq 1$.

4.3.4 The Born-Oppenheimer potentials evolving from the Rb($27p$) Rydberg state

Recently, rubidium Rydberg atoms in p-wave states have been experimentally created by single-photon transition from the ground state Rb($5s_{1/2}$) [105–107]. Opening the doorway to experimentally observe triatomic Rydberg molecules evolving from the Rydberg state Rb(np). We present in Fig. 4.8 the adiabatic electronic states with $M_J = 0$ involving Rb($27p$) and KRb with the field-free rotational states $N = 0, \ldots 5$. As in the previous two sections, the

calculations have been done including rotational excitations of KRb up to $N \leq 8$ to ensure that the results are properly converged.

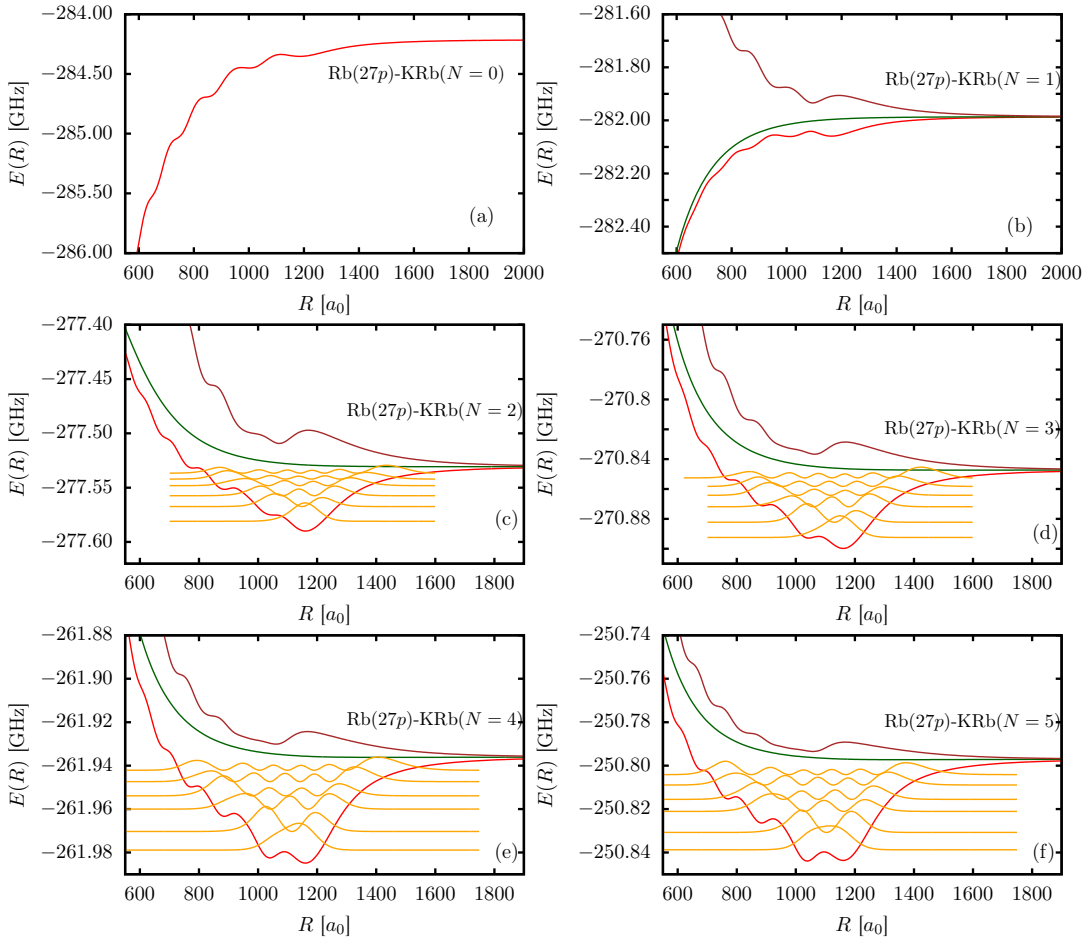

Figure 4.8: For the Rb-KRb Rydberg molecule, Born-Oppenheimer potentials with $M_J = 0$ evolving from the Rb($27p$) state and KRb in the rotational levels (a) $N = 0$, (b) $N = 1$, (c) $N = 2$, (d) $N = 3$, (e) $N = 4$ and (f) $N = 5$. The asymptotic limit Rb($27p$)-KRb(N) is indicated in each panel. In the potentials wells, the square of the vibrational wave functions are shown in arbitrary units. The zero energy has been set to the energy of the Rb($n = 25, l \geq 3$) degenerate manifold and the KRb in its ground state, i. e., Rb($n = 25, l \geq 3$)-KRb($N = 0$).

For these electronic states, the total angular momentum in the uncoupled system is $J = |1 - N|, \ldots N + 1$, and we encounter one BOP for $N = 0$, three for $N = 1, \ldots, 5$. In these case, the BOP approach the energy $\Delta E_{27p} + BN(N + 1)$, with $N = 0$, 1, 2, 3, 4 and 5, and $\Delta E_{27p} = E_{24,3} - E_{27p} = -284.21$ GHz, for $R \gtrsim 1700\ a_0$. As in the previous two Rydberg molecules, the BOPs with oscillatory behavior possess potential wells having depths of a few MHz or tens of MHz. These potential wells are deep enough to accommodate at least one vibrational level in which the polyatomic Rydberg molecule would exist. For a few vibrational levels, the square of the wave functions are shown in the potential wells in Fig. 4.8. For the BOPs evolving from $N = 2$ to $N = 5$ rotational states of KRb, we encounter several

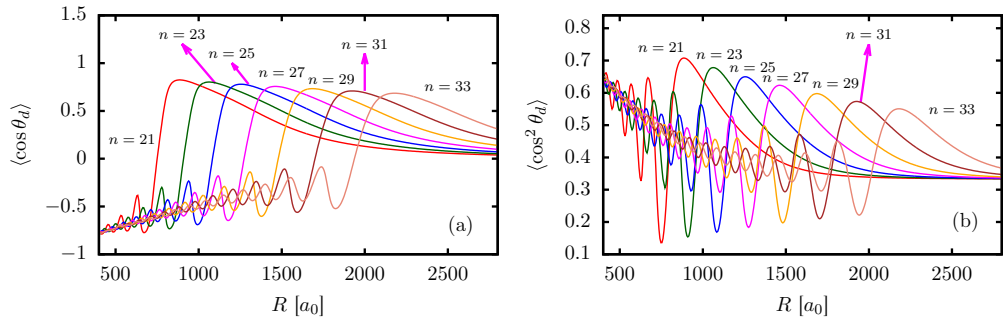

Figure 4.9: For the KRb molecule within the energetically lowest-lying BOPs with $M_J = 0$ of Rb$(n, l \geq 3)$-KRb with $n = 21, 23, 25, 27, 29, 31$, and 33, we show (a) the orientation $\langle\cos\theta_d\rangle$ and (b) the alignment $\langle\cos^2\theta_d\rangle$ along the LFF Z-axis versus the internuclear distance between Rb^+ and KRb.

vibrational bound states with wave functions extending over several potential wells.

4.3.5 Directional properties of the diatomic molecule within the triatomic Rydberg molecule

We analyze now the directional features of the KRb molecule within the Rb-KRb triatomic Rydberg molecule. For the lowest-lying electronic potentials evolving from the Rb$(n, l \geq 3)$ manifolds with $n = 21, 23, 25, 27, 29, 31$, and 33, for $M_J = 0$, the orientation, $\langle\cos\theta_d\rangle$, and alignment, $\langle\cos^2\theta_d\rangle$, of KRb along the LFF Z-axis are shown in Fig. 4.9 (a) and Fig. 4.9 (b), respectively. In addition, we present in Fig. 4.10, the orientation and alignment of KRb within the Rb-KRb in two manifolds Rb$(n = 25, l \geq 3)$ and Rb$(n = 29, l \geq 3)$ for $M_J = 0$, and the orientation and alignment of the rotational ground state of KRb in an electric field of varying field strength $5.14 a_0^2/R^2$ GV/cm, where R is given in atomic units and a_0 is the Bohr radius, i. e., the strength of the electric field due to the Rydberg core, being parallel and

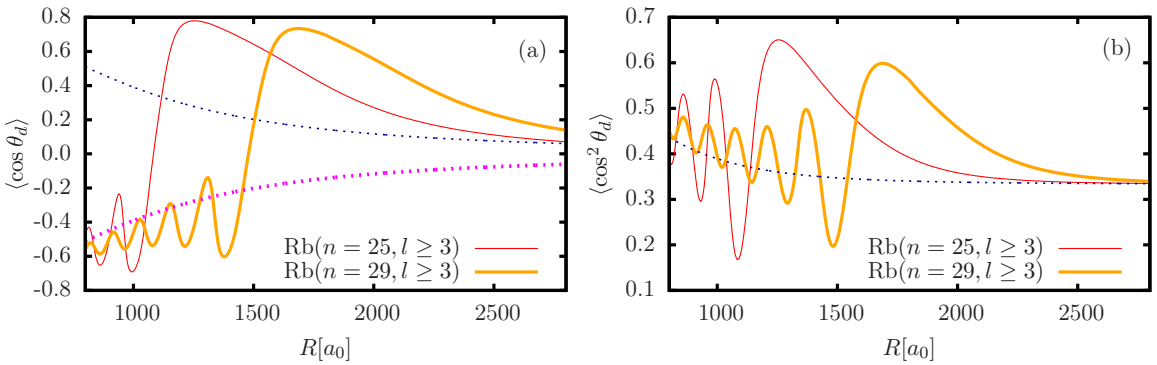

Figure 4.10: For the KRb molecule within the energetically lowest-lying BOPs with $M_J = 0$ of Rb$(n = 25, l \geq 3)$-KRb (thin solid) and Rb$(n = 29, l \geq 3)$-KRb (thick solid), we show (a) the orientation $\langle\cos\theta_d\rangle$ and (b) the alignment $\langle\cos^2\theta_d\rangle$ along the LFF Z-axis versus the internuclear distance between Rb^+ and KRb. We also present the orientation and alignment of KRb in an electric field parallel (thick dotted) and antiparallel (thin dotted) to the LFF Z-axis and strength $5.14 a_0^2/R^2$ GV/cm.

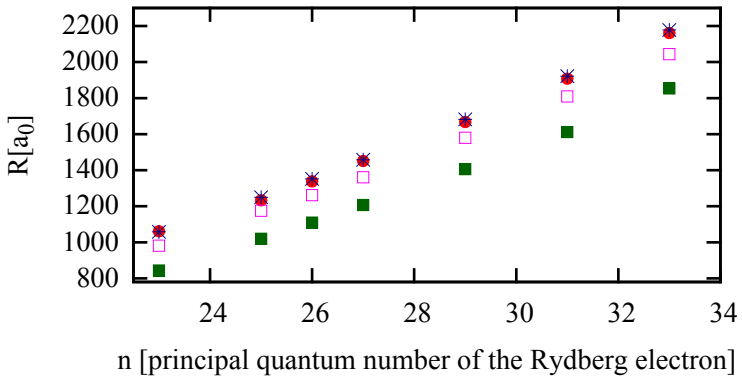

Figure 4.11: For the Rb-KRb Rydberg molecule, we show the distance between the Rb^+ core and KRb (•) at which the orientation of KRb is maximal within the lowest-lying $M_J = 0$ adiabatic potentials evolving from the $Rb(n, l \geq 3)$ manifolds for varying principal quantum number n. For these lowest-lying BOPs, we also present the internuclear separation R of Rb-KRb at which the one before the outermost (□) and the outermost (■) potential wells reach the minimum value. For comparison, we show the classical turning point $R \sim 2n^2 a_0$ ($\star$).

antiparallel to the LFF Z-axis. These results allow us to get a deeper physical insight into the interplay between the electric field due to the Rydberg electron and the Rb^+ core. Note that qualitatively similar behavior is obtained for the all the BOPs presented in Fig. 4.4.

For all BOPs, we encounter a regime where the electric field due to the Rydberg core is dominant, i. e., the total electric field is antiparallel to the LFF Z-axis, and KRb is anti-oriented. In this regime, the orientation of KRb within Rb-KRb is very close to the orientation of KRb in the $5.14 a_0^2/R^2$ GV/cm electric field. Let us comment, that for $R = 1000\ a_0$, the electric field strength due to the Rydberg core is 5 kV/cm. The oscillations of the orientation of the KRb within Rb-KRb are due to the electric field of the Rydberg electron, which oscillates resembling the behavior of its wave function. The amplitude of these oscillations increases as the electric field of the Rydberg electron becomes more important. When the contribution of this field becomes dominant, the orientation of KRb changes sign and KRb becomes oriented along the Z-axis. The differences in the electronic Rydberg wave function of $Rb(n = 29, l \geq 3)$ and $Rb(n = 25, l \geq 3)$, are reflected in the fact that the KRb molecule is anti-oriented for a larger range of values of R for $Rb(n = 29, l \geq 3)$-$KRb(N = 0)$. KRb is maximally oriented around the classical turning point $R \sim 2n^2 a_0$, and we have $\langle \cos\theta_d \rangle \approx 0.8$, which is the orientation of KRb in a strong electric field of 50 kV/cm strength [104]. The internuclear separation of Rb-KRb at which the KRb orientation reaches the maximum is shown versus the principal quantum number of the $Rb(n, l \geq 3)$ degenerate manifold in Fig. 4.11. We observe a very good agreement with the $2n^2 a_0$ behavior. In Fig. 4.11 we show also the internuclear separation of Rb-KRb at which the energetically lowest-lying BOP with $M_J = 0$ reaches the two outermost minima. The radial position of these two minima is shifted to lower values of R compared to the maximum of the KRb orientation. By further increasing R, the orientation decreases towards zero and approaches the orientation of KRb in the $5.14 a_0^2/R^2$ GV/cm electric field. Note that in the absence of an electric field, the KRb molecule is not oriented, see Appendix B.

The alignment along the LFF Z-axis of KRb within Rb-KRb also shows an oscillatory

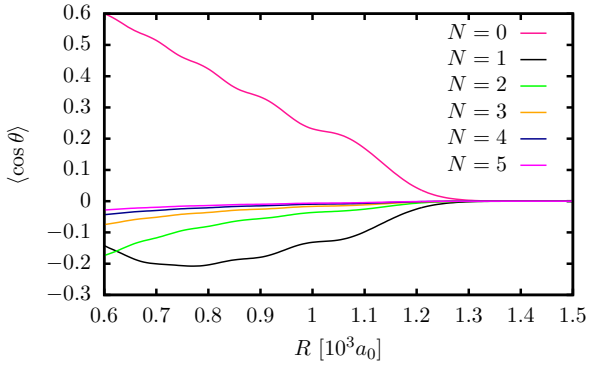

Figure 4.12: For the Rb-KRb Rydberg molecule, orientation of the diatomic molecule within the Born-Oppenheimer potentials with $M_J = 0$ evolving from the Rb($28s$) state and KRb in the rotational excitations $N = 0, 1, 2, 3, 4$ and 5. See Fig. 4.7 to identify the corresponding BOPs.

behavior around the alignment of the KRb in a $5.14a_0^2/R^2$ GV/cm electric field, cf. Fig. 4.9 (b) and Fig. 4.10 (b). As the coupling of the dipole moment of KRb with the electric field due to the Rydberg electron becomes dominant compared to the coupling with the Rb^+ electric field, the amplitude of the oscillations become very large. When the distance of KRb from the Rb^+ core is large, the alignment approaches the field-free value $\langle \cos^2 \theta_d \rangle = 1/3$.

We explore now the orientation of the KRb molecule within the BOP evolving from the Rb($28s$) state in Fig. 4.12. As the rotational excitation of KRb increases the orientation decreases. The rotational kinetic energy increases as $BN(N+1)$ with N being the rotational quantum number of KRb and B the rotational constant $B = 1.114$ GHz. This rotational kinetic energy become very large for these excited states, for instance, it is equal to 0, 6.68 and 33.4 GHz for $N = 0, 2$ and 5, respectively. These large kinetic energies should be compensated with the interaction between the permanent dipole moment of KRb and the electric fields due to the Rydberg core and electron. As a consequence, the impact of the Rydberg electric field on these rotational excitations decreases, and the diatomic molecule becomes significantly less oriented. In Fig. 4.12, we observe that only the KRb within the electronic state Rb($27p$)-KRb(N=0) shows a strong orientation for $R \sim 600\ a_0$, and $\langle \cos \theta \rangle$ shows smooth oscillations as R increases, which are due to the Rydberg electron electric field. In contrast to the behaviour observed for KRb within the lowest-lying BOPs evolving from the Rydberg degenerate manifold Rb($n, l \geq 3$)-KRb($N = 0$), the orientation does not change sign as R is increased. This is due to the weak electric fields produced by the Rydberg electron on $28s$ state, compared to the strong fields that are produced from the states in the degenerate manifold.

In Fig. 4.13 (a), we present the orientation of KRb within the lowest lying adiabatic electronic states evolving from Rb($27p$)-KRb(N) for $N = 0, \ldots, 5$, see Fig. 4.8 to identify the corresponding BOPs. Analogously, Fig. 4.14 (a) shows the orientation for KRb within the lowest lying adiabatic electronic states evolving from Rb($26d$)-KRb(N) for $N = 0, \ldots, 5$, see Fig. 4.6 to identify the corresponding BOPs. As in the BOPs evolving from Rb($28s$)-KRb(N), the orientation of KRb decreases as its rotational quantum number increases, and only on the $N = 0$ rotational states KRb reaches a significant orientation. As

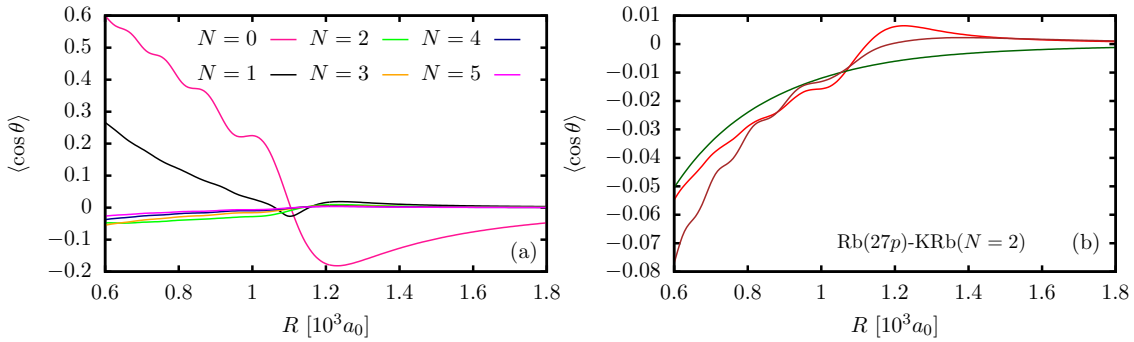

Figure 4.13: For the Rb-KRb Rydberg molecule, orientation of the diatomic molecule within (a) the lowest-lying Born-Oppenheimer potentials with $M_J = 0$ evolving from the Rb($27p$) state and KRb in the rotational levels $N = 0, 1, 2, 3, 4$ and 5, (b) the Born-Oppenheimer potentials with $M_J = 0$ evolving from the Rb($27p$) state and KRb in the rotational state $N = 2$. See Fig. 4.8 to identify the corresponding BOPs.

R increases the orientation of KRb in the Rb($27p$)-KRb($N = 0$) and Rb($26d$)-KRb($N = 0$) BOP changes sign once the interaction due to the Rb^+ electric field becomes dominant. This change on the sing of $\langle \cos\theta \rangle$ is also observed for KRb within the BOPs Rb($27p$)-KRb($N = 1$), Rb($26d$)-KRb($N = 1$) and Rb($26d$)-KRb($N = 2$). Finally, we analyze the orientation for KRb within all the BOPs evolving from Rb($27p$)-KRb($N = 2$) and Rb($26d$)- KRb($N = 2$) in Fig. 4.13 (b) and Fig. 4.14 (b), respectively. We observe two different behaviours of the orientation as a function of R, which are analogous to those observed for the BOP. For those BOPs showing oscillatory behaviour as R increases in Fig. 4.8 (c) and Fig. 4.6 (c), $\langle \cos\theta \rangle$ also shows smooth oscillations versus R. In contrast, $\langle \cos\theta \rangle$ shows a increasing or decreasing trend but without oscillations as their corresponding BOPs.

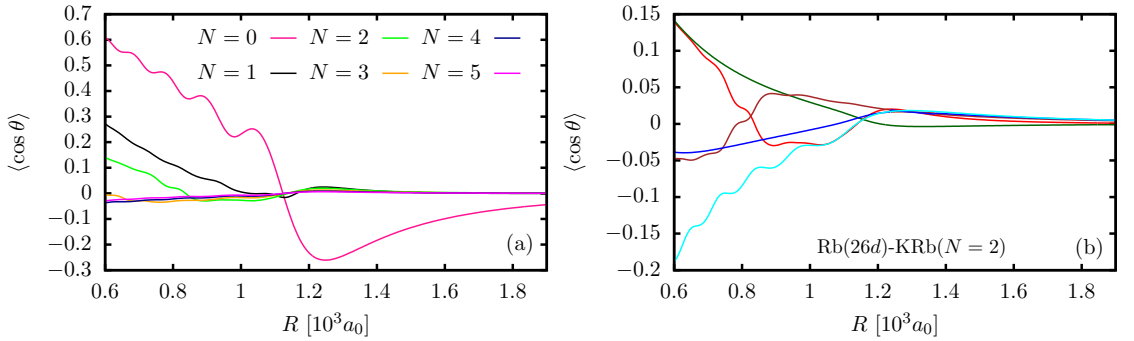

Figure 4.14: For the Rb-KRb Rydberg molecule, orientation of the diatomic molecule within (a) the lowest-lying Born-Oppenheimer potentials with $M_J = 0$ evolving from the Rb($26d$) state and KRb in the rotational levels $N = 0, 1, 2, 3, 4$ and 5, (b) the Born-Oppenheimer potentials with $M_J = 0$ evolving from the Rb($26ds$) state and KRb in the rotational state $N = 2$. See Fig. 4.6 to identify the corresponding BOPs.

Chapter 5

Ultralong-range Rydberg pentaatomic molecules with two polar diatomic molecules

5.1 Introduction

In an ultracold mixture of Rydberg atoms and molecules, more than one diatomic molecule might be immersed into the Rydberg wave function, opening the possibility of creating more complex polyatomic Rydberg molecules. In the present chapter, we consider a pentaatomic molecule formed by a Rydberg atom and two ground state heteronuclear diatomic molecules. As in our previous study on the triatomic Rydberg molecule, see Ref [77] and Chapter 4, we include the angular degrees of freedom of the diatomic molecules within the rigid rotor approximation. Such a realistic treatment of the internal motion of the diatomic molecules allows us to properly investigate the effect of the electric fields due to Rydberg core and Rydberg electron on their directional properties.

Our focus is on two collinear configurations of the pentaatomic Rydberg molecule: A symmetric one in which the two diatomic molecules are located at different sides of the Rydberg core, see Fig. 5.1 (a), and an asymmetric one with the two of them on the same side as plotted in Fig. 5.1 (b). As prototype ultralong-range molecules, we consider those formed by the Rubidium Rydberg atom and the diatomic molecules KRb. The rotational constant of KRb is $B = 1.114$ GHz [90], and electric dipole moment $d = 0.566$ D [89], which is well below the Fermi-Teller critical value 1.639 D [78, 79]. We analyze the adiabatic electronic potentials of the symmetric configurations KRb-Rb($n = 20, l \geq 3$)-KRb and KRb-Rb($23s$)-KRb Rydberg pentaatomic molecules as the internuclear separation between two KRb molecules and the Rb^+ core varies. We also explore the effects of the electric field due to the Rydberg atom on the rotational motion of diatomic molecules, by analyzing their orientation and alignment. For the asymmetric configuration, we study the BOPs for the Rb($n = 20, l \geq 3$)-KRb-KRb, as the distance of one or two of the diatomic molecules from the Rydberg core increases. For the adiabatic electronic states, we encounter oscillating BOPs having potentials wells with depths from a few MHz to a few GHz depending on the Rydberg state of Rb involved on the giant Rydberg molecule.

This chapter is organized as follows. The adiabatic Hamiltonian of the pentaatomic Rydberg molecule is described in Sec. 5.2, we also provide the coupled basis used to solve the Schrödinger equation. In Sec. 5.3 we analyze the electronic structure of the linear symmetric and asymmetric configurations as the distances of the diatomic molecules from the Rydberg core increase, we also study the directional properties of the diatomic molecules.

Part of the contents of this chapter is adapted from the reference: J. Aguilera-Fernández, H.R. Sadeghpour, P. Schmelcher, and R. González-Férez, *Electronic Structure of*

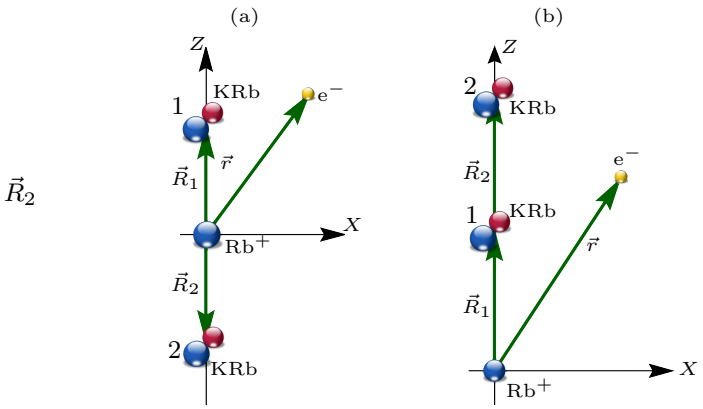

Figure 5.1: A sketch (not to scale) of the pentaatomic Rydberg molecule formed by a Rydberg atom and two diatomic polar molecules in the (a) symmetric and (b) asymmetric configurations.

Ultralong-Range Rydberg Pentaatomic Molecules with Two Polar Diatomic Molecules, arXiv:1710.01393, accepted for publication in Physical Review A (2017).

5.2 The adiabatic Hamiltonian

We consider a polyatomic molecule formed by a Rydberg atom and two ground state heteronuclear diatomic molecules. The ground-state diatomic molecules are described within the Born-Oppenheimer and rigid rotor approximations, i. e., we adiabatically separate first the electronic and vibrational motions, and then the vibrational and rotational motions. These approximations provide a good description of deeply bound diatomic molecules in the presence of moderate electric fields [102, 103]. The binding mechanism of the Rydberg molecule is due to the coupling between the electric dipole moments of the polar molecules with the electric field provided by the Rydberg core and electron [74–76], which reads

$$\mathbf{F}_{ryd}(\mathbf{R}_i, \mathbf{r}) = e\frac{\mathbf{R}_i}{R^3} + e\frac{\mathbf{r} - \mathbf{R}_i}{|\mathbf{r} - \mathbf{R}_i|^3}, \tag{5.1}$$

where e is the electron charge, $\mathbf{r}$ is the position of the Rydberg electron, and $\mathbf{R}_1$ and $\mathbf{R}_2$ the positions of the diatomic molecules. The expression of the Rydberg electron electric field is provided in Appendix A.

In the framework of the Born-Oppenheimer approximation, the adiabatic Hamiltonian of this polyatomic Rydberg molecule is given by

$$H_{ad} = H_A + H_{mol}, \tag{5.2}$$

where H_A represents the single electron Hamiltonian describing the Rydberg atom

$$H_A = -\frac{\hbar^2}{2m_e}\nabla_r^2 + V_l(r), \tag{5.3}$$

where $V_l(r)$ is the l-dependent model potential [97], with l being the angular momentum quantum number of the Rydberg electron.

The rigid-rotor Hamiltonian of the two polar molecules in the electric field created by the Rydberg electron and core reads

$$H_{mol} = \sum_{i=1,2} \left[B\mathbf{N}_i^2 - \mathbf{d}_i \cdot \mathbf{F}_{ryd}(\mathbf{R}_i, \mathbf{r})\right] + V_{12}(\Omega_1, \Omega_2), \tag{5.4}$$

with B being the rotational constant, $\mathbf{N}_1$ and $\mathbf{N}_2$ the molecular angular momentum operators and $\mathbf{d}_1$ and $\mathbf{d}_2$ the permanent electric dipole moments of the diatomic molecules. Note that for a linear molecule, the electric dipole moment is parallel to the molecular internuclear axis. The last term $V_{12}(\Omega_1, \Omega_2)$ stands for the dipole-dipole interaction between the two diatomic molecules. For the Rydberg peentaatomic molecules considered in this chapter, the distance between the two diatomic molecules is large enough so that the dipole-dipole interaction could be neglected. For each diatomic molecule, the internal rotational motion is described by the Euler angles $\Omega_i = (\theta_i, \phi_i)$ with $i = 1, 2$.

The total angular momentum of the Rydberg molecule, but excluding an overall rotation, is given by $\mathbf{J} = \mathbf{l} + \mathbf{N}$, where $\mathbf{l}$ is the orbital angular momentum of the Rydberg electron, and $\mathbf{N}$ is the coupled molecular angular momenta of the two diatomic molecules, $\mathbf{N} = \mathbf{N}_1 + \mathbf{N}_2$. To solve the Schrödinger equation associated with the Hamiltonian (5.2), we perform a basis set expansion in terms of the coupled basis

$$\Psi^{JM_J}_{nlm,NN_1N_2}(\mathbf{r}, \Omega_1, \Omega_2) = \sum_{m_l=-l}^{m_l=l} \sum_{M_N=-N}^{M_N=N} \langle lm_l NM_N | JM_J\rangle \Psi^{NM_N}_{N_1N_2}(\Omega_1, \Omega_2)\, \psi_{nlm}(\mathbf{r}), \tag{5.5}$$

where $\langle lm_l NM_N | JM_J\rangle$ is the Clebsch-Gordan coefficient, $J = |l-N|, \ldots, l+N$, and the total magnetic quantum number $M_J = -J, \ldots, J$. $\psi_{nlm}(\mathbf{r})$ is the Rydberg electron wave function with n, l and m being the principal, orbital and magnetic quantum numbers, respectively. For the two ground-state molecules, we use the coupled basis

$$\Psi^{NM_N}_{N_1N_2}(\Omega_1, \Omega_2) = \sum_{M_{N_1}=-N_1}^{M_{N_1}=N_1} \sum_{M_{N_2}=-N_2}^{M_{N_2}=N_2} \langle N_1 M_{N_1} N_2 M_{N_2} | NM_N\rangle Y_{N_1M_{N_1}}(\Omega_1)\, Y_{N_2M_{N_2}}(\Omega_2), \tag{5.6}$$

where N_i and M_{N_i}, with $i = 1, 2$, are the rotational and magnetic quantum numbers, and $Y_{N_iM_{N_i}}(\Omega_i)$, is the field-free rotational wave function of the diatomic molecules, i. e., the spherical harmonics. The coupled angular momentum of the two diatomic molecules satisfies $N = |N_1 - N_2|, \ldots, N_1 + N_2$, and its projections on the laboratory fixed frame $M_N = -N, \ldots, N$.

For the linear configurations, the electric field couples functions of the coupled basis (5.5) having the same total magnetic quantum numbers M_J because the system has azimuthal

Table 5.1: For the rubidium atom, energies and energies differences $\Delta E_{n,l} = E_{n,l} - E_{20,3}$ of the Rydberg levels close to the degenerate Rydberg manifold Rb($n = 20$, $l \geq 3$).

n	l	E_{nl}(THz)	ΔE_{nl}(GHz)
21	3	−7.4599	764.64
24	0	−7.5547	669.82
22	2	−7.7118	512.70
23	1	−7.9433	281.26
20	3	−8.2246	0
23	0	−8.3344	109.86
21	2	−8.5164	291.89
22	1	−8.5164	560.98
19	3	−9.1131	888.53
22	0	−9.2413	1016.78
20	2	−9.4538	1229.28
21	1	−9.7692	1544.67

symmetry. As a consequence, the basis set expansion of the wave functions is done in terms of functions of the coupled basis (5.5) with fixed total magnetic quantum number M_J, and reads

$$\Psi(\mathbf{r}, \Omega_1, \Omega_2; R_1, R_2) = \sum_{n,lN_1,N_2,J} C^J_{n,l,N,N_1,N_2}(R_1, R_2)\Psi^{JM_J}_{nlm,N}(\mathbf{r}, \Omega_1, \Omega_2), \tag{5.7}$$

where we have explicitly indicated that the coefficients of the expansion $C^J_{n,l,N,N_1,N_2}(R_1, R_2)$ depend on the distance between the two diatomic molecules and the ionic core R_1 and R_2. In this work, we have included the rotational excitations with $N_i \leq 4, 5$, and 6 for the two KRb molecules. For the Rydberg atom Rb*, we take into account the Rb($n, l \geq 3$) degenerate manifold, and the energetically neighboring level $(n + 3)s$. In this chapter, we focus on the Rydberg manifold Rb($n = 20, l \geq 3$) and the quantum-defect state Rb($23s$). In Table 4.1, we show the energies and energy differences of the quantum-defect states and the Rydberg manifolds close to Rb($n = 20, l \geq 3$). As in the previous two chapters, we neglect the quantum defect of the Rb(nf) Rydberg state. These large energy differences shown in Table 4.1 justify our approximation in reducing the number of Rydberg states used to solve the Schrödinger equation. In Sec. 5.3, we present a convergence study which shows how important are the contributions of rotationally excited states as well as of the Rydberg state Rb($23s$) on several electronic states.

The basis set expansion (5.7) transforms the partial differential equation given by the Schrödigner equation in a matrix eigenvalue problem. The matrix elements appearing are similar to those presented in Sec. 4.2. This Hamiltonian matrix is diagonalized using the restarted Lanczos procedure [93] implemented in the Arnoldi Package (ARPACK) [94, 95].

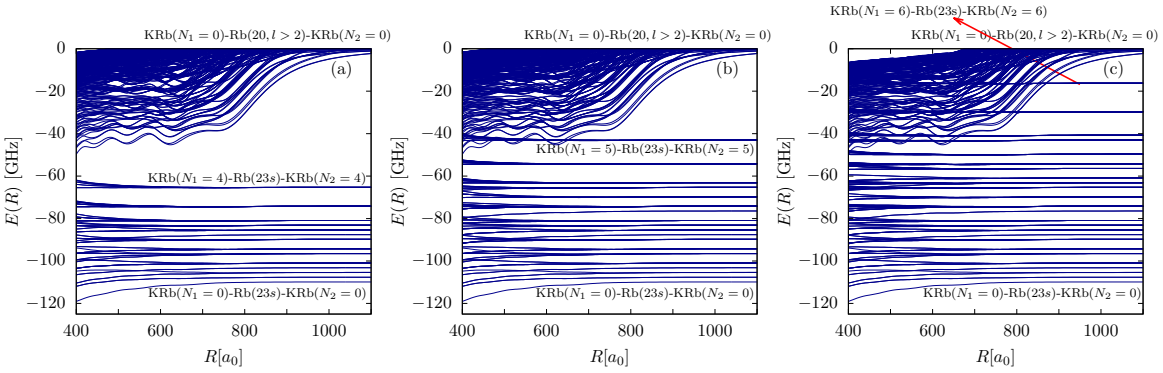

Figure 5.2: For the symmetric configuration of the pentaatomic Rydberg molecule, adiabatic electronic potentials evolving from the degenerate manifold Rb($n = 20$, $l \geq 3$) and the Rydberg state Rb($23s$) with total magnetic quantum number $M_J = 0$. The calculations have been done including in the coupled basis of the diatomic molecules (5.6) rotational excitations up to a) $N_i = 4$, b) $N_i = 5$, and c) $N_i = 6$, with $i = 1$ and 2.

For these pentaatomic Rydberg molecules, we have not solved the vibrational Scrödinger equation to determine the existence of bound states. We have approximated a harmonic oscillator to the minimum of the corresponding potential well. We have used the following expression $E_0 + \frac{1}{2}\beta(R - R_0)^2$ with fitting parameters E_0, β and R_0. The vibrational bound energies are then approximated by $\epsilon_n = \hbar(n + \frac{1}{2})\omega$, with $\omega = \sqrt{\beta/\mu}$ and the reduced mass by $\mu = 2m_{KRb}m_{Rb}/(m_{Rb} + 2m_{KRb})$, $m_{KRb} = m_K + m_{Rb}$, with m_K and m_{Rb} being the masses of the potassium and rubidium atoms, respectively.

5.3 The electronic structure of the linear symmetric pentaatomic Rydberg molecule

In this section, we explore the adiabatic potentials of the electronic states for the linear Rydberg pentaatomic molecule: a symmetric configuration, and two asymmetric ones, presented in Fig. 5.1.

We have first performed a numerical analysis of the convergence of the adiabatic electronic states for the symmetric configuration of the Rydberg molecule KRb-Rb*-KRb, i. e., $R_1 = R_2$, as the coupled basis (5.5) is changed. The basis set expansion of the total wave function includes the wave functions of the Rydberg degenerate manifold Rb($n = 20$, l$\geq$ 3) and of the energetically closest Rydberg state Rb($23s$) in the coupled basis (5.5). Note that we are neglecting the quantum defect of the nf Rydberg state. For the diatomic molecules, we take into account the rotational excitations up to $N_i = 4$, $N_i = 5$, and $N_i = 6$, with $i = 1$ and 2, in the coupled basis of the two diatomic molecules (5.6). The BOPs of the symmetric configuration of the pentamer molecule with $M_J = 0$ are presented in Fig. 5.2 (a), (b) and (c), for the rotational excitations of the two KRb molecules $N_i \leq 4$, $N_i \leq 5$, and $N_i \leq 6$, with $i = 1$ and 2, respectively. The zero energy has been set to the energy of the Rb($n = 20, l \geq 3$) degenerate manifold and the two KRb molecules on their rotational ground state $N_1 = N_2 = 0$.

The main difference between these three spectra are the electronic states evolving from the excited rotational states of KRb with $N_i = 5$ and $N_i = 6$, with $i = 1, 2$, which do not appear in Fig. 5.2 (a). The BOPs evolving from the Rydberg state Rb($23s$) can be easily identify on the electronic spectrum as almost horizontal lines on the scale of the this figure. These electronic states approach the asymptotic limit $\Delta E_{23s} + N_1(N_1+1)B + N_2(N_2+1)B$ for large values of R_1, with $\Delta E_{23s} = E_{23s} - E_{20,l\leq 3}$, E_{23s} and $E_{20,l\leq 3}$ being the energies of Rb($23s$) and Rb($n = 20$, l≥ 3), respectively. In the energy region of the electronic states evolving from the Rydberg manifold Rb($n = 20$, l≥ 3), i. e., $E(R) \gtrsim -50$ GHz, we encounter a few BOPs evolving from Rb($23s$) and the two KRb in a excited rotational state with $N_i \geq 5$. Due to high rotational excitations of the diatomic molecules, the effect of the Rydberg electric field is significantly reduced, since the electric-field interaction has to compensate the large rotational kinetic energies of each diatomic molecules, which are 33.4 GHz and 46.8 GHz for $N_1 = 5$ and $N_1 = 6$, respectively.

The relative errors of the six lowest-lying states evolving from the Rydberg manifold Rb($n = 20$, l≥ 3) are smaller than 1% when the rotational excitations of KRb are increased from $N_i \leq 4$ to $N_i \leq 5$, these relative errors are even smaller if we compare the BOP with $N_i \leq 5$ and $N_i \leq 6$. Let us emphasize that these six lowest-lying electronic states evolve from the manifold Rb($n = 20$, l≥ 3) and the two KRb being initially in their rotational ground state. Thus, these small relative errors indicate that the contribution of highly excited rotational states with $N_i \geq 5$ do not have a significant contribution on the field-dressed ground state of KRb. For the electronic states evolving from the Rydberg state Rb(23s) and the two KRb molecules with rotational excitations $N_i \leq 3$, the comparison between the calculations done using $N_i \leq 5$ and $N_i \leq 6$ shows relative errors smaller than 1%, which also indicates the small contribution of partial waves on the rotational dynamics of KRb. Finally, if only the states within the degenerate manifold are included in the basis set expansion, the relative error is smaller than 0.8% for the six lowest-lying states, and smaller than 0.4% for the ground state. This is due to the large energy separation between the Rydberg state Rb(23s) and the manifold Rb($n = 20$, l≥ 3), and that those electronic state lying energetically close are due to the KRb molecules being in a excited rotational states, which reduces the coupling between these electronic states.

5.3.1 The Born-Oppenheimer potentials evolving from the Rydberg degenerate manifold Rb($n = 20$, l≥ 3)

In Fig. 5.3 (b) and (d), we show the BOPs with $M_J = 0$, and 1, respectively, for the collinear Rydberg pentaatomic molecule where the two diatomic molecules are located on LFF Z-axis at the same distance from the core $R_1 = R_2$, but on different sides of Rb^+, see the sketch presented in Fig. 5.1 (a). For comparison, the corresponding adiabatic potentials for a Rb-KRb triatomic molecule, with Rb^+ located at the center of the LFF, and the diatomic molecule is on the Z-axis at a distance $R = R_1$, are shown in Fig. 5.4. Note that the BOPs of the triatomic Rydberg molecule also evolve from the Rb($n = 20$, l≥ 3) manifold. This triatomic molecule is numerically described with a coupled basis analogous to the one used for the pentaatomic molecule, see Ref. [77].

As for the Rydberg triatomic system, the electronic potentials oscillate as the internuclear distance $R_1 = R_2$ increases, which reflects the oscillatory behaviour of the Rydberg electron

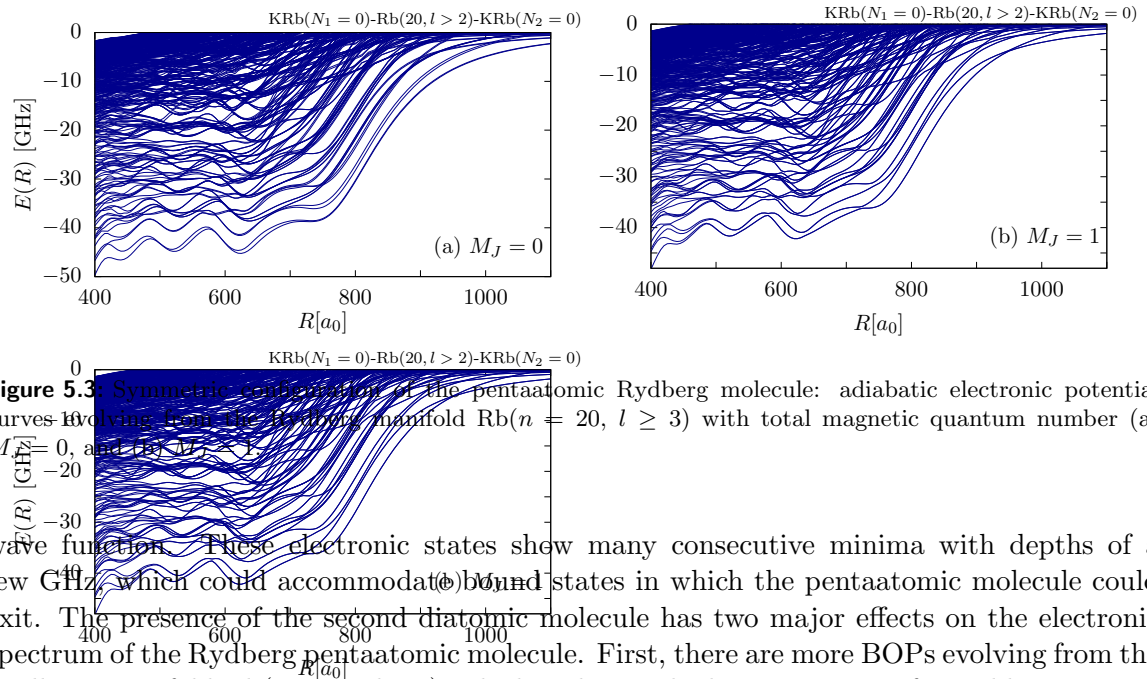

Figure 5.3 Symmetric configuration of the pentaatomic Rydberg molecule: adiabatic electronic potential curves evolving from the Rydberg manifold Rb($n = 20$, $l \geq 3$) with total magnetic quantum number (a) $M_J = 0$, and (b) $M_J = 1$.

wave function. These electronic states show many consecutive minima with depths of a few GHz, which could accommodate bound states in which the pentaatomic molecule could exit. The presence of the second diatomic molecule has two major effects on the electronic spectrum of the Rydberg pentaatomic molecule. First, there are more BOPs evolving from the Rydberg manifold Rb($n = 20$, l≥ 3), which is due to the larger amount of possible rotational excitations of the two diatomic molecules, i. e., $\Psi^{NM_N}_{N_1N_2}(\Omega_1, \Omega_2)$ with $N_i \leq 4$, to be combined with the Rydberg states from the degenerate manifold Rb($n = 20$, l≥ 3). As a consequence, the complexity of the electronic structure is significantly enhanced, and these neighbouring electronic states undergo narrow avoided crossings. Second, the energy shifts of the two lowest-lying BOPs evolving from the Rydberg manifold Rb($n = 20$, l≥ 3) are a bit larger than the corresponding shifts of the lowest-lying one in the Rydberg triatomic molecule, but the differences are not significant. Indeed, for the Rydberg pentaatomic molecule, we also encounter pairs of electronic states having similar energies, which at large internuclear separations, once the effect of the electric field due to the Rydberg core becomes dominant,

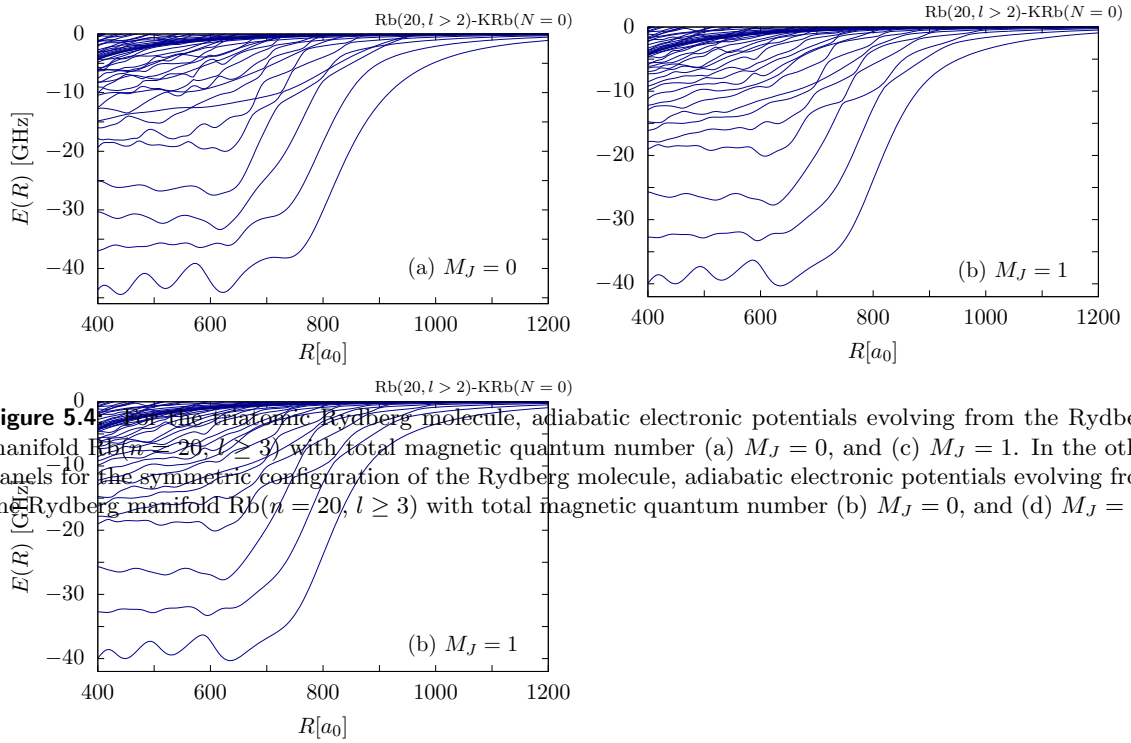

Figure 5.4 For the triatomic Rydberg molecule, adiabatic electronic potentials evolving from the Rydberg manifold Rb($n = 20, l \geq 3$) with total magnetic quantum number (a) $M_J = 0$, and (c) $M_J = 1$. In the other panels for the symmetric configuration of the Rydberg molecule, adiabatic electronic potentials evolving from the Rydberg manifold Rb($n = 20, l \geq 3$) with total magnetic quantum number (b) $M_J = 0$, and (d) $M_J = 1$.

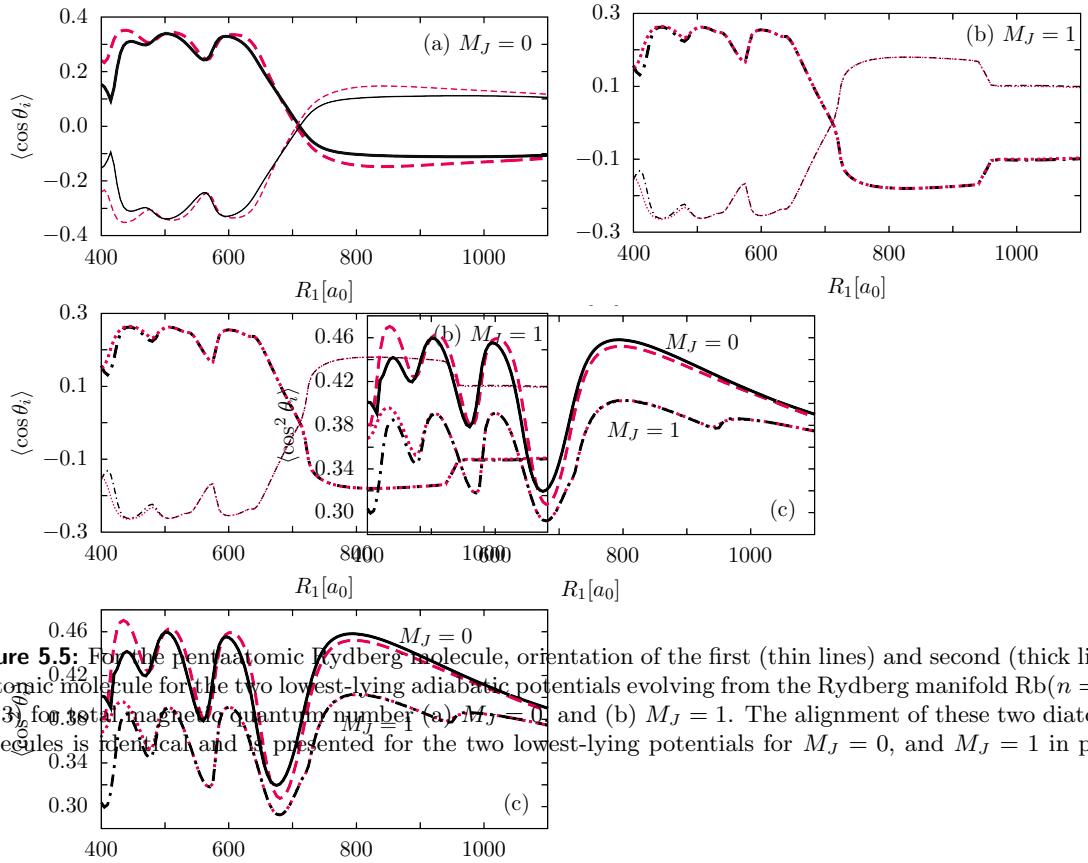

Figure 5.5: For the pentaatomic Rydberg molecule, orientation of the first (thin lines) and second (thick lines) diatomic molecule for the two lowest-lying adiabatic potentials evolving from the Rydberg manifold Rb($n = 20$, $l \geq 3$) for total magnetic quantum number (a) $M_J = 0$, and (b) $M_J = 1$. The alignment of these two diatomic molecules is identical and is presented for the two lowest-lying potentials for $M_J = 0$, and $M_J = 1$ in panel (c).

become equal. For $M_J = 1$ the degeneracy between pairs of consecutive states is manifested even at lower values of the internuclear separation R. The two KRb molecules are exposed to the Rydberg atom electric field, whose matrix elements on the Rydberg electron wave function basis have the same strength but differ on sign due to their different location on the Z-axis, see appendix A. In addition, the dipole-dipole interaction between the two KRb molecules is rather small due to the large spatial separation, and can be neglected. These two facts give rise to similar energy shifts for the BOPs that are due to the presence of the first or second diatomic molecules.

The KRb molecules within the Rydberg pentaatomic molecule are oriented and aligned. Fig. 5.5 (a) and Fig. 5.5 (b) present the orientation of the two diatomic molecules with the adiabatic electronic potentials with $M_J = 0$ and $M_J = 1$, respectively. The two KRb are oriented in opposite directions but having the same absolute value. Within the BOPs with $M_J = 0$ and $R \lesssim 700\ a_0$, the first diatomic molecule shows a moderate orientation against the Rydberg core, whereas the second one is oriented towards Rb^+. In both cases, their orientations show an oscillatory behaviour reflecting the radial dependence of the Rydberg electron wave function. By further increasing the internuclear separation, the orientation of the two diatomic molecules is reversed. A similar behaviour is observed for the orientation of the two KRb within BOPs with $M_J = 1$. For the orientation within the $M_J = 1$ BOPs in Fig. 5.5 (b), the sudden changes of the orientations around $R \approx 980\ a_0$ are due to the avoided crossing between these two potentials and the two neighbouring ones which is observed in Fig. 5.4 (d). Within a certain electronic state, the alignment of the two diatomic molecules

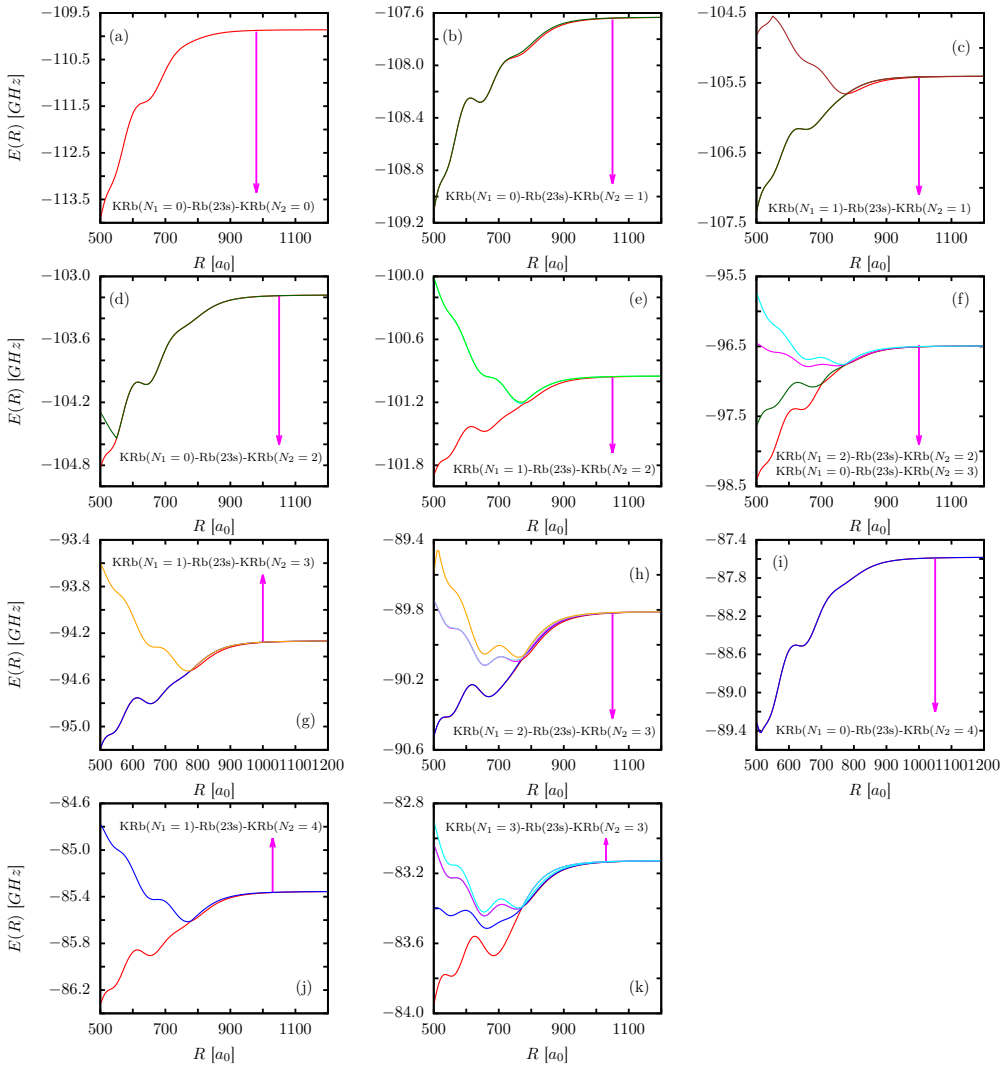

Figure 5.6: For the symmetric configuration of the Rydberg molecule, adiabatic electronic potentials versus the internuclear separation $R_1 = R_2 = R$ evolving from the Rydberg state Rb($23s$) and the diatomic molecules in rotational excitations in the coupled basis $N_i = 6$ with $i = 1, 2$. The total magnetic quantum number of the adiabatic electronic potentials is $M_J = 0$.

is the same, in Fig. 5.5 (c) we present $\langle \cos^2 \theta_1 \rangle$ within these two lowest-lying BOPs with $M_J = 0$ and $M_J = 1$. The changes on the direction of the orientation, i. e., $\langle \cos \theta_i \rangle \approx 0$ corresponds with the diatomic molecules having their field-free alignment $\langle \cos^2 \theta_1 \rangle \approx 1/3$. After the oscillatory behaviour, the alignment approach the field-free value $\frac{1}{3}$ as R_1 increases and the effect of the electric field due to the Rydberg core decreases.

5.3.2 The Born-Oppenheimer potentials evolving from the Rb($23s$) Rydberg state.

We explore now a set of electronic states evolving from the Rydberg state Rb($23s$). The BOPs for $M_J = 0$ evolving from the Rydberg state and the two diatomic molecules in the rotational excitations states up to $N_i = 6$, $i = 1, 2$, are shown in Fig. 5.6. At large separation between the diatomic molecules and the ionic core, the system could be considered uncoupled and the adiabatic electronic states approach a limit which depend on the states of the KRb molecules and of the Rydberg electron. For these electronic states, we have the following energetical limits:

- In Fig. 5.6 (a), the BOP approaches to the asymptotic limit $\Delta E_{23s} + 0B$ and correspond to the two diatomic molecules being in the rotational ground state with the wave function on the coupled basis (5.6) $|N, M_N, N_1, N_2\rangle = |0, 0, 0, 0\rangle$.
- In Fig. 5.6 (b), the BOPs approach to the asymptotic limit $\Delta E_{23s} + 2B$ and correspond to one diatomic molecule being in the rotational ground state, and the other one in the first excited state, with the wave functions on the coupled basis (5.6) $|1, 0, 1, 0\rangle$ and $|1, 0, 0, 1\rangle$.
- In Fig. 5.6 (c), the BOPs approach to the asymptotic limit $\Delta E_{23s} + 4B$ and correspond to the two diatomic molecules being in the first rotational excited state, with the wave functions on the coupled basis (5.6) $|N, 0, 1, 1\rangle$ with $N = 0, 1, 2$.
- In Fig. 5.6 (d), the BOPs approach to the asymptotic limit $\Delta E_{23s} + 6B$ and correspond to one diatomic molecules being in the ground state, and the other one in the second rotational excited state, with the wave functions on the coupled basis (5.6) $|2, 0, 0, 2\rangle$ and $|2, 0, 2, 0\rangle$.
- In Fig. 5.6 (e), the BOPs approach to the asymptotic limit $\Delta E_{23s} + 8B$ and correspond to one diatomic molecules being in the first excited state, and the other one in the second rotational excited state, with the wave functions on the coupled basis (5.6) $|N, 0, 1, 2\rangle$ and $|N, 0, 2, 1\rangle$ with $N = 1, 2, 3$.
- In Fig. 5.6 (f), the BOPs approach to the asymptotic limit $\Delta E_{23s} + 12B$ and correspond to the two diatomic molecules being in the second rotational excited state, or one of them in the third excited state and the second one in the ground state, with the wave functions on the coupled basis (5.6) $|N, 0, 2, 2\rangle$ with $N = 0, 1, 2, 3, 4$ and $|N, 0, 3, 0\rangle$ and $|N, 0, 0, 3\rangle$, respectively.
- In Fig. 5.6 (g), the BOPs approach to the asymptotic limit $\Delta E_{23s} + 14B$ and correspond to one KRb being in the third excited state and the second one in the first excited state, with the wave functions on the coupled basis (5.6) $|N, 0, 3, 1\rangle$ and $|N, 0, 1, 3\rangle$ with $N = 2, 3, 4$.
- In Fig. 5.6 (h), the BOPs approach to the asymptotic limit $\Delta E_{23s} + 18B$ and correspond to one KRb being in the third excited state and the second one in the second excited state, with the wave functions on the coupled basis (5.6) $|N, 0, 3, 2\rangle$ and $|N, 0, 2, 3\rangle$ with $N = 1, 2, 3, 4, 5$.
- In Fig. 5.6 (i), the BOPs approach to the asymptotic limit $\Delta E_{23s} + 20B$ and correspond to one KRb being in the fourth excited state and the second one in the ground state, with the wave functions on the coupled basis (5.6) $|4, 0, 4, 0\rangle$ and $|4, 0, 0, 4\rangle$.
- In Fig. 5.6 (j), the BOPs approach to the asymptotic limit $\Delta E_{23s} + 22B$ and correspond

to one KRb being in the fourth excited state and the second one in the first excited state, with the wave functions on the coupled basis (5.6) $|N, 0, 4, 1\rangle$ and $|N, 0, 1, 4\rangle$ with $N = 3, 4, 5$.

- In Fig. 5.6 (k), the BOPs approach to the asymptotic limit $\Delta E_{23s}+24B$ and correspond to the two KRb being in the third excited state, with the wave functions on the coupled basis (5.6) $|N, 0, 3, 3\rangle$ with $N = 0, 1, 2, 3, 4, 5, 6$.

Many of the electronic states presented in the panels of Fig. 5.6 are double degenerate. As in the electronic states analyzed in the previous section, these BOPs show an oscillatory behaviour as R increases but now they possess potential wells with depths reaching a few tens to few hundreds MHz. In these adiabatic electronic states, we find unstable and stable configurations of the Rydberg pentaatomic with adiabatic potential energy curves overall decreasing and increasing, respectively, as R decreases and having wells too shallow to accommodate bound vibrational levels. We can observe that some of the BOPs present an asymmetric double-well structure in the electronic states: $\Delta E_{23s} + 12B$, $\Delta E_{23s} + 18B$, $\Delta E_{23s} + 24B$, see panels Fig. 5.6 (f), Fig. 5.6 (h), and Fig. 5.6 (k), respectively. In the latter potential wells, a few vibrational states exist with vibrational wave functions being delocalized with respect to the two wells.

The energy shifts of these electronic sates evolving from Rb($23s$) from the corresponding asymptotic limits, i. e., $\Delta E_{23s} + 12B$ and $\Delta E_{23s} + 24B$, are smaller than 2 GHz at $R = 500a_0$, and are significantly smaller than the shifts of the BOPs from the Rydberg manifold Rb($n = 20$, $l \geq 3$), which reach approximately ~ 45 GHz at $R = 500$ a_0, see Fig. 5.3. This can be explained in terms of the smaller state space, formed by the Rydberg state Rb($23s$), that can mix to generate these adiabatic electronic states compared to the large number of Rydberg states with $n = 20$, $l \geq 3$ and m_l forming the degenerate manifold Rb($n = 20$, $l \geq 3$) contributing to the BOPs presented in Fig. 5.3. In addition, the electric fields due to the Rydberg electron of Rb($23s$) are weaker than those from the Rydberg manifold Rb($n = 20$, $l \geq 3$). As an example, we present in Fig. 5.7 the absolute value of the matrix elements of the electric field along the Z axis for a separation between Rb^+ and each KRb of $R = 600$ a_0. These matrix elements are defined in Appendix A. Due to the larger spatial extension of the radial wave function of the Rydberg state Rb($23s$) compared to those from Rb($n = 20$, $l \geq 3$), the matrix elements $\langle 0, 0|F^{e,Z}_{ryd}(R, 0, 0, \mathbf{r})|l_2, 0\rangle$ with $l_2 \geq 3$ are in most cases smaller than those involving two wave functions of the degenerate manifold. In addition, within the degenerate manifold there are many non-zero matrix elements of the electric field components, $\langle l_1, m_1|F^{e,Z}_{ryd}(R, 0, 0, \mathbf{r})|l_2, m_2\rangle$, $l_1, l_2 \geq 3$, affecting the two diatomic molecules, compared to the few non-zero components due to the coupling of Rb($23s$), with the Rb($n = 20$, $l \geq 3$) states, i. e., $\langle 0, 0|F^{e,Z}_{ryd}(R, 0, 0, \mathbf{r})|l_j, 0\rangle$ and $\langle 0, 0|F^{e,Z}_{ryd}(R, 0, 0, \mathbf{r})|l_j, \pm 1\rangle$. Since the interaction with the electric field produces the same impact on both diatomic molecules the BOPs become degenerate.

The BOPs for total magnetic quantum number $M_J = 1$ evolving from the Rydberg state and the two diatomic molecules in the rotational excitations states up to $N_i = 6$, $i = 1, 2$, are shown in Fig. 5.8. At large separations between the diatomic molecules and the ionic core, the system could be considered uncoupled and the adiabatic electronic states approach a limit which depend on the states of the KRb molecules and of the Rydberg electron. For these electronic states, we have the following energetical limits:

- In Fig. 5.8 (a), the BOPs approach to the asymptotic limit $\Delta E_{23s}+2B$ and correspond

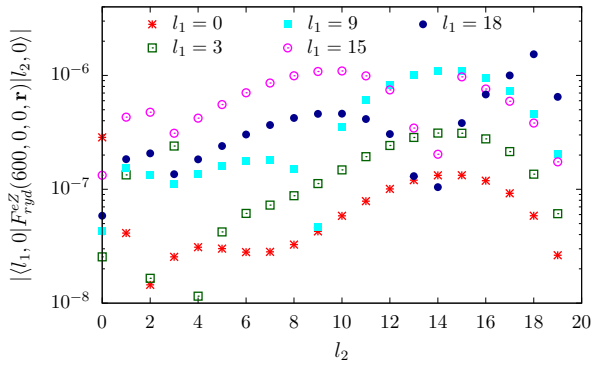

Figure 5.7: Expectation values of the Z component of the electric field due to the Rydberg electron $|\langle l_1, 0|F_{ryd}^{e,Z}(600, 0, 0, \mathbf{r})|l_2, 0\rangle|$.

to one diatomic molecule being in the rotational ground state, and the other one in the first excited state, with the wave functions on the coupled basis (5.6) $|1, 1, 1, 0\rangle$ and $|1, 1, 0, 1\rangle$.

- In Fig. 5.8 (b), the BOPs approach to the asymptotic limit $\Delta E_{23s} + 4B$ and correspond to the two diatomic molecules being in the first rotational excited state, with the wave functions on the coupled basis (5.6) $|N, 1, 1, 1\rangle$ with $N = 1, 2$.
- In Fig. 5.8 (c), the BOP approach to the asymptotic limit $\Delta E_{23s} + 6B$ and correspond to one diatomic molecules being in the ground state, and the other one in the second rotational excited state, with the wave functions on the coupled basis (5.6) $|2, 1, 0, 2\rangle$ and $|2, 1, 2, 0\rangle$.
- In Fig. 5.8 (d), the BOPs approach to the asymptotic limit $\Delta E_{23s} + 8B$ and correspond to one diatomic molecules being in the first excited state, and the other one in the second rotational excited state, with the wave functions on the coupled basis (5.6) $|N, 1, 1, 2\rangle$ and $|N, 1, 2, 1\rangle$ with $N = 1, 2, 3$.
- In Fig. 5.8 (e), the BOPs approach to the asymptotic limit $\Delta E_{23s} + 12B$ and correspond to the two diatomic molecules being in the second rotational excited state, or one of them in the third excited state and the second one in the ground state, with the wave functions on the coupled basis (5.6) $|N, 1, 2, 2\rangle$ with $N = 1, 2, 3, 4$ and $|N, 1, 3, 0\rangle$ and $|N, 1, 0, 3\rangle$, respectively.
- In Fig. 5.8 (f), the BOPs approach to the asymptotic limit $\Delta E_{23s} + 14B$ and correspond to one KRb being in the third excited state and the second one in the first excited state, with the wave functions on the coupled basis (5.6) $|N, 1, 3, 1\rangle$ and $|N, 1, 1, 3\rangle$ with $N = 2, 3, 4$.
- In Fig. 5.8 (g), the BOPs approach to the asymptotic limit $\Delta E_{23s} + 18B$ and correspond to one KRb being in the third excited state and the second one in the second excited state, with the wave functions on the coupled basis (5.6) $|N, 1, 3, 2\rangle$ and $|N, 1, 2, 3\rangle$ with $N = 1, 2, 3, 4, 5$.
- In Fig. 5.8 (h), the BOPs approach to the asymptotic limit $\Delta E_{23s} + 20B$ and correspond to one KRb being in the fourth excited state and the second one in the ground state, with the wave functions on the coupled basis (5.6) $|4, 1, 4, 0\rangle$ and $|4, 1, 0, 4\rangle$.

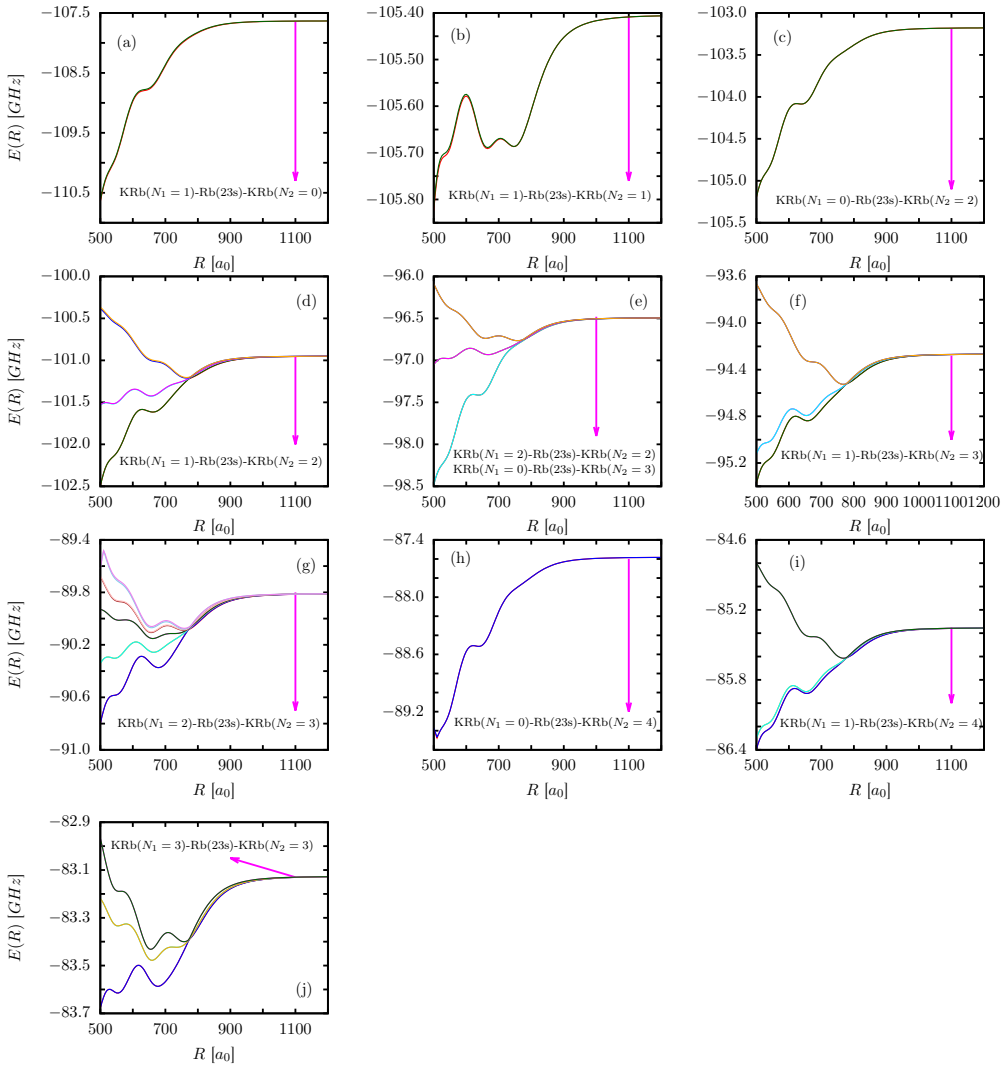

Figure 5.8: For the symmetric configuration of the Rydberg molecule, adiabatic electronic potentials versus the internuclear separation $R_1 = R_2 = R$ evolving from the Rydberg state Rb($23s$) and the diatomic molecules in rotational excitations in the coupled basis $N_i = 6$ with $i = 1, 2$. The total magnetic quantum number of the adiabatic electronic potentials is $M_J = 1$.

- In Fig. 5.8 (i), the BOPs approach to the asymptotic limit $\Delta E_{23s} + 22B$ and correspond to one KRb being in the fourth excited state and the second one in the first excited state, with the wave functions on the coupled basis (5.6) $|N, 1, 4, 1\rangle$ and $|N, 1, 1, 4\rangle$ with $N = 3, 4, 5$.
- In Fig. 5.8 (j), the BOPs approach to the asymptotic limit $\Delta E_{23s} + 24B$ and correspond to the two KRb being in the third excited state, with the wave functions on the coupled basis (5.6) $|N, 1, 3, 3\rangle$ with $N = 1, 2, 3, 4, 5, 6$.

These $M_J = 1$ adiabatic electronic states show similar features as those discussed for the $M_J = 0$ ones. They are double degenerate, and possess potential wells with depths reaching

a few tens to few hundreds MHz, some of them having an asymmetric double-well structure, which could accommodate vibrational bound states. Again, there are unstable and stable configurations of the Rydberg pentaatomic with adiabatic potential energy curves overall decreasing and increases, respectively, as R decreases.

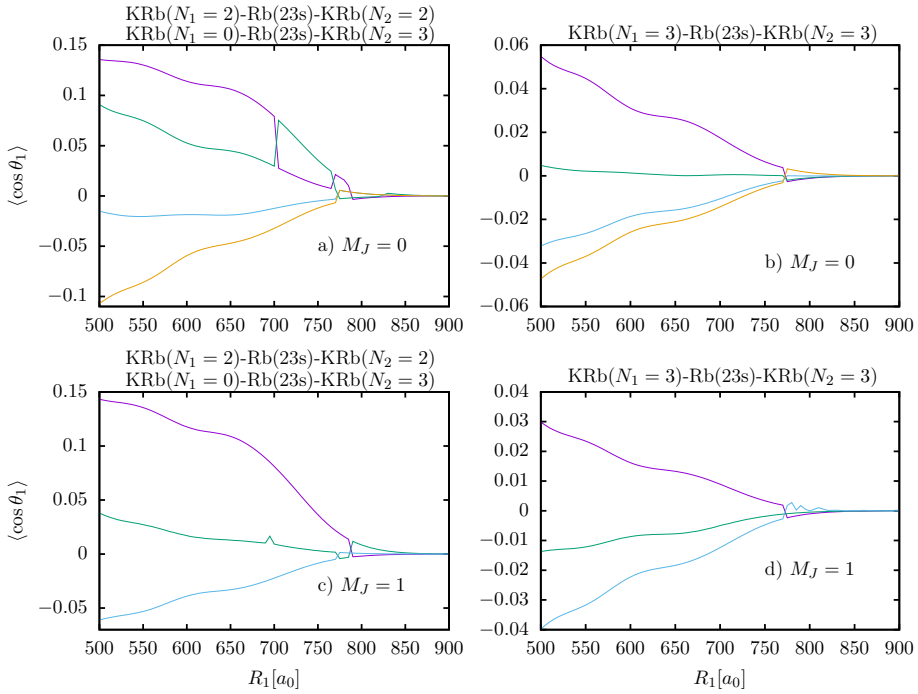

Figure 5.9: For the symmetric configuration of the Rydberg molecule, adiabatic electronic potentials versus the internuclear separation $R_1 = R_2 = R$ evolving from the Rydberg state Rb($23s$) and the diatomic molecules in rotational excitations $|N, M_N, 3, 3\rangle$. The total magnetic quantum number of the results is (a) $M_J = 0$, and (b) $M_J = 1$.

Regarding the directional properties of the KRb molecules, we present only the orientation of the first ditomic molecule, since for the orientation of the second one, it holds $\langle \cos\theta_2 \rangle = -\langle \cos\theta_1 \rangle$, for the electronic states evolving from the Rydberg state Rb($23s$), $\Delta E_{23s} + 12B$ Fig. 5.9 (a) and (c) with the magnetic quantum number $M_J = 0$ and $M_J = 1$ respectively, and the other electronic state $\Delta E_{23s} + 24B$ Fig. 5.9 (b) and (d) with $M_J = 0$ and $M_J = 1$ respectly. The adiabatic electronic states are presented in Fig. 5.6 (f) and Fig. 5.8 (e) for the the Rydberg pentaatomic molecules KRb($N = 3$)-Rb($23s$)-KRb($N = 0$), KRb($N = 0$)-Rb($23s$)-KRb($N = 3$) and KRb($N = 2$)-Rb($23s$)-KRb($N = 2$), and in Fig. 5.6 (k) and Fig. 5.8 (j) for the Rydberg pentaatomic molecule KRb($N = 3$)-Rb($23s$)-KRb($N = 3$). As can be observed in the panels of Fig. 5.9, the orientation is very small due to the weak electric fields created by the Rydberg electron in Rb($23s$). Additionally, the large rotational excitations give rise to large kinetic energies which should be compensated by the interaction with the Rydberg electric field. In contrast, for the two diatomic molecules within the lowest lying potential evolving from Rb($23s$), i. e., the KRb molecules in $N_1 = N_2 = 0$, not shown here, we obtain $|\langle \cos\theta_i \rangle| = 0.32$ for $R = 500\ a_0$, which is similar to the orientation achieved

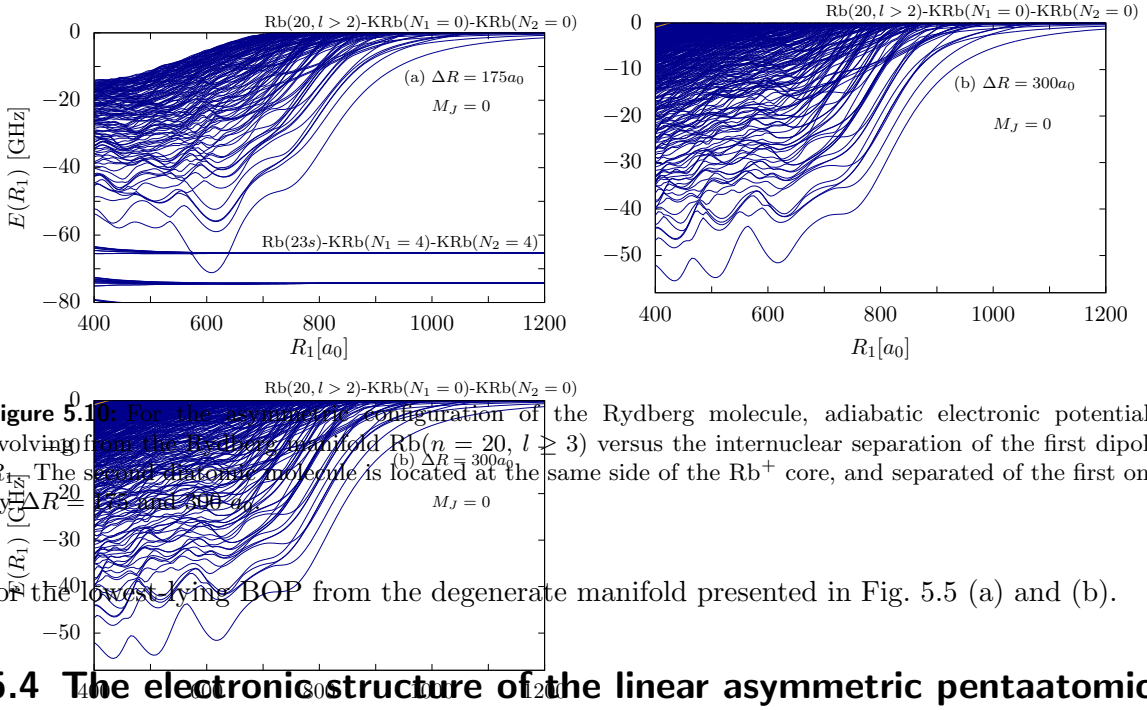

Figure 5.10: For the asymmetric configuration of the Rydberg molecule, adiabatic electronic potentials evolving from the Rydberg manifold Rb($n = 20$, $l \geq 3$) versus the internuclear separation of the first dipole R_1. The second diatomic molecule is located at the same side of the Rb^+ core, and separated of the first one by $\Delta R = 175$ and 300 a_0.

for the lowest-lying BOP from the degenerate manifold presented in Fig. 5.5 (a) and (b).

5.4 The electronic structure of the linear asymmetric pentaatomic Rydberg molecule

In this section, we explore the asymmetric configuration of the Rydberg molecule with the two diatomic molecules located at the same side of the Rydberg core Rb-KRb-KRb, see the sketch presented in Fig. 5.1 (b). The separation between the two diatomic molecules is kept large enough so that the dipole-dipole interaction between both of them could be neglected. For instance, this dipole-dipole interaction amounts approximately to 0.11 GHz for two fully oriented KRb molecules separated by 150 a_0, which is significantly smaller than the few tens of GHz energy shifts from the Rydberg manifold obtained for both the symmetric and asymmetric configurations of the pentaatomic ultralong-range molecule.

First, we consider the Rydberg molecule in which the distances of the two KRb molecules from the Rydberg core increase, while their relative separation is kept constant to $\Delta R = R_2 - R_1 = 175$ a_0 and 300 a_0. The adiabatic potentials curves with $M_J = 0$ are shown in Fig. 5.10 as a function of the internuclear distance of the first dipole R_1. Since $R_2 = R_1 + \Delta R$, the two diatomic molecules are exposed to electric fields with different strengths but along the same direction. The lowest-lying BOP from this Rydberg manifold is energetically well separated from the rest of the electronic states. Compared to the triatomic Rydberg molecule and to the symmetric configuration of KRb-Rb*-KRb, the energy shifts of the adiabatic potentials from the Rydberg manifold Rb($n = 20$, l≥ 3) are larger. For these Rydberg molecule, the two diatomic molecules are exposed to electric fields of different strengths but since they have the same direction, the energies shifts are larger than those of the symmetric Rydberg molecule. For $\Delta R = 175$ a_0, the minimum of the lowest-lying adiabatic potential is below the BOP evolving from Rb($23s$) and the diatomic molecules in the rotational excitations $|N, M_N, 4, 4\rangle$, and these two sets of adiabatic electronic states suffer several avoided crossings.

We analyze now the directional properties of the KRb molecules in this asymmetric

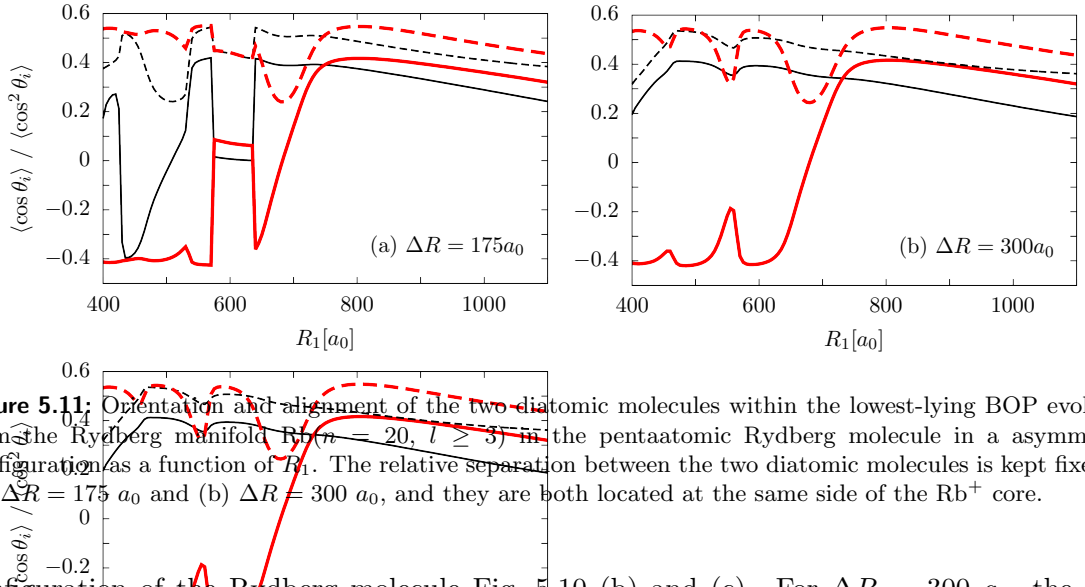

Figure 5.11: Orientation and alignment of the two diatomic molecules within the lowest-lying BOP evolving from the Rydberg manifold Rb($n = 20$, $l \geq 3$) in the pentaatomic Rydberg molecule in a asymmetric configuration as a function of R_1. The relative separation between the two diatomic molecules is kept fixed to (a) $\Delta R = 175\ a_0$ and (b) $\Delta R = 300\ a_0$, and they are both located at the same side of the Rb^+ core.

configuration of the Rydberg molecule Fig. 5.10 (b) and (c). For $\Delta R = 300\ a_0$, the first diatomic molecule shows a similar orientation and alignment as in the first diatomic molecule in the symmetric configuration. The second KRb is located further 300 a_0 away from the Rb^+ than the first one, as a consequence, it is oriented against the Rydberg core, and after a weak oscillation its value monotonically decreases. For $\Delta R = 175\ a_0$, the orientation and alignment of the two KRb show a more complex behaviour as R_1 increases, which is characterized by the sudden change for $R_1 \approx 580\ a_0$ and $R_1 \approx 640\ a_0$, due to the avoided crossings with the BOPs evolving from Rb($23s$) and the diatomic molecules in the rotational excitations $|N, M_N, 4, 4\rangle$. Between these two values of R_1, the alignment and orientation keep an almost constant value. For $R_1 \gtrsim 640\ a_0$, the orientation and alignment behaviour of the two diatomic molecule resemble those from the configuration with the relative separation $\Delta R = 300\ a_0$, monotonically decreasing and approaching the corresponding field-free limits.

In the second asymmetric configuration, we assume that the position of the first diatomic

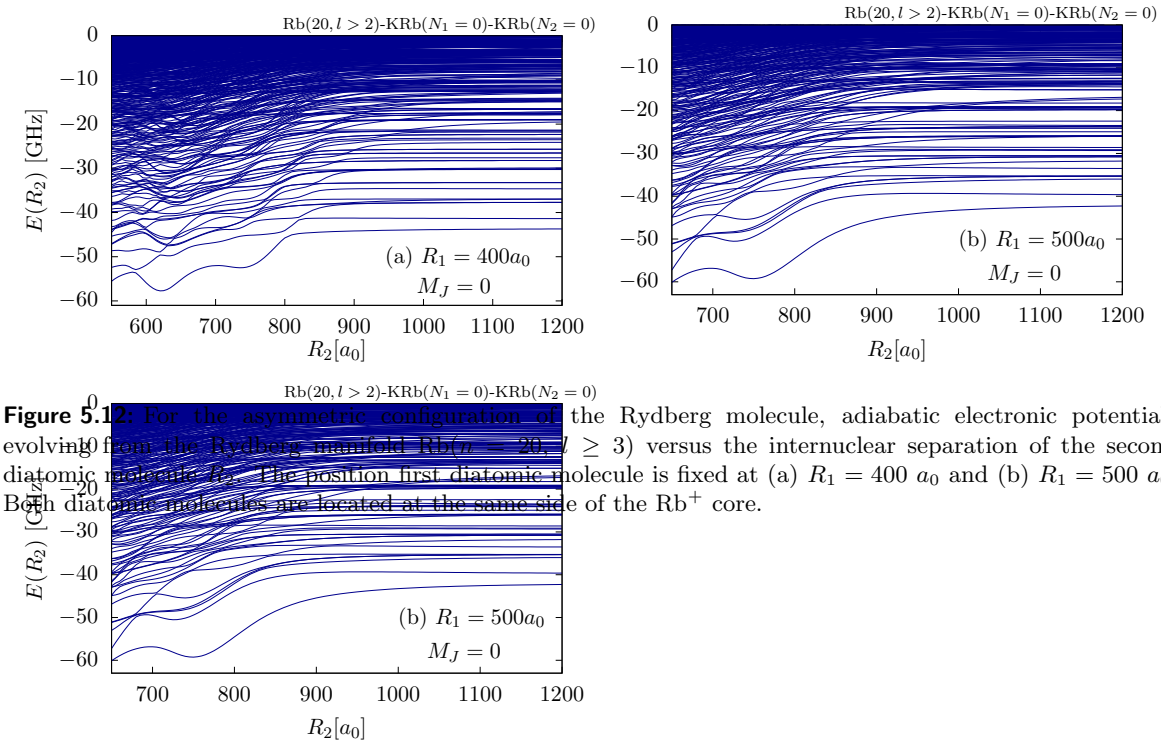

Figure 5.12: For the asymmetric configuration of the Rydberg molecule, adiabatic electronic potentials evolving from the Rydberg manifold Rb($n = 20$, $l \geq 3$) versus the internuclear separation of the second diatomic molecule R_2. The position first diatomic molecule is fixed at (a) $R_1 = 400\ a_0$ and (b) $R_1 = 500\ a_0$. Both diatomic molecules are located at the same side of the Rb^+ core.

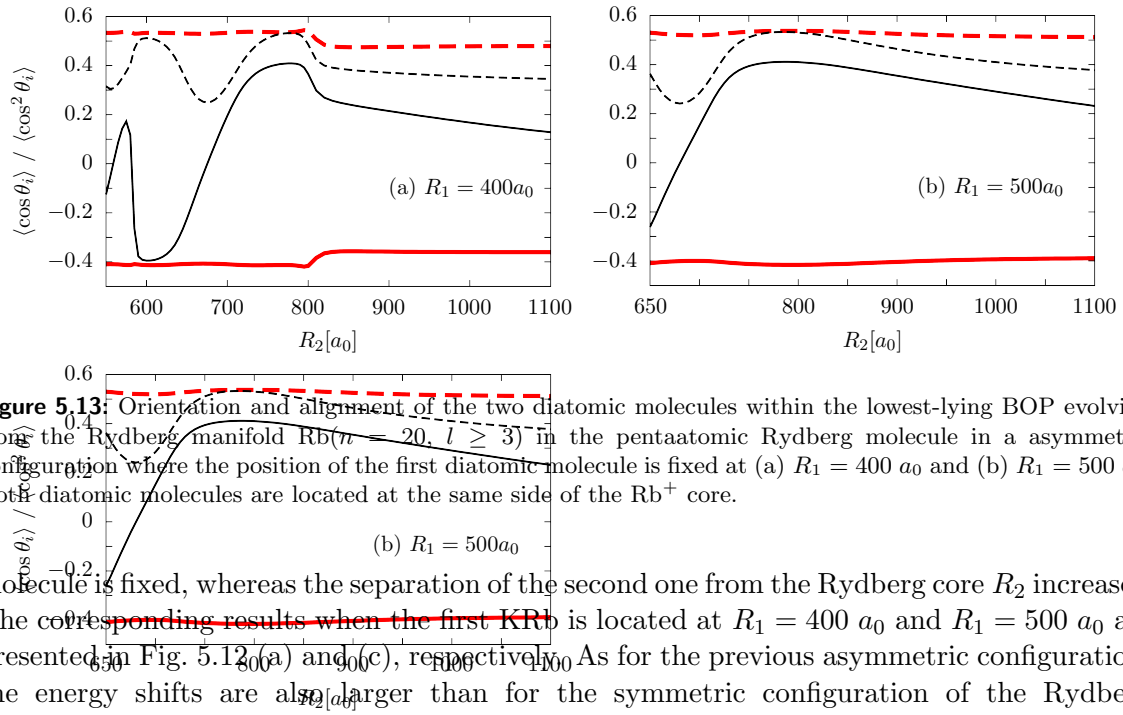

Figure 5.13: Orientation and alignment of the two diatomic molecules within the lowest-lying BOP evolving from the Rydberg manifold Rb($n = 20$, $l \geq 3$) in the pentaatomic Rydberg molecule in a asymmetric configuration where the position of the first diatomic molecule is fixed at (a) $R_1 = 400\ a_0$ and (b) $R_1 = 500\ a_0$. Both diatomic molecules are located at the same side of the Rb^+ core.

molecule is fixed, whereas the separation of the second one from the Rydberg core R_2 increases. The corresponding results when the first KRb is located at $R_1 = 400\ a_0$ and $R_1 = 500\ a_0$ are presented in Fig. 5.12 (a) and (c), respectively. As for the previous asymmetric configuration, the energy shifts are also larger than for the symmetric configuration of the Rydberg pentaatomic molecule, which is due to the cooperative effect of the electric fields in both diatomic molecules. The lowest-lying potential from the Rydberg manifold Rb($n = 20$, $l \geq 3$) present an oscillatory behavior with broad minima of a few GHz depths, before they reach a plateau like behavior for large values of R_2. In this limit, the BOPs approach the energies of the trimer Rydberg molecule with the KRb located at either at $R_1 = 400\ a_0$ or $R_1 = 500\ a_0$.

Finally, we analyze the rotational dynamics of the two diatomic molecules within the pentaatomic Rydberg molecule in this asymmetric configuration presented in Fig. 5.12 (b) and (d). In both cases, the fist diatomic molecule is moderately anti-oriented and aligned, both expectation values present a plateau-like behaviour as R_2 increases. In contrast, the directional properties of the second KRb oscillate as R_2 increases, it is firstly anti-oriented, and becomes oriented once the interaction due to the Rydberg core starts to dominate. For large values of R_2, the orientation and alignment of this second diatomic molecule approach the field-free values 0 and 1/3, respectively.

Chapter 6

Conclusions and outlook

Let us finish by summing up our findings and providing an outlook on perspectives of future research on Rydberg molecules, which are a natural continuation of the results presented here. In this thesis, we have theoretically investigated the electronic structure and properties of two types of polyatomic Rydberg molecules, which differ on the biding mechanism that create them. The first Rydberg molecule is formed by a Rydberg rubidium atom and two ground-state Rb atoms, which are bound due to the low-energy collisions between the Rydberg electron and the ground state perturbers. The second Rydberg molecule is formed by a Rydberg atom and one or two diatomic heteronuclear molecules. In this case, the anisotropic scattering of the Rydberg electron from the permanent electric dipole moment of the polar molecules allows for the creation of the ultralong-range Rydberg molecules. We now describe in more detail the conclusions obtained in the two parts of this dissertation, and for each part, we provide an extensive list of open problems related to these Rydberg molecules, which are a natural continuation of the work performed in this thesis.

In the first part of this thesis, we have investigated the impact of an external electric field in an ultralong-range triatomic Rydberg molecules formed by a Rydberg rubidium atom and two ground-state Rb atoms in the presence of an external electric field. Although previous works have studied triatomic molecules formed by a Rydberg rubidium atom and a ground state diatomic molecule KRb in an electric field [76, 77], this was the first investigation of a triatomic ULRM formed by two ground state atoms and a Rydberg atom in an electric field. We have considered the symmetric and asymmetric linear configurations, as well as a planar one with the neutral atoms located at the same distance from the Rydberg core. We have performed an analysis of the electronic structure for the Rb Rydberg atom in the degenerate manifold Rb($n = 35, l \geq 3$). For the linear configurations, in the absence of the electric field several molecular states, with Σ and Π symmetry, are split from the Rb($n = 35, l \geq 3$) manifold, showing an oscillatory behaviour with many wells accommodating vibrational levels where the Rydberg molecule would exist. For the planar configuration, we encounter that the molecular states only show a significant dependence on angle formed by the two straight lines from the ionic core to each of the ground-state atoms. The interaction with the electric field favouors the symmetric linear configuration and strengthen the bound state character of molecular states, and vibrational states with the spatial extensions of a few hundreds Bohr radii could appear. In addition, we have investigated the impact of the electric field on electronic states of Rb-Rb-Rb evolving from the low-angular momentum states of the Rydberg electron. We have considered a planar configuration, where we have investigate the lowest-lying BOP evolving from the Rb($n = 35, l \geq 3$) manifold, as well as the BOP from Rb-Rb($38s$)-Rb. Both electronic states

show a weak dependence on the angle formed by the internuclear axis of the ground state atoms and the Rydberg one, and that the electric field tends to favour the linear configuration.

For diatomic Rydberg molecules, it has been shown that the Rydberg-atom fine structure and the hyperfine coupling of the ground-state atom significantly alter the adiabatic electronic potentials evolving from the Rydberg atom in such excited states [54, 62, 64, 65]. Thus, an immediate extension of the work presented in this thesis would be to investigate the impact of an external electric field on electronic structure and vibrational properties of an ultralong-range diatomic and triatomic molecules, but including the Rydberg-atom fine structure and the hyperfine coupling of the ground-state atoms. By including these couplings for a diatomic Rydberg molecule, the potential energy surfaces depend on the hyperfine states of the ground-state atoms as well as on the fine structure of the Rydberg atom, and, the complexity of the molecular electronic states is significantly enhanced. Analogously, the complexity of the electronic structure of the Rydberg triatomic molecule should be also enhanced. Another posible extension would be to explore the impact of only a magnetic field, or combined electric and magnetic fields on these ultralong-range triatomic molecules. Analogously to the diatomic Rydberg molecule, one might expect a strong level repulsion in the presence of a pure magnetic field, which might provoke that the field-free potential wells vanish [66, 69]. In an experimental set up, it is extremely complicated to reduce the impact of static electric fields, the so-called stray fields, on Rydberg atoms [108]. Taking into account that experimentally more complex polyatomic Rydberg molecules formed by more than three ground state rubidium atoms [73], it might be interesting to investigate the impact of an external electric fields in these tetraatomic Rydberg molecules.

The second part of the thesis is devoted to investigate ultralong-range Rydberg polyatomic molecules formed by a Rydberg Rubidium atom and one or two KRb diatomic rotational molecules. The binding mechanism of these exotic molecules is due to the interaction of the electric dipole moments of the diatomic molecules with the electric fields due to the Rydberg electron and Rydberg core. We have described the hybridization of the rotational motion of the diatomic molecules due to the Rydberg electric fields within the rigid rotor approximation. In the framework of the Born-Oppenheimer approximation, we have obtained and analyzed the adiabatic electronic potentials with total magnetic quantum numbers $M_J = 0, 1$ and 2 for the Rydberg triatomic molecules, and with $M_J = 0$ and 1 for the pentaatomic one, as a function of the separations between the Rb^+ core and one or two KRb molecules. The electronic structure of these Rydberg molecules strongly depends on the Rydberg state of the rubidium atom involved in their formation.

For the triatomic Rydberg molecule, we have investigated the adiabatic electronic states evolving from the degenerate manifolds Rb(n, $l \geq 3$) as the principal quantum number n of the Rydberg state increases. We observe that by increasing the excitation of the Rydberg electron, i. e., increasing n, the energy shift of these electronic states from the degenerate manifold decreases, which indicates that the KRb molecule is exposed to weaker electric fields. In addition, the depths of the potential wells within these BOPs also decrease and they become more shallow. By solving the Schrödinger equation of the Rydberg triatomic molecule, we have computed the vibrational spectrum of these electronic states. The outermost minimum of the lowest-lying adiabatic electronic potential evolving from the Rydberg manifold Rb(n,

$l \geq 3$) can accommodate several vibrational levels, with vibrational energy spacing on the GHz regime. As the principal quantum number n of the involved Rydberg manifold increases, the number of vibrational bound states decreases. These vibrational energy spacing in the few GHz range could be resolved with current experimental techniques. Experimentally, it is very challenging to create and observe these Rydberg triatomic molecule because it is complicated to create a Rydberg atom with a high orbital angular momentum state $l \geq 3$. Normally, alkali Rydberg atoms are created using a standard two-photon excitation scheme, and have orbital quantum number $l = 0$ and $l = 2$. Recently, strongly polar trilobite Rydberg molecules have been experimentally created in an electronic states evolving from a high-orbital angular momentum Rydberg electron [63]. Due to the ground-state hyperfine interaction, the electron-neutral singlet and triplet scattering channels are coupled, which allows to access Rb_2 Rydberg molecules in these electronic states evolving from a high-orbital angular momentum Rb^* via two-photon laser excitation. These experimental results open the doorway to design a similar experimental technique to access the electronic states of the Rydberg trimer presented in this thesis.

Regarding the linear symmetric and asymmetric configurations of the Rydberg pentaatomic molecule, we have demonstrated the existence of stable adiabatic electronic states evolving from the degenerate manifold $\mathrm{Rb}(n = 20, l \geq 3)$. For the linear symmetric configuration, we have observed that the presence of the second diatomic molecule strongly affect the electronic structure, where we encounter more electronic states and it is more complex. However, the energy shift from the Rydberg manifold $\mathrm{Rb}(n = 20, l \geq 3)$ are not significantly modified, and compared to the corresponding BOPs of the Rydberg triatomic molecule, we encounter shifts of a few MHz. This can be explained in terms of the Rydberg-electron electric fields that suffer the two diatomic molecules, which possess the same strengths but different directions due to the symmetric arrangement of the two KRb. These adiabatic electronic potentials also show an oscillatory behaviour and possess potential wells with depths of a few GHz. In contrast, the electronic structures of the Rydberg pentaatomic molecule in the analyzed asymmetric configurations significantly differs from the corresponding spectrum of the symmetric Rydberg pentaatomic molecule, and the energies shifts from the Rydberg manifold are larger than in the symmetric configuration and in the Rydberg triatomic molecule. In these asymmetric arrangements, the two diatomic molecules are exposed to Rydberg-induced electric fields with different strengths, whose effects becomes additive, and the energies shifts become larger. For the symmetric and asymmetric configurations, we have estimated the vibrational biding energies of the potential wells in these BOPs by fitting a harmonic oscillator potential to these wells. We have obtained that they can accommodate a few vibrational bound levels where the Rydberg pentaatomic and triatomic molecules exist, and that the biding energies are on the GHz regime. In addition, we have studied the directional properties, i. e., orientation and alignment, of the two KRb molecules within the Rydberg pentaatomic molecule. The diatomic molecules show a significant orientation and alignment in the BOPs evolving from the Rydberg degenerate manifold.

Motivated by the experimental accessibility to the Rydberg states with low orbital angular momentum, we have also investigated the adiabatic states of the Rydberg triatomic and pentaatomic molecules evolving from these quantum defect states and the diatomic molecule in the ground state but also in excited rotational states. For both Rydberg molecules, we encounter unstable electronic states, but also stable ones possessing potential wells with

depths of a few hundreds MHz. For the Rydberg triatomic molecule, we have computed the binding energies of these stable electronic states by solving the Schrödinger equation of the rovibrational Hamiltonian, and we have found that they can support several vibrational bound levels with energy spacing on the MHz regime. For the electronic states of the Rydberg pentaatomic molecule, we have estimated the binding energies of the vibrational spectrum are also on the MHz regime. Let us remark that the small energy spacing in the vibrational bound states, with the vibrational transition frequencies in the few MHz range requieres small laser line widths to resolve them. For instance, the group of Prof. T. Killian (Rice University, Houston) have a the 319 nm laser with linewidth of $\sim$ 400 kHz [57] which could help to experimentally resolve these individual molecular levels. The diatomic molecules forming these Rydberg species show small degrees of orientation, which can explained by two different effects. First, the electric fields produced by the Rydberg electron on these Rydberg excited states is smaller due the different spatial extension of the radial wave function of the Rydberg state $\mathrm{Rb}(n_1 l_1)$, with $l_1 = 0, 1, 2$, compared to those from $\mathrm{Rb}(n, l \geq 3)$, as a consequence the matrix elements involving one state from the quantum-defect Rydberg state are in most cases smaller than those involving two wave functions of the degenerate manifold. In addition, there is a smaller state space, formed by the Rydberg state $\mathrm{Rb}(n's)$, that can mix to generate these adiabatic electronic states compared to the large number of Rydberg states with $n, l \geq 3$ and m_l forming the degenerate manifold $\mathrm{Rb}(n, l \geq 3)$. Second, the KRb molecules are in excited rotational states and have large rotational kinetic energies to be compensated by the electric-field interaction, therefore, stronger fields are needed to produce a similar effect as in the electronic states evolving from the Rydberg degenerate manifold $\mathrm{Rb}(n, l \geq 3)$.

The studies presented in this thesis about the polyatomic Rydberg molecules formed by a Rydberg atom and one or more diatomic polar molecules could be continued in several ways. Using the computational techniques developed within the group, one could perform an exhaustive study of other possible candidates to create these triatomic Rydberg molecules. Currently, many experiments around the world have a hybrid systems of two species of ultracold atoms where diatomic heteronuclear molecules in their absolute ground states have been produced, such as RbCs [109, 110], KCs [111], NaK [113], KRb [112], LiNa [114], NaCs [115–117], YbRb [118], OH [119], SrF [120], among others. The selection of the diatomic polar molecule should be based on their permanent electric dipole moment, which should be subcritical $d < 1.639$ D, in order to prevent binding of the Rydberg electron to the diatomic molecule [78–81]. Among the ultracold molecules experimentally available listed above, some candidates are LiNa, RbCs, KRb and YbRb, having permanent electric dipole moments at the equilibrium distance $d = 0.561, 1.238, 0.615$, and 0.987 D, respectively, [121, 122]. The Rydberg spectra of the alkali atoms forming these diatomic molecules has been investigated both theoretically and experimentally in detail. Furthermore, it is also interesting to compare the electronic structure of the Rydberg triatomic molecule depending on the involved Rydberg atom. Since the quantum defects are specific of each Rydberg atom, the Rydberg energies for the states with low rotational angular momentum $l \lesssim 3$ shifted from the degenerate manifold of $\mathrm{Rb}(n, l \gtrsim 4)$ and $\mathrm{K}(n, l \gtrsim 4)$ are different. Thus, the adiabatic electronic structure of K^*-KRb as well as the vibrational binding energies should significantly be different from the results presented in this thesis for the Rydberg molecule Rb^*-KRb.

Regarding the Rydberg pentaatomic molecules, one could explore the potential energy curves in a planar triangular configuration. For instance, we could considered the two diatomic molecules located at the minima of an optical lattice and the Rydberg atom above them. In such a planar configuration, the azimuthal symmetry is lost and the total magnetic quantum number is not conserved, which significantly increases the numerical complexity to solve the Schrödinger equation of this Rydberg molecule. In particular, the basis set expansion of the wave function should include all possible values of the magnetic quantum number, i. e., M_J, i. e., $|M_J| \leq J$ in the coupled wave functions (5.5). For instance, including the Rydberg manifold Rb($n = 20$, $l \geq 3$) and Rb($23s$), and rotational excitations up to $N_i = 5$, the dimension of the Hamiltonian matrix is larger than half a million being computationally very challenging to obtain the eigenvalues of the Rydberg pentaatomic molecule in this planar configuration.

In addition, more complex ultralong-range Rydberg molecules formed by one Rydberg atom and several diatomic polar molecules could be investigated. Due to the numerical complexity of the theoretical description of a Rydberg pentaatomic molecule in a planar configuration explained above, these polyatomic Rydberg systems could be analyzed for diatomic open-shell diatomic molecules, such as OH, OD, LiO and NaO. The field-dressed rotational spectra of these molecules are characterized by fine-structure interactions and the Λ-doubling effects [82]. As a consequence, the rotational motion of these molecules in sufficiently weak electric fields can be approximately described by a two state model [83, 84]. Such an approximation facilitates the computational analysis because the size of the Hamiltonian matrix is drastically reduced, i. e., from more half a million to $4n^2$, with n the principal quantum number, for the pentaatomic molecule, being then realistic to compute the adiabatic electronic potential curves and surfaces of these molecules as it was previously done for the triatomic ones [74–76]. The first step should be to investigate if the description of these polyatomic Rydberg molecules should include the three cartesian componentes produced by the Rydberg electron and core electric field, or only the component along the Z-axis as it has been done in previous studies [74–76]. One could consider several configurations in two- and three-dimensions. For a pentaatomic Rydberg molecule, the planar and collinear configurations could be analyzed and compared seeking for the deepest potential well in the adiabatic electronic states which will give rise to the most stable configuration. More complex polyatomic Rydberg molecules in symmetric configurations based on geometric figures could also be investigated. Some of examples of planar configurations are: three Λ-doublet molecules located on the corners of an equilateral triangle and the Rydberg core at the center, and four of them located on the corners of a square and the ionic at the center, and so on. One could even design three-dimensional polyatomic molecule with eight polar molecules located at the corners of a cube and the Rydberg core at its center. For these polyatomic Rydberg molecules, one could explore the potential energy curves of the adiabatic electronic states, and the directional properties of the diatomic molecules, where frustration effects on the orientation of the molecules due to these symmetric arrangements might be expected.

Chapter 7

Conclusiones y perspectivas

Por último, resumimos los resultados obtenidos en esta tesis doctoral, e indicamos varios posibles trabajos de investigación sobre estas moléculas Rydberg, que suponen una continuación natural de los estudios llevados a cabo en esta tesis. En esta tesis hemos investigado teóricamente la estructura electrónica y las propiedades de dos tipos de moléculas Rydberg poliatómicas que difieren en su mecanismo de enlace. La primera molécula Rydberg está formada por un átomo de rubidio en un estado Rydberg y otros dos átomos de Rb en el estado fundamental. En este caso, la ligadura aparece debido a la colisión a baja energía entre el electrón Rydberg y cada uno de los dos átomos de Rb en el estado fundamental. La segunda molécula Rydberg está formada por un átomo Rydberg y una molécula o dos moléculas diatómicas heteronucleares. En este caso, la dispersión anisotrópica del electrón Rydberg con el momento dipolar eléctrico permanente de las moléculas polares permite la creación de estas moléculas Rydberg de alcance ultra-largo. A continuación describimos, en detalle las conclusiones obtenidas en las dos partes de esta tesis doctoral, y proporcionamos una listado de problemas abiertos relacionados con estas moléculas Rydberg, que suponen una continuación natural de los resultados aquí obtenidos.

En la primera parte de esta tesis, hemos investigado el impacto de un campo eléctrico externo en una molécula Rydberg triatómica de alcance ultra largo formada por un átomo de rubidio en estado Rydberg y dos átomos de Rb en el estado fundamental. Aunque en trabajos previos se habían estudiado moléculas triatómicas Rydberg formadas por un átomo de Rb en un estado Rydberg y una molécula diatómica de KRb en el estado fundamental, en un campo eléctrico [76, 77], esta es la primera vez que se ha investigado una molécula Rydberg formada por dos átomos en el estado fundamental y un átomo Rydberg en un campo eléctrico. Hemos considerado configuraciones lineales simétricas y asimétricas, así como, una configuración plana con los átomos neutros situados a la misma distancia del core Rb^+. Se ha realizado un análisis de la estructura electrónica de la molécula Rydberg cuando el átomo de Rb está en un estado Rydberg del multiplete degenerado $Rb(n = 35, l \geq 3)$. Para las configuraciones lineales, en ausencia de campo eléctrico, algunos estados moleculares con simetría Σ y Π, se desdoblan del nivel principal $Rb(n = 35, l \geq 3)$, mostrando un carácter oscilatorio con muchos pozos de potencial en los que se pueden acomodar niveles vibracionales donde la molécula Rydberg podría existir. Para la configuración plana, hemos encontrado que los estados moleculares muestran una dependencia significativa con el ángulo que forman las líneas rectas del núcleo Rydberg con cada uno de los átomos en el estado fundamental. La interacción con el campo eléctrico favorece la configuración simétrica lineal de la molécula triatómica, refuerza el carácter de estado ligado de los estados moleculares y hace posible la aparición de más estados vibracionales, que están caracterizados por

extensiones espaciales de algunos cientos de radios de Bohr. Además, se ha investigado el impacto del campo eléctrico en los estados electrónicos de Rb-Rb*-Rb, que surgen de los estados del electrón Rydberg con $l = 0$. Para la configuración plana, se han analizado los estados electrónicos de las moléculas Rydberg Rb- Rb($n = 35, l \geq 3$)-Rb y Rb-Rb($38s$)-Rb. En ambos casos, se observa una dependencia muy débil en el ángulo formado por los dos ejes internucleares, y que el campo eléctrico favorece la configuración lineal.

Para las moléculas Rydberg diatómicas, se ha demostrado que la estructura fina del átomo Rydberg y el acoplamiento hiperfino del átomo en el estado fundamental afectan significativamente los estados electrónicos adiabáticos creados a partir de un átomo Rydberg con momento angular orbital bajo [54, 62, 64, 65]. Por lo tanto, una continuación inmediata del trabajo presentado en esta tesis sería investigar el impacto de un campo eléctrico en la estructura electrónica y en las propiedades vibracionales de una molécula Rydberg diatómica y triatómica inlcuyendo la estructura fina del átomo Rydberg y el acoplamiento hiperfino de los átomos en el estado fundamental. Al incluir estos acoplamientos para una molécula Rydberg diatómica, las curvas de energía potencial dependen de los estados hiperfinos de los átomos en el estado fundamental así como de la estructura fina del átomo Rydberg aumentando la complejidad de las mismas. Análogamente, la estructura electrónica de la molécula Rydberg triatómica será también más compleja.

Otra posible extensión es el análisis del impacto de un campo magnético, o la combinación de campos eléctricos y magnéticos, en estas moléculas Rydberg triatómicas. Al igual que para molécula Rydberg diatómica, es de esperar una fuerte repulsión entre los niveles electrónicos debido al campo magnético, lo que provoca que lo profundidad de los pozos de potencial disminuya [66, 69]. En los experimentos con átomos y moléculas Rydberg, es extremadamente difícil reducir el impacto de los campos eléctricos remanentes, los llamados *stray fields*, [108]. Teniendo en cuenta que experimentalmente ya se han creado moléculas Rydberg poliatómicas más complejas formadas por más de tres átomos de rubidio en el estado fundamental [73], se debe investigar el impacto de un campo eléctrico externo en estas moléculas Rydberg poliatómicas.

La segunda parte de esta tesis está dedicada a la investigación de moléculas Rydberg poliatómicas formadas por un átomo de rubidio y una o dos moléculas diatómicas de KRb. El mecanismo de enlace de estas moléculas Rydberg se debe a la interacción entre el momento dipolar eléctrico de la molécula diatómica con el campo eléctrico producido por el átomo Rydberg. Hemos descrito la hibridización del movimiento rotacional de la molécula diatómica debido al campo eléctrico del átomo Rydberg dentro de la aproximación del rotor rígido. En el marco de la aproximación de Born-Oppenheimer, se han obtenido y analizado los estados electrónicos adiabáticos con número cuántico magnético $M_J = 0, 1$ y 2 para las moléculas Rydberg triatómicas y con $M_J = 0$ y 1 para la pentaatómica al variar la separación entre el core Rb^+ y una o las dos moléculas de KRb. La estructura electrónica de estas moléculas Rydberg depende de los estados Rydberg del átomo de rubidio involucrados en su formación.

Para la molécula Rydberg triatómica se ha estudiado los estados electrónicos adiabáticos creados a partir del multiplete degenerado Rb($n, l \geq 3$) al aumentar número cuántico principal n. Se ha observado que con el incremento de la excitación del electrón Rydberg, es decir, con el incremento de n, los desplazamientos energéticos de estos estados electrónicos disminuyen,

lo que indica que la molécula de KRb está expuesta a un campo eléctrico más débil. Además, la profundidad de los pozos de potencial de estos estados electrónicos también disminuye. Al resolver la ecuación de Schrödinger de la molécula Rydberg triatómica se ha calculado el espectro vibracional para estos estados electrónicos. El pozo de potencial más alejado del core Rb^+ del estado electrónico adiabático más bajo en energía de KRb-Rb(n, $l \geq 3$) posee varios estados vibracionales, con un espaciamiento energético del orden los GHz. Al aumentar el número cuántico principal n del estado Rydberg, el número de estados vibracionales ligados disminuye. Merece la pena destacar, que las técnicas experimentales actuales pueden discernir los estados vibracionales en un espectro caracterizado una separación energética en el rango de unos GHz o incluso de los MHz. Experimentalmente, es muy difícil observar y crear estas moléculas Rydberg triatómicas debido a la complejidad experimental asociada a la excitación de un átomo Rydberg con momento angular orbital $l \geq 3$. Normalmente, se usan técnicas experimentales basadas en la absorción de dos fotones, y se producen átomos alcalinos Rydberg $l = 0$ y $l = 2$. Recientemente se han creado experimentalmente moléculas trilobites de Rydberg fuertemente polares en estados electrónicos que surgen a partir de un estado con un alto valor de momento angular-orbital del electrón Rydberg [63]. Debido a la interacción hiperfina del estado fundamental, los canales de dispersión de triplete y singlete de espín del átomo en el estado fundamental están acoplados, lo que permite acceder a moléculas Rydberg Rb_2 en estos estados electrónicos que surgen a partir de un momento angular orbital alto usando la ténica estándar de absorción de dos fotones. Estos resultados experimentales permiten pensar en diseñar de una técnica experimental similar para acceder a los estados electrónicos de la molécula Rydberg triatómica presentadados en esta tesis.

Para moléculas Rydberg pentaatómicas se ha mostrado la existencia de estados electrónicos adiabáticos creados a partir del multiplete degenerado Rb($n = 20$, $l \geq 3$) para las configuraciones lineales simétricas y asimétricas. Para la molécula Rydberg lineal simétrica, la presencia de una segunda molécula diatómica afecta de manera considerable la estructura electrónica, donde aparecen más estados electrónicos y más complejos. Sin embargo, el desplazamiento en energía del nivel electrónico más bajo de KRb-Rb($n = 20$, $l \geq 3$)-KRb no se modifica significativamente, y comparado con el correspondiente nivel de la molécula Rydberg triatómica varía unos pocos MHz. Esto se puede explicar en términos del campo eléctrico del electrón Rydberg que sufren las dos moléculas diatómicas, el cual posee la misma intensidad pero direcciones contrarias debido a las posiciones espaciales de las dos KRb en esta configuración simétrica. Estos potenciales electrónicos adiabáticos también muestran un carácter oscilatorio y poseen pozos con profundidades de unos pocos GHz. Por el contrario, las estructuras electrónicas de la molécula Rydberg pentaatómica en las configuraciones asimétricas analizadas difieren significativamente del espectro correspondiente para la configuración simétrica. Los desplazamientos energéticos de los estados electrónicos son mucho mayores que en la configuración simétrica, y que en la molécula Rydberg triatómica. En estas configuraciones asimétricas, las dos moléculas diatómicas estan expuestas a campos eléctricos inducidos por el átomo Rydberg con intensidades diferentes y en la misma dirección, cuyos efectos se vuelven aditivos provocando un mayor impacto. La molécula Rydberg pentaatómica en configuraciones simétrica y asimétrica tiene las energías de enlace vibracional de unos GHz, que se han estimado aproximando el mínimo del pozo del potencial con un oscilador armónico. Se ha obtenido que dichos pozos poseen unos pocos estados vibracionales ligados donde la molécula pentatómica existiría. Sus energías de enlace están en

el orden de los GHz. Además, se ha analizado el movimiento rotacional de las dos moléculas de KRb dentro de la molécula pentaatómica, y se ha mostrado que los dos KRb están ligeramente orientadas y alineadas.

Motivados por su accesibilidad experimental, se han analizado los estados electrónicos adiabáticos con bajo momento angular de moléculas Rydberg triatómicas y pentaatómicas, formadas por una molécula diatómica en el estado fundamental y en estados rotacionalmente excitados. Ambas moléculas Rydberg poseen tanto estados electrónicos inestables como estables. Éstos últimos tienen pozos de potencial, algunos de ellos con una estructura de doble pozo asimétrico, que alcanzan profundidades de unos pocos cientos de MHz. Para la molécula Rydberg triatómica, hemos calculado las energías de enlace del espectro vibracional en estos estados eletrónicos estables resolviendo la correspondiente la ecuación de Schrödinger del Hamiltoniano rovibracional. Estos estados tienen varios niveles vibracionales ligados con un espaciamiento energético del orden de los MHz. En el caso de la molécula Rydberg pentaatómica, se ha estimado que estas energías de enlace vibracional son también de unos pocos MHz. Para poder distinguir experimentalmente estos estados vibracionales ligados, con separaciones energéticas del orden de los MHz, se necesita un láser con un ancho de línea pequeño. Por ejemplo, el grupo del Prof. T. Killian (Rice University, Houston, EEUU) tiene un láser de 319 nm con ancho de línea ~ 400 kHz [57], que permitiría discernir experimentalmente estos niveles vibracionales. Las moléculas diatómicas que forman estas especies Rydberg están débilmente orientadas, lo que puede explicarse por dos efectos diferentes. En primer lugar, los campos eléctricos producidos por el electrón Rydberg en estos estados excitados Rydberg son muy pequeños debido a las diferentes extensiones espaciales de la funciones de onda radiales de los estados $\mathrm{Rb}(n_1, l_1)$, con $l_1 = 0, 1, 2$ en comparación con las del multiplete degenerado $\mathrm{Rb}(n, l \geq 3)$; como consecuencia, los elementos de matriz que mezclan estos estados Rydberg son más pequeños que aquellos involucrando sólo niveles del multiplete degenerado. Además, el número de niveles Rydberg que se pueden acoplar con el estado Rydberg $\mathrm{Rb}(n's)$ para generar el campo eléctrico es más reducido que los estados del multiplete $\mathrm{Rb}(n, l \geq 3)$ que se pueden acoplar entre sí. Por tanto, están expuestas a menos componentes del campo eléctrico. En segundo lugar, las moléculas de KRb se encuentran en estados rotacionales excitados y, por tanto, tienen energías cinéticas de rotación altas, que han de ser compensadas con la interacción del momento dipolar eléctrico y el campo eléctrico del átomo Rydberg. Por ello, se necesitan campos eléctricos más fuertes para conseguir un efecto similar al observado en el estado rotacional fundamental, es decir aquellos estados que participan en la formción de la molécula Rydberg $\mathrm{KRb}(N = 0)$-$\mathrm{Rb}(n, l \geq 3)$-$\mathrm{KRb}(N = 0)$.

Los estudios presentados en esta tesis sobre las moléculas Rydberg pentaatómicas se pueden extender en diferentes aspectos. Usando técnicas computacionales desarrolladas en el grupo de investigación donde se ha realizado esta tesis doctoral, se puede llevar cabo un estudio exhaustivo de otras posibles moléculas diatómicas candidatas para crear estas moléculas Rydberg poliatómicas. Recientemente, muchos grupos experimentales han creado sistemas híbridos de dos especies de átomos ultrafríos, en los que se han producido moléculas diatómicas heteronucleares ultrafrías en el estado fundamental, tales como RbCs [109, 110], KCs [111], NaK [113], KRb [112], LiNa [114], NaCs [115–117], YbRb [118], OH [119], SrF [120], entre otras. La molécula diatómica polar elegida ha de tener un momento dipolar eléctrico permanente subcrítico $d < 1.639$ D, para evitar el enlace del electrón Rydberg a la molécula

diatómica [78–81]. Entre las moléculas ultrafrías accesibles experimentalmente, posibles candidatas para formar moléculas Rydberg son el LiNa, RbCs, KRb y YbRb, cuyos momentos dipolares eléctricos valen $d = 0.561, 1.238, 0.615$, y 0.987 D, respectivamente [121, 122]. El espectro Rydberg de los átomos alcalinos que forman estas moléculas diatómicas ya se ha investigado en detalle tanto teórica como experimentalmente. Además, es interesante comparar la estructura electrónica de la molécula Rydberg triatómica al cambiar el átomo Rydberg involucrado, por ejemplo Rb*-KRb y K*-KRb. Dado que los defectos cuánticos son específicos de cada átomo, las energías Rydberg de los estados con bajo momento angular orbital $l \lesssim 2$, que se desdoblan de los multipletes degenerados Rb$(n, l \gtrsim 3)$ y K$(n, l \gtrsim 3)$ son diferentes. Por lo tanto, la estructura electrónica de K*-KRb, así como las energías vibracionales de enlace también difieren de las obtenidas en esta tesis para Rb*-KRb.

Para las moléculas Rydberg pentaatómicas, se puede considerar una configuración triangular. Por ejemplo, las dos moléculas diatómicas están ubicadas en dos mínimos consecutivos de una red óptica y el átomo Rydberg encima de ellas. En tal configuración triangular, la simetría azimutal de la molécula Rydberg se pierde y el número cuántico magnético total M_J no se conserva. Esto aumenta la complejidad numérica asociada a la resolución de la ecuación de Schrödinger para esta molécula Rydberg. En particular, el desarrollo en serie de la función de onda debe incluir todos los valores del número cuántico magnético, es decir, $|M_J| \leq J$ en las funciones de onda acopladas (5.5). Por ejemplo, teniendo en cuenta sólo el multiplete Rydberg Rb$(n = 20,\, l \geq 3)$ y el estado Rb$(23s)$, y para KRb las excitaciones rotacionales hasta $N_i = 5$, la dimensión de la matriz Hamiltoniana es superior a medio millón. Es por tanto, un reto computacional obtener los autovalores de una molécula Rydberg pentaatómica triangular.

Además, podrían investigarse moléculas Rydberg de alcance ultra-largo más complejas, formadas por un átomo en estado Rydberg y por varias moléculas diatómicas polares. Debido a la complejidad numérica de la descripción teórica de la molécula Rydberg pentaatómica en una configuración triangular, como la mencionada anteriormente, estos sistemas poliatómicos podrían formarse a partir de moléculas diatómicas de capa abierta, tales como OH, OD, LiO y NaO. Cuyos espectros rotacionales un campo eléctrico están caracterizados por las interacciones de la estructura fina y los efectos del doblete-Λ [82], y pueden describirse de forma aproximada por un modelo de dos estados [83, 84]. Tal aproximación facilita el análisis computacional porque el tamaño de la matriz del hamiltoniana se reduce drásticamente, es decir, de más de medio millón pasa a $4n^2$, con n es el número cuántico principal del átomo Rydberg. Es por tanto posible, llevar a cabo un estudio del espectro electrónico, como ya ha sido realizado previamente para la molécula Rydberg triatómica [74–76]. El primer paso debe ser investigar si la descripción de estas moléculas Rydberg poliatómicas debe incluir las tres componentes cartesianas del campo eléctrico del átomo Rydberg, o si es suficiente considerar solo la componente a lo largo del eje Z como en los trabajos previos [74–76]. Se pueden considerar muchas configuraciones en dos y tres dimensiones. Para la molécula Rydberg pentaatómica, las configuraciones lineal y triangular, deben ser analizadas y comparadas con los resultados presentados en esta tesis, y se ha de buscar la configuración más estable. Se pueden explorar moléculas Rydberg poliatómicas más complejas utilizando configuraciones simétricas basadas en figuras geométricas. Por ejemplo, tres moléculas doblete-Λ ubicadas en los vértices de un triángulo equilátero, y el core Rydberg en el centro, y cuatro moléculas doblete-Λ localizadas en los vértices de un cuadrado, y el core iónico en el centro, y así

sucesivamente. Incluso, diseñar una molécula Rydberg poliatómica tridimensioal con ocho moléculas polares ubicadas en los vértices de un cubo y el core Rydberg localizado en el centro de este, una estructura cúbica centrada en el cuerpo. Para estas moléculas poliatómicas, se pueden explorar las curvas de energía potencial de los estados electrónicos adiabáticos, y sus propiedades direccionales de las moléculas diatómicas, donde podrían aparecer efectos de frustración en la orientación de estas moléculas debido a la distribución simétrica de las moléculas diatómicas.

Appendix A

The Rydberg electron electric field

In this appendix we provide the expression of the electric field created by the Rydberg electron at the position of the diatomic molecules which is given by the relation

$$\mathbf{F}^{e}_{ryd}(\mathbf{R}_i,\mathbf{r}) = e\frac{\mathbf{r}-\mathbf{R}_i}{|\mathbf{r}-\mathbf{R}_i|^3} = \nabla_{\mathbf{R}_i}\frac{1}{|\mathbf{r}-\mathbf{R}_i|} \tag{A.1}$$

where $\nabla_{\mathbf{R}_i}$ is the Laplacian with respect to the molecular coordinate $\mathbf{R}_i = (R_i\hat{R}_i, \theta_{R_i}\hat{\theta}_i, \phi_{R_i}\hat{\phi}_i)$ with $i = 1, 2$, see Ref. [101]. The electric field reads

$$\mathbf{F}^{e}_{ryd}(R_i,\Omega_i,\mathbf{r}) = F^{e,X}_{ryd}(R_i,\Omega_i,\mathbf{r})\hat{X} + F^{e,Y}_{ryd}(R_i,\Omega_i,\mathbf{r})\hat{Y} + F^{e,Z}_{ryd}(R_i,\Omega_i,\mathbf{r})\hat{Z} \tag{A.2}$$

$$F^{e,K}_{ryd}(R_i,\Omega_i,\mathbf{r}) = e\sum_{l=0}^{\infty}\frac{4\pi}{2l+1}\begin{cases} -(l+1)\frac{r^l}{R_i^{l+2}}\sum_m Y_{lm}(\Omega)A^K_{lm}(\Omega_i)\hat{K} & \text{if} \quad r<R, \\ l\frac{R_i^{l-1}}{r^{l+1}}\sum Y_{lm}(\Omega)A^K_{lm}(\Omega_i)\hat{K} & \text{if} \quad r>R, \end{cases} \tag{A.3}$$

with $K = X, Y$ and Z. The coordinates of the Rydberg electron are $\Omega = (\theta, \phi)$ and $\mathbf{r} = (r\hat{R}, \theta\hat{\theta}, \phi\hat{\phi})$, whereas $(R_i, \theta_{R_i}, \phi_{R_i})$ and $\Omega_i = (\theta_i, \phi_i)$ are the coordinates of the center of mass of the diatomic molecules with $i = 1, 2$. The components $A^K_{lm}(\Omega_i)$ read

$$\begin{aligned} A^X_{lm}(\Omega_i) &= \Big[Y^*_{lm}(\Omega_i)\sin\theta_i\cos\phi_i \\ &+ \big(Y^*_{lm+1}(\Omega_i)e^{i\phi_i}a_{lm} - Y^*_{lm-1}(\Omega_i)e^{-i\phi_i}b_{lm}\big)\cos\theta_i\cos\phi_i \\ &- i\big(Y^*_{lm+1}(\Omega_i)e^{-i\phi_i}a_{lm} + Y^*_{lm-1}(\Omega_i)e^{+i\phi_i}b_{lm}\big)\sin\theta_i\Big], \end{aligned} \tag{A.4}$$

$$\begin{aligned} A^Y_{lm}(\Omega_i) &= \Big[Y^*_{lm}(\Omega_i)\sin\theta_i\sin\phi_i \\ &+ \big(Y^*_{lm+1}(\Omega_i)e^{i\phi_i}a_{lm} - Y^*_{lm-1}(\Omega_i)e^{-i\phi_i}b_{lm}\big)\cos\theta_i\sin\phi_i \\ &+ i\big(Y^*_{lm+1}(\Omega_i)e^{-i\phi_i}a_{lm} + Y^*_{lm-1}(\Omega_i)e^{+i\phi_i}b_{lm}\big)\cos\theta_i\Big], \end{aligned} \tag{A.5}$$

$$\begin{aligned} A^Z_{lm}(\Omega_{R_i}) &= \Big[Y^*_{lm}(\Omega_{R_i})\cos\theta_{R_i} \\ &- \big(Y^*_{lm+1}(\Omega_{R_i})e^{i\phi_{R_i}}a_{lm} - Y^*_{lm-1}(\Omega_{R_i})e^{-i\phi_{R_i}}b_{lm}\big)\sin\theta_{R_i}\Big], \end{aligned} \tag{A.6}$$

with

$$a_{lm} = \sqrt{l(l+1)-m(m+1)}, \tag{A.7}$$

$$b_{lm} = \sqrt{l(l+1)-m(m-1)}. \tag{A.8}$$

If the two diatomic molecules are located along the Z axis, the expression of the electric field is significantly simplified because $\theta_{R_i} = 0$ or $\theta_{R_i} = \pi$, and $\phi_{R_i} = 0$. For $\theta_{R_i} = 0$ and $\phi_{R_i} = 0$, we obtain

$$A^X_{lm}(0,0) = \sqrt{\frac{2l+1}{4\pi}}\left(\delta_{m,-1}a_{lm} - \delta_{m,1}b_{lm}\right), \tag{A.9}$$

$$A^Y_{lm}(0,0) = -i\sqrt{\frac{2l+1}{4\pi}}(\delta_{m,-1}a_{lm} + \delta_{m,1}b_{lm}), \tag{A.10}$$

$$A^Z_{lm}(0,0) = \sqrt{\frac{2l+1}{4\pi}}\delta_{m,0}, \tag{A.11}$$

where δ_{m_1,m_2} is the Kronecker delta. If the diatomic molecule is located at the other side of the Rydberg core, we have that $\theta_{R_i} = \pi$ and $\phi_{R_i} = 0$, and we obtain

$$A^X_{lm}(\pi,0) = (-1)^{l+1}\sqrt{\frac{2l+1}{4\pi}}(\delta_{m,-1}a_{lm} - \delta_{m,1}b_{lm}), \tag{A.12}$$

$$A^Y_{lm}(\pi,0) = i(-1)^{l}\sqrt{\frac{2l+1}{4\pi}}(\delta_{m,-1}a_{lm} + \delta_{m,1}b_{lm}), \tag{A.13}$$

$$A^Z_{lm}(\pi,0) = (-1)^{l+1}\sqrt{\frac{2l+1}{4\pi}}\delta_{m,0}. \tag{A.14}$$

For the Z-component of $\mathbf{F}^e_{ryd}(\mathbf{R}_i, \mathbf{r})$ in (A.3), the sum in the magnetic quantum number m is restricted to $m = 0$, whereas for the X and Y components, only the terms with $m = 1$ and -1 contribute.

For the symmetric configuration, i. e., the two diatomic molecules are located at different sides of the Rb^+ core, the l-dependent components of the electric field are of the same strength but differ on the sign depending on the orbital angular momentum of the Rydberg electron l. As a consequence, the matrix elements of the electric field components satisfy the following relation

$$\langle l_1, m_1|F^{e,K}_{ryd}(R_1, 0, 0, \mathbf{r})|l_2, m_2\rangle = -(-1)^{l_1-l_2}\langle l_1, m_1|F^{e,K}_{ryd}(R_2, \pi, 0, \mathbf{r})|l_2, m_2\rangle\,, \tag{A.15}$$

with $K = X, Y, Z$ and $R_1 = R_2$. The matrix element of the Z electric field is non-zero if $m_1 = m_2$, whereas non-zero contributions of the electric field along the X- and Y-axes are obtained if $m_2 = m_1 \pm 1$. In addition, the following relations between the electric field in the X- and Y-axes are satisfied

$$\langle l_1, m_1|F^{e,X}_{ryd}(R_i, \theta_i, 0, \mathbf{r})|l_2, m_1+1\rangle = i\langle l_1, m_1|F^{e,Y}_{ryd}(R_i, \theta_i, 0, \mathbf{r})|l_2, m_1+1\rangle\,, \tag{A.16}$$

$$\langle l_1, m_1|F^{e,X}_{ryd}(R_i, \theta_i, 0, \mathbf{r})|l_2, m_1-1\rangle = -i\langle l_1, m_1|F^{e,Y}_{ryd}(R_i, \theta_i, 0, \mathbf{r})|l_2, m_1-1\rangle\,, \tag{A.17}$$

with $i = 1, 2$ and $\theta_1 = 0$ and $\theta_2 = \pi$. Note that although the electric field component along the Y-axis is imaginary, the Hamiltonian matrix is real because the matrix elements of the electric dipole moment along of the diatomic molecules along the LFF Y-axis is also imaginary.

Our study is restricted to linear configurations of the Rydberg molecule with the diatomic

molecule located on the Z-axis of the laboratory fixed frame (LFF). Thus $\phi_1 = \phi_2 = 0$ or $\phi_2 = \pi$. For one diatomic molecule, $\theta_2 = 0$, and $\phi_1 = 0$ the matrix elements of the $\mathbf{F}^e_{ryd}(R_1, 0, 0, \mathbf{r})$ read:

$$\langle l_1, m_1|\mathbf{F}^e_{ryd}(R_1, 0, 0, \mathbf{r})|l_2, m_2\rangle = F^{e,X}_{l_1 m_1, l_2 m_2}(R_1)\hat{X} + F^{e,Y}_{l_1 m_1, l_2 m_2}(R_1)\hat{Y} + F^{e,Z}_{l_1 m_1, l_2 m_2}(R_1)\hat{Z}, \tag{A.18}$$

$$F^{e,X}_{l_1 m_1, l_2 m_2}(R_1) = e\sqrt{2\pi} \sum_{l''=|l_1-l_2|}^{l_1+l_2} \sqrt{2\pi}\sqrt{\frac{l''(l''+1)}{2l''+1}}\Re_{l'',l_1 l_2}(R_1) \cdot \int_\Omega Y^*_{l_2,m_2}(\Omega) Y^-_{l''1}(\Omega) Y_{l_1,m_1}(\Omega) d\Omega \tag{A.19}$$

$$F^{e,Y}_{l_1 m_1, l_2 m_2}(R_1) = -ie\sqrt{2\pi} \sum_{l''=|l_1-l_2|}^{l_1+l_2} \sqrt{\frac{l''(l''+1)}{2l''+1}}\Re_{l'',l_1,l_2}(R_1) \cdot \int_\Omega Y^*_{l_2,m_2}(\Omega) Y^+_{l''1}(\Omega) Y_{l_1,m_1}(\Omega) d\Omega \tag{A.20}$$

$$F^{e,Z}_{l_1 m_1, l_2 m_2}(R_1) = e \sum_{l''=|l_1-l_2|}^{l_1+l_2} \sqrt{\frac{4\pi}{2l''+1}}\Im_{l'',l_1,l_2}(R_1) \int_\Omega Y^*_{l_2,m_2}(\Omega) Y_{l''0}(\Omega) Y_{l_1,m_1}(\Omega) d\Omega \tag{A.21}$$

where $\Omega = (\theta, \phi)$ and $r = (r\hat{R}, \theta\hat{\theta}, \phi\hat{\phi})$ are the coordinates of the Rydberg electron. The radial integrals are given by:

$$\Re_{l'',l_1,l_2}(R_1) = \int_0^{R_1} \frac{r^{l''}}{R_1^{l''+2}} \psi^*_{l_2}(r)\psi_{l_1}(r) r^2 dr + \int_{R_1}^\infty \frac{R_1^{l''-1}}{r^{l''+1}} \psi^*_{l_2}(r)\psi_{l_1}(r) r^2 dr \tag{A.22}$$

$$\Im_{l'',l_1,l_2}(R_1) = -(l''+1) \int_0^{R_1} \frac{r^{l''}}{R_1^{l''+2}} \psi^*_{l_2}(r)\psi_{l_1}(r) r^2 dr + l'' \int_{R_1}^\infty \frac{R_1^{l''-1}}{r^{l''+1}} \psi^*_{l_2}(r)\psi_{l_1}(r) r^2 dr \tag{A.23}$$

where the terms $R_{l_1}(r)$ and $R_{l_2}(r)$ are the radial part of the Rydberg electron wave function.

Appendix B

A heteronuclear diatomic molecule in a static electric field

In this appendix we consider the diatomic heteronuclear molecule in a static electric field. We assume that the molecule can be described within the Born-Oppenheimer and rigid rotor approximations, and that the electric field is weak enough to have a significant impact only on the rotational dynamics. As prototype molecule we consider KRb, with rotational constant $B = 1.114$ GHz [90], and electric dipole moment $d = 0.566$ D [89]. The rotational motion is described be means of the Euler angles (θ, ϕ), which relate the molecular fixed frame, having the z axis parallel to the molecular internuclear axis, and the laboratory fixed frame [123].

Within the rigid rotor approximation, the Hamiltonian of a diatomic molecule in a static electric field reads

$$H = B\mathbf{N}^2 - \mathbf{d} \cdot \mathbf{F}, \tag{B.1}$$

where the first term is the field-free rotational kinetic energy with $B = \frac{\hbar^2}{2I}$ being the rotational constant, I the moment of inertia, and $\mathbf{N}$ the angular momentum operator. The eigenfunctions of the field-free Hamiltonian, i. e., $H_0 = B\mathbf{N}^2$, are the spherical harmonics, $Y_{NM_N}(\theta, \phi)$, with N being the rotational quantum number and M_N the magnetic quantum number, that is, the eigenvalue of the projection of $\mathbf{N}$ on the Z axis of the laboratory fixed frame N_Z. The field-free eigenenergies are $E_N = BN(N + 1)$ and are $2N + 1$ degenerate.

The second term in the Hamiltonian (B.1) stands for the interaction of the external electric field $\mathbf{F}$ with the permanent electric dipole moment of the molecule $\mathbf{d}$. For diatomic molecules, the permanent electric dipole moment $\mathbf{d}$ is parallel to the internuclear axis, i. e., to the z axis of the molecular fixed frame. The electric field is taken parallel to the Z axis of the laboratory fixed frame, i. e., $\mathbf{F} = F\hat{Z}$, and the field-dressed Hamiltonian reads

$$H = B\mathbf{N}^2 - dF\cos\theta, \tag{B.2}$$

where θ is the angle formed by the internuclear z axis and the electric field. Note that we are neglecting the interaction of the electric field with the molecular polarizability, hyperpolarizability, and higher order terms. Since the electric field is parallel to the Z axis of the laboratory fixed frame, the rigid rotor Hamiltonian preserves the azimuthal symmetry, and the magnetic quantum number is a good quantum number.

To investigate the impact of the electric field on the rotational spectrum, we have to solve the time-independent Schrödinger equation associated to the Hamiltonian (B.3). To do so, we expand the wave function in terms of the field-free eigenfunctions, which are the spherical Harmonics, taking into account that M_J is a good quantum number due to the azymutal symmetry of the system. This basis set expansion allows us to transform the time-independent

Schrödinger equation, which is a second order differential equation in θ and ϕ, in a matrix eigenvalue problem. The wave function is given by

$$\Psi(\theta,\phi) = \sum_{N_1=M_N}^{N_{max}} C_{N_1}^{M_N} Y_{N_1 M_N}(\theta,\phi) \quad . \tag{B.3}$$

The complete basis contains infinite functions, and, therefore, set the expansion of the wave function (B.3) should contain infinite terms. However, for computational reasons, we cut this infinite series to a finite one including $N_{max} - M_J$ elements of the basis.

Applying the Ritz variational method or linear variational principle, see Appendix C, we obtain the Hamiltonian matrix and search for upper bounds of the eigenvalues of the field-dressed Hamiltonian. The elements of the Hamiltonian matrix read:

$$\langle N_1, M_N|H_0|N_2, M_N\rangle = \langle N_1, M_N|B\mathbf{N^2}|N_2, M_N\rangle = BN_1(N_1+1)\delta_{N_1,N_2}, \tag{B.4}$$

$$\begin{aligned}\langle N_1, M_N|DF\cos\theta|N_2, M_N\rangle &= \sqrt{\frac{(N_2+M_N)(N_2-M_N)}{(2N_2-1)(2N_2+1)}}\delta_{N_1,N_2-1} \\ &+ \sqrt{\frac{(N_2+M_N+1)(N_2-M_N+1)}{(2N_2+1)(2N_2+3)}}\delta_{N_1,N_2+1}.\end{aligned} \tag{B.5}$$

The Hamiltonian matrix is tridiagonal. We diagonalize it using the restarted Lanczos procedure [93] implemented in the Arnoldi Package (ARPACK) [94, 95].

In Fig. B.1, we present the energy of the lower-lying states of KRb as a function of the

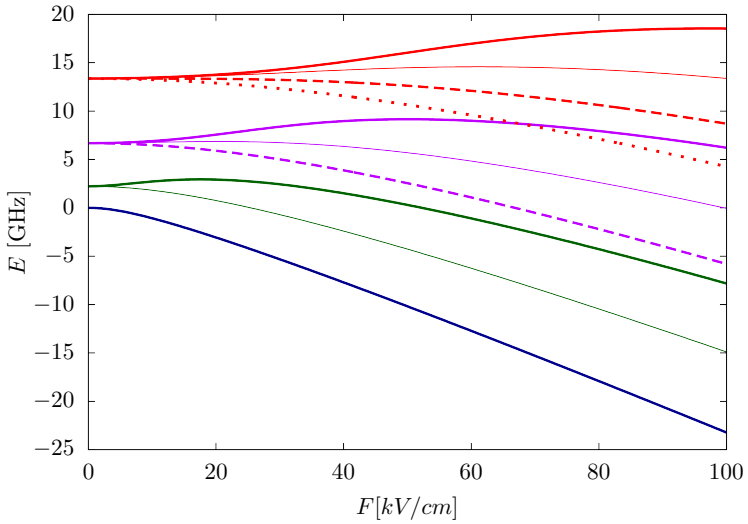

Figure B.1: For KRb molecule, energy of the states with field-free rotational quantum number $N \leq 3$ as a function of the static electric field strength. We use thick solid lines for the states with field-free $M_J = 0$ thin solid lines for the $M_J = 1$ states, dashed lines for the $M_J = 2$ states, and dotted lines for the $M_J = 3$ states.

electric field strength F. Here, we focus on the rotational states with field-free rotational quantum number $N \leq 3$. We observe two different behaviours as F varies. The energy of high-field seeking states decreases as F increases, i. e., they become more bound for stronger electric fields, see for instance the states $|N, N\rangle = |0, 0\rangle, |1, 1\rangle, |2, 2\rangle$ and $|3, 3\rangle$. In contrast, for the low-field seeking states, their energy initially increases and only for strong enough electric fields they show the decreasing behaviour. This low-field seeking behaviour is observed for the rest of states, such as $|1, 0\rangle, |2, 0\rangle, |2, 1\rangle$ and so on. As the rotational excitation of the states increases, the impact of the electric field decreases. This effect can be explained in terms of the competition between the rotational kinetic energy, which increases as $BN(N + 1)$, and the interaction with the electric fields. Compared to the rotational ground state $|0, 0\rangle$, as the rotational excitation N increases, stronger fields are needed to have the same impact. This effect is also observed for the expectation values that we analyze in the next paragraphs.

Due to the interaction with the electric field, the rotational quantum number is not a good quantum number, and states with different field-free rotational quantum number are mixed. This effect is called the hybridization of the rotational motion, and it is illustrated in Fig. B.2 with the expectation value $\langle \mathbf{N}^2 \rangle$. For the high-field seeking states, $\langle \mathbf{N}^2 \rangle$ increases as F increases, due to the contribution to the field-dressed wave function of states with larger field-free rotational quantum number. For the low-field seeking behaviour and sufficiently weak electric fields, $\langle \mathbf{N}^2 \rangle$ decreases due to the contribution of lower-lying states having smaller N. Once the electric field is strong enough, the contribution of higher rotational excitations dominates, and $\langle \mathbf{N}^2 \rangle$ increases as F increases.

Another effect of the electric field is to induce orientation on the molecule, which mean a spatial confinement with a well define direction. In case of polar molecules, the molecule fixed axis is confined in the laboratory fixed axis, and the permanent electric dipole moment

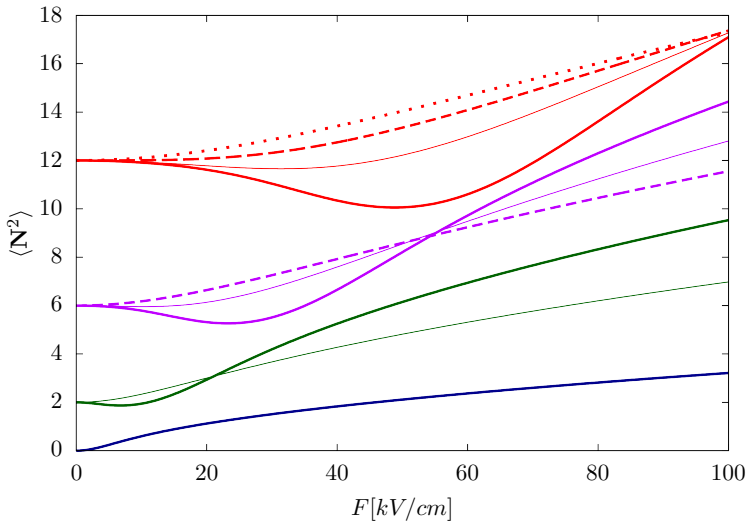

Figure B.2: For KRb molecule, expectation value $\langle \mathbf{N}^2 \rangle$ of the states with field-free rotational quantum number $N \leq 3$ as a function of the static electric field strength. We use thick solid lines for the states with field-free $M_J = 0$ thin solid lines for the $M_J = 1$ states, dashed lines for the $M_J = 2$ states, and dotted lines for the $M_J = 3$ states.

is pointing in along the electric field. This orientation is characterized by the expectation value $\langle \cos\theta \rangle$, and $|\langle \cos\theta \rangle|$ approach 1 as the orientation increases. In Fig. B.3, we show the orientation of the KRb states with field-free rotational quantum number $N \leq 3$ as a function of the static electric field strength. Note that for all the states, $\langle \cos\theta \rangle = 0$ in the absence of the electric field $F = 0$ kV/cm, i. e., the fied-free rotational states are not oriented, which is due to their defined parity at $F = 0$ kV/cm. As in the case of the energy and $\langle \mathbf{N}^2 \rangle$, the low- and high-field seeking states show a different behaviour as F increases. The orientation of the high-field seekers is always parallel to the electric field direction and increased with F. In contrast, the low-field seekers are anti-oriented for weak fields, and only for strong fields $\langle \cos\theta \rangle$ monotonically increases approaching the upper limit of 1. On the strong field regime, all the states are strongly oriented. Note that this regime is reached at stronger field strengths as the rotational excitation of the state increases. Due to the large rotational constant and small electric dipole moment of KRb, even for very strong electric fields as $F = 100$ kV/cm, only the ground state $|0, 0\rangle$ shows a strong orientation with $\langle \cos\theta \rangle > 0.8$. For higher rotational excitations, the orientation is very weak even in this strong field regime. For $F = 100$ kV/cm, we obtain $\langle \cos\theta \rangle = 0.02$ and 0.19 for the $|3, 0\rangle$ and $|3, 1\rangle$ states, respectively.

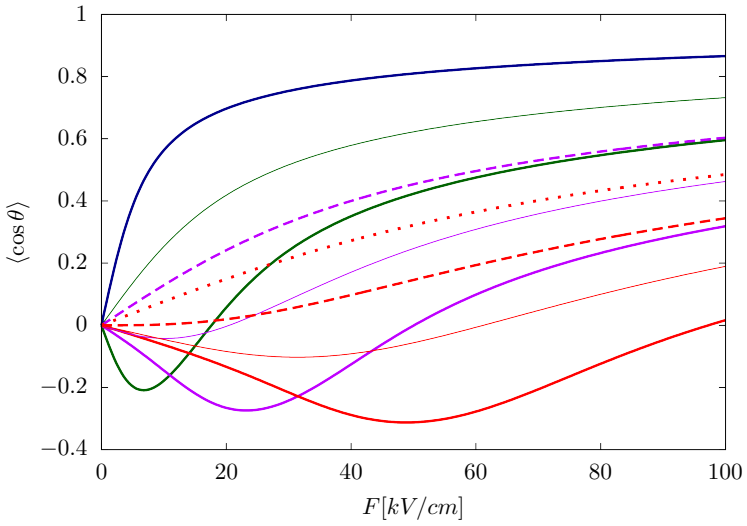

Figure B.3: For KRb molecule, expectation value $\langle \cos\theta \rangle$ of the states with field-free rotational quantum number $N \leq 3$ as a function of the static electric field strength. We use thick solid lines for the states with field-free $M_J = 0$ thin solid lines for the $M_J = 1$ states, dashed lines for the $M_J = 2$ states, and dotted lines for the $M_J = 3$ states.

Appendix C

Numerical Methods

In this appendix we describe the two numerical methods: the basis set expansion and discrete variable representation used in this thesis to solve the time-independent Schrödinger equation.

Basis Set Expansion or Finite Basis Representation

Let us assume a one dimensional Hamiltonian $H(r)$, a way to solve the time-independent Schrödinger equation

$$H\Psi(r) = E\Psi(r) \tag{C.1}$$

is to expand the wave function $\Psi(r)$ in terms of the functions of a complete and orthonormal basis $\{\phi_i(r)\}_{i=1}^{\infty}$ as follows

$$\Psi(r) = \sum_{i=1}^{N} c_i \phi_i(r), \tag{C.2}$$

where c_i is the coefficient of the function $\phi_i(r)$. In principle, this basis set expansion (C.2) should contain the infinite terms of the complete basis, which could not be computationally treated. As a consequence, this infinite series is truncated and we only consider the first N elements of the complete series. In this expansion (C.2), we also require the wave function is normalized to one

$$\langle \Psi | \Psi \rangle = 1 \tag{C.3}$$

The upper bounds of the eigenvalues of the Hamiltonian are obtained minimizing the expectation value of the Hamiltonian $\langle \Psi | H | \Psi \rangle$ and using the restriction of the normalization of the wave function, which is imposed via a real Lagrange multiplier λ

$$\langle \Psi | H | \Psi \rangle - \lambda \langle \Psi | \Psi \rangle = 0 \tag{C.4}$$

Using the expression of the wave function (C.2), and taking derivatives with respect to the coefficients c_i, we obtain

$$\sum_{i=1}^{N} c_i \langle \phi_j | H | \phi_i \rangle = \lambda c_j, \tag{C.5}$$

The time-independent Schrödinger equation has been transformed in this matrix eigenvalue problem. Due to the Ritz variational method or linear variational principle [124, 125], the eigenvalue of the Hamiltonian matrix $\langle \phi_j | H | \phi_i \rangle$ given by λ is an upper bound of the eigenvalue E of the Schrödinger equation (C.1). To ensure that our results are numerically converged, they should be independent of the number of basis functions N used in the expansion (C.2).

As indicated in Chapters 3, 4 and 5, the Hamiltonian matrix is diagonalized using the restarted Lanczos procedure [93] implemented in the Arnoldi Package (ARPACK) [94, 95].

The Discrete Variable Representation

In the previous section, the wave function $\Psi(r)$ is then represented by its projection on the basis functions $\{\phi_i(r)\}$, i. e., by the coefficients $\{c_i\}$, this is the so-called Finite Basis Representation (FBR).

In addition, we could assume that the functions of the complete and orthonormal basis $\{\phi_i(r)\}_{i=1}^{\infty}$ are square integrable, with derivatives $\phi_i^{'}(r)$ and $r\phi_i(r)$ also being square integrable, and that they satisfy a Gaussian quadrature:

$$\int_a^b w(r)f(r)dr = \sum_{\alpha=0}^{N-1} w_\alpha f(r_\alpha), \tag{C.6}$$

with w_α and r_α being the weights and nodes, respectively, and $w(r)$ the weight function of this family of orthogonal polynomials in the interval $[a, b]$. The quadrature is exact for all polynomials $f(r)$ of degree lower or equal to $2N-1$. The orthonormal relation and matrix elements of the position operator given by quadrature relations

$$\langle\phi_j|\phi_k\rangle = \sum_{\alpha=0}^{N-1} w_\alpha \phi_j(r_\alpha)^* \phi_k(r_\alpha) = \delta_{jk}, \tag{C.7}$$

$$\langle\phi_j|r|\phi_k\rangle = \sum_{\alpha=0}^{N-1} w_\alpha r\phi_j(r_\alpha)^* \phi_k(r_\alpha) = \hat{X}_{jk}, \tag{C.8}$$

with $\hat{X}_{jk}$ being the position operator matrix.

The weights w_α of the Gaussian quadrature are determined by:

$$w_\alpha^{1/2} = \frac{U_{n\alpha}^*}{\phi_n(r_\alpha)}$$

where $U_{n\alpha}$ is the unitary matrix diagonalizing the position operator matrix $\hat{X}_{jk}$, which means that

$$(U^\dagger \hat{X} U)_{\alpha,\beta} = r_\alpha \delta_{\alpha,\beta}.$$

The eigenvectors of the matrix $\hat{X}$ are defined as

$$\chi_\alpha(r) = \sum_{n=0}^{N-1} \phi_n(r) U_{n\alpha}, \tag{C.9}$$

which form an orthonormal basis, i. e., they satisfy that $\langle\chi_\alpha|\chi_\beta\rangle = \delta_{\alpha\beta}$ and $\langle\chi_\alpha|r|\chi_\beta\rangle = r_\alpha\delta_{\alpha\beta}$.

The unitary matrix U allows us to transform from the finite basis representation of the wavefunction

$$\Psi(r) \to \psi^{FBR} = (c_1, c_2, \cdots, c_N), \tag{C.10}$$

to its Discrete Variable Representations (DVR) [126], which consists on representing $\Psi(R)$ by its values in the grid points of the quadrature $\{r_\alpha\}$

$$\Psi(r) \to \psi^{DVR} = (w_1^{1/2}\psi(r_0), w_2^{1/2}\psi(r_1), \cdots, w_{N-1}^{1/2}\psi(r_{N-1})). \tag{C.11}$$

Let us emphasize that both representations are related by the unitary matrix U.

The numerical advantage of the DVR is that the matrix elements of the potentials become a diagonal matrix

$$V^{DVR} = U^\dagger V^{FBR} U = V(r_\alpha)\delta_{\alpha\beta} \tag{C.12}$$

where

$$V_{jk}^{FBR} = \sum_{\alpha=0}^{N-1} U_{j\alpha} V(r_\alpha) U_{k\alpha}, \tag{C.13}$$

Computationally, it is easy to evaluate the potential in the grid points $V_l(r_\alpha)$, than to perform the numerical integral of the matrix elements $\langle\phi_n|V_l(r_\alpha)|\phi_m\rangle$, which in most cases are not analitically known.

To solve the time-independent Schrödinger equation associated to the Hamiltonian of the vibrational problem of the Rydberg molecules we use a equidistant grid. We consider now a particle in a box with boundaries r_0 and r_{N+1}. The basis functions are given by

$$\varphi_j(r) = \begin{cases} \sqrt{2/L}\sin(j\pi(r-r_0)/L) & \text{for} \quad r_0 \le r \le r_{N+1}, \\ 0 & \text{else.} \end{cases} \tag{C.14}$$

The derivative matrices, needed to evaluate the matrix elements of the kinetic energy, are thus:

$$\left\langle \varphi_j | \frac{d}{dr} | \varphi_k \right\rangle = mod(j-k,2)\frac{4}{L}\frac{jk}{j^2-k^2}, \qquad j \neq k, \tag{C.15}$$

$$\left\langle \varphi_j | \frac{d^2}{dr^2} | \varphi_k \right\rangle = -\delta_{jk}(j\pi/L)^2, \tag{C.16}$$

where $mod(j-k,2) = 0$ if $j-k$ is even and $mod(j-k,2) = 1$ if $j-k$ is odd. The first derivative vanishes when $j = k$.

To obtain a tridiagonal matrix for the position operator r, we define the transformation

$$z = \cos(\pi(r-r_0)/L). \tag{C.17}$$

Then, the position operator matrix reads

$$z_{jk} = \langle\varphi_j|\hat{z}|\varphi_k\rangle = \frac{1}{2}(\delta_{j,k+1} + \delta_{j,k-1}). \tag{C.18}$$

This matrix can be diagonalized analytically, having as eigenvectors and eigenvalues s

$$U_{j\alpha} = \sqrt{\frac{2}{N+1}}\sin\left(\frac{j\alpha\pi}{N+1}\right), \tag{C.19}$$

and

$$z_\alpha = \cos\left(\frac{\alpha\pi}{N+1}\right). \tag{C.20}$$

We obtain the grid points in DVR:

$$r_\alpha = r_0 + \frac{L}{\pi}\arccos(z_\alpha) = r_0 + \alpha\frac{L}{N+1} = r_0 + \Delta r. \tag{C.21}$$

where $\Delta r = L/(N+1)$ is the constant spacing in the grid. The boundaries of the box, i. e., the points r_0 and r_{N+1}, do not belong to the set of grid points, and the wave functions is zero on these points. Since the grid is equidistant, the weights are constant

$$w_\alpha^{1/2} = U_{j\alpha}/\varphi_j(r_\alpha) = \sqrt{\Delta r}. \tag{C.22}$$

Finally, the DVR expressions of the first and second derivative matrix elements are

$$D_{\alpha\beta}^{(1),DVR} = \left\langle \varphi_\alpha | \frac{d}{dr} | \varphi_\beta \right\rangle = \sum_{j,k=0}^{N-1} U_{j\alpha}^* \left\langle \varphi_j | \frac{d}{dr} | \varphi_k \right\rangle U_{k\beta}, \tag{C.23}$$

and

$$D_{\alpha\beta}^{(2),DVR} = \left\langle \varphi_\alpha | \frac{d^2}{dr^2} | \varphi_\beta \right\rangle = -\left(\frac{\pi}{\Delta r}\right)^2 \begin{cases} -\frac{1}{3} + \frac{1}{6(N+1)^2} - \frac{1}{2(N+1)^2 \sin^2\left(\frac{\alpha\pi}{N+1}\right)}, & \alpha = \beta, \\ \frac{2(-1)^{\alpha-\beta}}{(N+1)^2} \frac{\sin\left(\frac{\alpha\pi}{N+1}\right)\sin\left(\frac{\beta\pi}{N+1}\right)}{\left(\cos\left(\frac{\alpha\pi}{N+1}\right) - \cos\left(\frac{\beta\pi}{N+1}\right)\right)^2}, & \alpha \neq \beta \end{cases} \tag{C.24}$$

Appendix D

Spherical Harmonics

In this appendix, we provide the main properties used in this thesis of the spherical harmonics, which are defined as

$$Y_{lm}(\theta,\phi) = (-1)^m \sqrt{\frac{(2l+1)(l+m)!}{4\pi(l+m)!}} P_l^m(\cos\theta) e^{im\phi}, \tag{D.1}$$

where $l = 0, 1, \ldots$ and $m = -l, \ldots, l$, and $P_l^m(\cos\theta)$ is associated Legendre polynomial [123].

In Chapter 3, the p-wave pseudo-potential (3.1) includes the gradient of the wave function. This means, that we have to compute the partial derivative of the spherical harmonics with respect to θ and ϕ. The partial derivative with respect to θ is given by

$$\frac{\partial}{\partial\theta} Y_{lm}(\theta,\phi) = (-1)^m \sqrt{\frac{(2l+1)(l+m)!}{4\pi(l+m)!}} e^{im\phi} \frac{\partial}{\partial\theta} P_l^m(\cos\theta). \tag{D.2}$$

With the change of variable

$$x = \cos\theta,$$

the derivative of the associated Legendre polynomial can be written as

$$\frac{\partial}{\partial\theta} P_l^m(\cos\theta) = \frac{\partial\cos\theta}{\partial\theta} \frac{\partial P_l^m(\cos\theta)}{\partial\cos\theta}\,. \tag{D.3}$$

obtaining

$$\frac{\partial}{\partial\theta} P_l^m(\cos\theta) = -\sin\theta \frac{\partial}{\partial x} P_l^m(x) = -\sqrt{1-x^2} \frac{\partial}{\partial x} P_l^m(x)\,. \tag{D.4}$$

Using the following recurrence relation

$$\frac{\partial}{\partial x} P_l^m(x) = -\frac{1}{2}\left[(l+m)(l-m+1)P_l^{m-1}(x) - P_l^{m+1}(x)\right], \tag{D.5}$$

it yields

$$\frac{\partial}{\partial\theta} Y_{lm}(\Omega) = \frac{1}{2}\left[D_{lm}^{(1)} e^{i\phi} Y_{l,m-1}(\Omega) - D_{lm}^{(2)} e^{-i\phi} Y_{l,m+1}(\Omega)\right], \tag{D.6}$$

with $D_{lm}^{(1)} = \sqrt{(l+m)(l-m+1)}$ and $D_{lm}^{(2)} = \sqrt{(l-m)(l+m+1)}$.

The term of the gradient due to the ϕ-component, it reads

$$\frac{1}{\sin\theta}\frac{\partial}{\partial\phi}Y_{lm}(\theta,\phi) = \frac{im}{\sin\theta}\left[\sqrt{\frac{(2l+1)(l+m)!}{4\pi(l+m)!}}e^{im\phi}P_l^m(\cos\theta)\right]. \tag{D.7}$$

To avoid the singularity at $\theta = 0$, we use another recurrence formula for the associated Legendre polynomial

$$\frac{mP_l^m(x)}{\sqrt{1-x^2}} = -\frac{1}{2x}\left[(l+m)(l-m+1)P_l^{m-1}(x) + P_l^{m+1}(x)\right], \tag{D.8}$$

obtaining the final expression

$$\frac{\partial}{\partial\phi}Y_{lm}(\Omega) = \frac{i}{2\cos\theta}\left[D_1 e^{i\phi}Y_{l,m-1}(\Omega) + D_2 e^{-i\phi}Y_{l,m+1}(\Omega)\right]. \tag{D.9}$$

Note that in this case the singularity arise for $\theta = \pi/2$. Thus, in the triatomic Rydberg molecules we have avoided that the ground state atoms are located at this angle $\theta = \pi/2$.

In Chapters 4 and 5, we have to compute the matrix elements of the permanent dipole moment of the diatomic molecules, whose spatial components on the laboratory fixed frame are given by

$$\begin{aligned} d_x &= \sin\theta\cos\phi, \\ d_y &= \sin\theta\sin\phi, \\ d_z &= \cos\theta, \end{aligned}$$

and their expressions in terms of the spherical harmonics are

$$\begin{aligned} d_x &= \sqrt{\frac{2\pi}{3}}\left[Y_{1-1}(\theta,\phi) - Y_{11}(\theta,\phi)\right], \\ d_y &= \sqrt{\frac{2\pi}{3}}\left[Y_{1-1}(\theta,\phi) + Y_{11}(\theta,\phi)\right], \\ d_z &= \sqrt{\frac{4\pi}{3}}Y_{10}(\theta,\phi). \end{aligned}$$

We have used the following analytical expressions of the spherical harmonics:

$$Y_{10}(\theta,\phi) = \frac{1}{2}\sqrt{\frac{3}{\pi}}\cos\theta, \tag{D.10}$$

$$Y_{11}(\theta,\phi) = -\frac{1}{2}\sqrt{\frac{3}{2\pi}}\sin\theta e^{i\phi}, \tag{D.11}$$

$$Y_{1-1}(\theta,\phi) = \frac{1}{2}\sqrt{\frac{3}{2\pi}}\sin\theta e^{-i\phi}. \tag{D.12}$$

We present now the matrix elements $\langle N_1 M_{N_1}|d_i|N_1' M_{N_1'}'\rangle$ with $i = x, y$ and z of the

permanent electric dipole moment:

$$d^X_{NM_NN'M'_N} = (-1)^{M'_{N'_1}} 2\sqrt{\frac{2\pi}{3}} \int_\Omega Y_{N_1M_{N_1}}(\Omega) Y_{N'_1-M'_{N_1}}(\Omega)[Y_{1-1}(\Omega) - Y_{11}(\Omega)](\Omega)d\Omega\,. \quad \text{(D.13)}$$

$$d^Y_{NM_NN'M'_N} = i(-1)^{M'_{N'_1}} 2\sqrt{\frac{2\pi}{3}} \int_\Omega Y_{N_1M_{N_1}}(\Omega) Y_{N'_1-M'_{N_1}}(\Omega)[Y_{1-1}(\Omega) + Y_{11}(\Omega)](\Omega)d\Omega, \quad \text{(D.14)}$$

$$d^Z_{NM_NN'M'_N} = (-1)^{M'_{N'_1}} 2\sqrt{\frac{\pi}{3}} \int_\Omega Y_{N_1M_{N_1}}(\Omega) Y_{N'_1-M'_{N_1}}(\Omega) Y_{10}(\Omega)d\Omega\,. \quad \text{(D.15)}$$

To evaluate these integrals, we use the following expression [123]

$$\int_0^{2\pi}\int_0^{\pi} Y_{J_3M_3}(\theta,\phi) Y_{J_2M_2}(\theta,\phi) Y_{J_1M_1}(\theta,\phi)\sin\theta d\theta d\phi$$
$$= \left[\frac{(2J_1+1)(2J_2+1)(2J_3+1)}{4\pi}\right]^{\frac{1}{2}} \begin{pmatrix} J_1 & J_2 & J_3 \\ 0 & 0 & 0 \end{pmatrix} \begin{pmatrix} J_1 & J_2 & J_3 \\ M_1 & M_2 & M_3 \end{pmatrix},$$

we finally obtain:

$$d^X_{N_1M_{N_1}N'_1M'_{N_1}} = C_{MN_1N'_1} \begin{pmatrix} N_1 & N'_1 & 1 \\ 0 & 0 & 0 \end{pmatrix} \begin{pmatrix} N_1 & N'_1 & 1 \\ M_{N_1} & -M'_{N_1} & -1 \end{pmatrix} -$$
$$- \begin{pmatrix} N_1 & N'_1 & 1 \\ 0 & 0 & 0 \end{pmatrix} \begin{pmatrix} N_1 & N'_1 & 1 \\ M_{N_1} & -M'_{N_1} & 1 \end{pmatrix} \quad \text{(D.16)}$$

$$d^Y_{N_1M_{N_1}N'_1M'_{N_1}} = C_{MN_1N'_1} \begin{pmatrix} N_1 & N'_1 & 1 \\ 0 & 0 & 0 \end{pmatrix} \begin{pmatrix} N_1 & N'_1 & 1 \\ M_{N_1} & -M'_{N_1} & -1 \end{pmatrix} +$$
$$+ \begin{pmatrix} N_1 & N'_1 & 1 \\ 0 & 0 & 0 \end{pmatrix} \begin{pmatrix} N_1 & N'_1 & 1 \\ M_{N_1} & -M'_{N_1} & 1 \end{pmatrix}, \quad \text{(D.17)}$$

$$d^Z_{N_1M_{N_1}N'_1M'_{N_1}} = C_{MN_1N'_1} \begin{pmatrix} N_1 & N'_1 & 1 \\ 0 & 0 & 0 \end{pmatrix} \begin{pmatrix} N_1 & N'_1 & 1 \\ M_{N_1} & -M'_{N'_1} & 0 \end{pmatrix}, \quad \text{(D.18)}$$

with $C_{MN_1N'_1} = (-1)^{M'_{N'_1}} \left[\frac{2(2N_1+1)(2N'_1+1)}{3}\right]^{1/2}$.

Note that for these matrix elements to be non-zero, the following selections rules must be satisfied $\Delta N_1 = N_1 - N'_1 = \pm 1$, and $\Delta M_{N_1} = M_{N_1} - M'_{N'_1} = 0$ for the Z component of the electric dipole moment, and $\Delta M_{N_1} = M_{N_1} - M'_{N'_1} = \pm 1$ for the x and y components.

Bibliography

[1] H. J. Metcalf, and P. van der Straten, *Laser Cooling and Trapping*, Springer, New York, (1999).

[2] K. M. Jones, E. Tiesinga, P. D. Lett, and P. S. Julienne, *Ultracold Photoassociation Spectroscopy: Long-range Molecules and Atomic Scattering*, Rev. Mod. Phys. **78**, 483 (2006).

[3] T. Köhler, K. Góral, and P. S. Julienne, *Production of Cold Molecules via Magnetically Tunable Feshbach Resonances*, Rev. Mod. Phys. **78**, 1311 (2006).

[4] C. J. Pethick and H. Smith, *Bose-Einstein Condensation in Dilute Gases*, Cambridge University Press, (2008).

[5] M. H. Anderson, J. R. Ensher, M. R. Matthews, C. E. Wieman, and E. A. Cornell, *Observation of Bose-Einstein Condensation in a Dilute Atomic Vapor*, Science **269**, 198 (1995).

[6] K. B. Davis, M. O. Mewes, M. R. Andrews, N. J. van Druten, D. S. Durfee, D. M. Kurn, and W. Ketterle, *Bose-Einstein Condensation in a Gas of Sodium Atoms*, Phys. Rev. Lett. **75**, 3969 (1995).

[7] I. Bloch, J. Dalibard, and W. Zwerger, *Many-body Physics with Ultracold Gases*, Rev. Mod. Phys. **80**, 885 (2008).

[8] M. Lewenstein, A. Sanpera, and V. Ahufinger, *Ultracold Atoms in Optical Lattices: Simulating quantum many-body systems*, Oxford University Press, Oxford, (2012).

[9] L. D Carr and D. DeMille and R. V Krems and J.Ye, *Cold and Ultracold molecules: Science, Technology and Applications*, New J. Phys. **11**, 055049 (2009).

[10] D. Jin and J. Ye, *Introduction to Ultracold Molecules: New Frontiers in Quantum and Chemical Physics*, Chem. Rev. **112**, 4801 (2012).

[11] D. Jin and J. Ye (Editors), *Ultracold Molecules. Special Issue*, Chem. Rev. **112**, 4801 (2012).

[12] A. Krükow, A. Mohammadi, A. Härter, and J. Hecker Denschlag, *Reactive Two-Body and Three-Body Collisions of Ba^+ in an Ultracold Rb Gas*, Phys. Rev. A **94**, 030701(R) (2016).

[13] S. Kotler, R. W. Simmonds, D. Leibfried, and D. J. Wineland,*Hybrid Quantum Systems with Trapped Charged Particles*, Phys. Rev. A **95**, 022327 (2017).

[14] M. Gröbner, P. Weinmann, F. Meinert, K. Lauber, E. Kirilov, and H.-C. Nägerl, *A New Quantum Gas Apparatus for Ultracold Mixtures of K and Cs and KCs Ground-State Molecules*, Journal of Modern Optics **63**, 1829 (2016).

[15] R. Côté, V. Kharchenko, and M. D. Lukin, *Mesoscopic Molecular Ions in Bose-Einstein Condensates*, Phys. Rev. Lett. **89**, 093001 (2002).

[16] F. H. J. Hall and S. Willitsch, *Millikelvin Reactive Collisions between Sympathetically Cooled Molecular Ions and Laser-Cooled Atoms in an Ion-Atom Hybrid Trap*, Phys. Rev. Lett. **109**, 233202 (2012).

[17] M. Schlagmüller, T. C. Liebisch, F. Engel, K. S. Kleinbach, F. Böttcher, U. Hermann, K. M. Westphal, A. Gaj, R. Löw, S. Hofferberth, T. Pfau, J. Pérez-Ríos, and C. H. Greene, *Alignment of D-State Rydberg Molecules*, Phys. Rev. X **6**, 031020 (2016).

[18] V Giovannetti, S Lloyd, L Maccone, *Quantum-enhanced Measurements: Beating the Standard Quantum Limit*, Science **306**, 1330 (2004).

[19] V. Giovannetti, S. Lloyd, and L. Maccone, *Quantum Metrology*, Phys. Rev. Lett. **96**, 010401 (2006).

[20] J. Ye, H. J. Kimble, and H. Katori, *Quantum State Engineering and Precision Metrology Using State-Insensitive Light Traps*, Science **320**, 1734 (2008).

[21] T. Secker, R. Gerritsma, A. W. Glaetzle, and A. Negretti, *Controlled Long-Range Interactions between Rydberg Atoms and Ions*, Phys. Rev. A **94**, 013420 (2016).

[22] T. Softley, and M. Bell, *Ultracold Molecules and Ultracold Chemistry*, Mol. Phys. **107**, 99 (2009).

[23] P. Eberle, A. D. Dörfler, C. von Planta, K. Ravi, and S. Willitsch, *A Dynamic Ion-Atom Hybrid Trap for High-Resolution Cold-Collision Studies*, ChemPhysChem **17**, 3769 (2016).

[24] S. Ospelkaus, K.-K. Ni, D. Wang, M. H. G. De Miranda, B. Neyenhuis, G. Quéméner, P. S. Julienne, J. L. Bohn, D. S. Jin, J. Ye, *Quantum-State Controlled Chemical Reactions of Ultracold Potassium-Rubidium Molecules*, Science **327**, 853 (2010).

[25] G. Kurizki, P. Bertet, Y. Kubo, K. Mølmer, D. Petrosyan, P. Rabl, and J. Schmiedmayer, *Quantum Technologies with Hybrid Systems*, Proc. Natl. Acad. Sci. USA. **112**, 3866 (2015).

[26] M. A. Nielsen and I. L. Chuang, *Quantum Computation and Quantum Information*, Cambridge University Press, Cambridge, U.K., (2000).

[27] H. Häffner, C. F. Roos, and R. Blatt, *Quantum Computing with Trapped Ions*, Phys. Rep. **469**, 155 (2008).

[28] T. F. Gallagher, *Rydberg Atoms*, Cambridge University Press, Cambridge, U.K., (1994).

[29] J. J. Balmer, *Notiz über die Spectrallinien des Wasserstoffs*, Ann. Phys. Chem. **25**, 80 (1885).

[30] J. R. Rydberg, *On the Structure of the Line-Spectra of the Chemical Elements*, Philosophical Magazine 5th Ser. **29**, 331 (1890).

[31] R. F. Stebbings and F. B. Dunning, Editors, *Rydberg States of Atoms and Molecules*, Cambridge University Press, (1983).

[32] T. C. Killian, T. Pattard, T. Pohl, J. M. Rost, *Ultracold neutral plasmas*, Phys. Rep. **449**, 77 (2007).

[33] T. Pohl, C. S. Adams and H. R. Sadeghpour *Cold Rydberg Gases and Ultra-Cold Plasmas. Special issue*, J. Phys. B **44**, 180201 (2011).

[34] H. Weimer, M. Müller, I. Lesanovsky, P. Zoller, and H. P. Büchler,*A Rydberg Quantum Simulator*, Nat.Phys. **6**, 382 (2010).

[35] D. Jaksch, J.I. Cirac, P. Zoller, S.L. Rolston, R. Côté, and M.D.Lukin, *Fast Quantum Gates for Neutral Atoms*, Phys. Rev. Lett. **85**, 2208 (2000).

[36] M. D. Lukin, M. Fleischhauer, R. Côté, L. M. Duan D. Jaksch, J. I. Cirac, and P. Zoller, *Dipole Blockade and Quantum Information Processing in Mesoscopic Atomic Ensembles*, Phys. Rev. Lett. **87**, 037901 (2001).

[37] M. Saffman, T. G. Walker, and K. Molmer, *Quantum Information with Rydberg Atoms*, Rev. Mod. Phys. **82**, 2313 (2010).

[38] R. Heidemann, U. Raitzsch, V. Bendkowsky, B. Butscher, R. Löw, L. Santos, and T. Pfau, *Evidence for Coherent Collective Rydberg Excitation in the Strong Blockade Regime*, Phys. Rev. Lett. **99**, 163601 (2007).

[39] R. Heidemann, U. Raitzsch, V. Bendkowsky, B. Butscher, R. Löw, and T. Pfau, *Rydberg Excitation of Bose-Einstein Condensates*, Phys. Rev. Lett. **100**, 033601, (2008).

[40] E. Urban, T. A. Johnson, T. Henage, L. Isenhower, D. D. Yavuz, T. G. Walker, and M. Saffman, *Observation of Rydberg Blockade between Two Atoms*, Nat. Phys. **5**, 110 (2009).

[41] J. B. Balewski, A. T. Krupp, A. Gaj, D. Peter, H. P. Büchler, R. Löw, Sebastian Hofferberth, and T. Pfau, *Coupling a Single Electron to a Bose-Einstein Condensate*, Nature **502**, 664 (2013).

[42] C. H. Greene, A. S. Dickinson, and H. R. Sadeghpour, *Creation of Polar and Nonpolar Ultra-Long-Range Rydberg Molecules*, Phys. Rev. Lett. **85**, 2458 (2000).

[43] A. Duncan, *Rydberg Series in Atoms and Molecules*, Academic Press, (1971).

[44] M. S. Child, *Theory of Molecular Rydberg States*, Cambridge University Press, Cambridge, (2011).

[45] E. Fermi, *Sopra lo Spostamento per Pressione delle Righe Elevate delle Serie Spettrali*, Nuovo Cimento **11**, 157 (1934).

[46] A. Omont, *On the Theory of Collisions of Atoms in Rydberg States with Neutral Particles*, J. Phys. **38**, 1343 (1977).

[47] E. L. Hamilton, C. H Greene and H. R. Sadeghpour,*Shape-Resonance-Induced Long-Range Molecular Rydberg States*, J. Phys. B **35**, L199 (2002).

[48] W. Li, T. Pohl, J. M. Rost, S. T. Rittenhouse, H. R. Sadeghpour, J. Nipper, B. Butscher, J. B. Balewski, V. Bendkowsky, R. Löw and T. Pfau, *A Homonuclear Molecule with a Permanent Electric Dipole Moment*, Science **334**, 1110 (2011).

[49] V. Bendkowsky, B. Butscher, J. Nipper, J. P. Shaffer, R. Löw and T. Pfau, *Observation of Ultralong-Range Rydberg Molecules*, Nature **458**, 1005 (2009).

[50] B. Butscher, V. Bendkowsky, J. Nipper, J. B. Balewski, L. Kukota, R. Löw, T. Pfau W. Li, T. Pohl, and J. M. Rost, *Lifetimes of Ultralong-Range Rydberg Molecules in Vibrational Ground and Excited States*, J. Phys. B **44**, 184004 (2011).

[51] V. Bendkowsky, B. Butscher, J. Nipper, J. B. Balewski, J. P. Shaffer, R. Löw, T. Pfau, W. Li, J. Stanojevic, T. Pohl, and J. M. Rost, *Rydberg Trimers and Excited Dimers Bound by Internal Quantum Reflection.*, Phys. Rev. Lett. **105**, 163201 (2010).

[52] J. Tallant, S. T. Rittenhouse, D. Booth, H. R. Sadeghpour, and J. P. Shaffer, *Observation of Blueshifted Ultralong-Range Cs_2 Rydberg Molecules* Phys. Rev. Lett. **109**, 173202 (2012).

[53] D. Booth, S. T. Rittenhouse, J. Yang, H. R. Sadeghpour, and J. P. Shaffer, *Molecular Physics. Production of Trilobite Rydberg Molecule Dimers with Kilo-Debye Permanent Electric Dipole Moments*, Science **348**, 99 (2015).

[54] H. Saßmannshausen, F. Merkt, and J. Deiglmayr, *Experimental Characterization of Singlet Scattering Channels in Long-Range Rydberg Molecules*, Phys. Rev. Lett. **114**, 133201 (2015).

[55] B. J. DeSalvo, J. A. Aman, F. B. Dunning, T. C. Killian, H. R. Sadeghpour, S. Yoshida and J. Burgdörfer, *Ultra-Long-Range Rydberg Molecules in a Divalent Atomic System*, Phys. Rev. A **92**, 031403 (2015).

[56] F. Camargo, J. D. Whalen, R. Ding, H. R. Sadeghpour, S. Yoshida, J. Burgdörfer, F. B. Dunning, and T. C. Killian, *Lifetimes of Ultra-Long-Range Strontium Rydberg Molecules*, Phys. Rev. A **93**, 022702 (2016).

[57] J. D. Whalen, F. J. D. Whalen, F. Camargo, R. Ding, T. C. Killian, F. B. Dunning, J. Pérez-Ríos, S. Yoshida, J. Burgdörfer, *Lifetimes of Ultralong-Range Strontium Rydberg Molecules in a Dense BEC*, arXiv:1707.02354 (2017).

[58] M. A. Bellos, R. Carollo, J. Banerjee, E. E. Eyler, P. L. Gould, and W. C. Stwalley, *Excitation of Weakly Bound Molecules to Trilobitelike Rydberg States*, Phys. Rev. Lett. **111**, 053001 (2013).

[59] D. A. Anderson, S. A. Miller, and G. Raithel, *Photoassociation of Long-Range nD Rydberg Molecules*, Phys. Rev. Lett. **112**, 163201 (2014).

[60] A. T. Krupp, A. Gaj, J. B. Balewski, S. Hofferberth, R. Löw, T. Pfau, M. Kurz, and P. Schmelcher, *Alignment of D-state Rydberg Molecules*, Phys. Rev. Lett. **112**, 143008 (2014).

[61] T. Niederprüm, O. Thomas, T. Eichert, C. Lippe, J. Pérez-Ríos, C. H. Greene, and H. Ott, *Observation of Pendular Butterfly Rydberg Molecules*, Nature Comm. **7**, 12820 (2016).

[62] D. A. Anderson, S. A. Miller, and G. Raithel, *Angular-Momentum Couplings in Long-Range Rb_2 Rydberg Molecules*, Phys. Rev. A **90** 062518 (2014).

[63] K. S. Kleinbach, F. Meinert, F. Engel, W. J. Kwon, R. Löw, T. Pfau, and G. Raithel, *Photoassociation of Trilobite Rydberg Molecules via Resonant Spin-Orbit Coupling*, Phys. Rev. Lett. **118**, 223001 (2017).

[64] S. Markson, S. T. Rittenhouse, R. Schmidt, J. P. Shaffer, and H. R. Sadeghpour, *Theory of Ultralong-Range Rydberg Molecule Formation Incorporating Spin-Dependent Relativistic Effects: Cs(6s)–Cs(np) as Case Study*, ChemPhysChem, **17**, 3683 (2016).

[65] M. T. Eiles and C. H. Greene, *Hamiltonian for the Inclusion of Spin Effects in Long-Range Rydberg Molecules*, Phys. Rev. A **95**, 042515 (2017).

[66] I. Lesanovsky, H. R. Sadeghpour, and P. Schmelcher, *Ultra-Long-Range Rydberg Molecules Exposed to a Magnetic Field*, J. Phys. B **39**, L69 (2007).

[67] M. Kurz, M. Mayle and P. Schmelcher, *Ultra-Long-Range Giant Dipole Molecules in Crossed Electric and Magnetic Fields*, Europhys. Lett. **97** 43001 (2012).

[68] M. Kurz and P. Schmelcher, *Electrically Dressed Ultra-Long-Range Polar Rydberg Molecules*, Phys. Rev. A. **88**, 022501 (2013).

[69] M. Kurz and P. Schmelcher, *Ultralong-Range Rydberg Molecules in Combined Electric and Magnetic Fields*, J. Phys. B **47**, 165101 (2014).

[70] I. C. H. Liu and J. M. Rost, *Polyatomic Molecules Formed with a Rydberg Atom in an Ultracold Environment*, Eur. Phys. J. D **40**, 65 (2006).

[71] I. C. H. Liu, J. Stanojevic, and J. M. Rost, *Ultra-Long-Range Rydberg Trimers with a Repulsive Two-Body Interaction*, Phys. Rev. Lett. **102** 173001 (2009).

[72] M. T. Eiles J. Pérez-Ríos, F. Robicheaux, and C. H. Greene, *Ultracold Molecular Rydberg Physics in a High Density Environment*, J. Phys. B **49**, 114005 (2016).

[73] A. Gaj, A. T. Krupp, J. B. Balewski, R. Löw, S. Hofferberth and T. Pfau, *From Molecular Spectra to a Density Shift in dense Rydberg Gases*, Nature Comm. **5**, 4546 (2014).

[74] S. T. Rittenhouse, and H. R. Sadeghpour, *Ultracold Giant Polyatomic Rydberg Molecules: Coherent Control of Molecular Orientation*, Phys. Rev. Lett. **104**, 243002 (2010).

[75] S. T. Rittenhouse, M. Mayle, P. Schmelcher, and H. R. Sadeghpour, *Ultralong-Range Polyatomic Rydberg Molecules formed by a Polar Perturber*, J. Phys. B **44**, 184005 (2011).

[76] M. Mayle, S. T. Rittenhouse, P. Schmelcher, and H. R. Sadeghpour, *Electric Field Control in Ultralong-Range Triatomic Polar Rydberg Molecules*, Phys. Rev. A **85**, 052511 (2012).

[77] R. González-Férez, H. R. Sadeghpour, and P. Schmelcher, *Rotational Hybridization, and Control of Alignment and Orientation in Triatomic Ultralong-Range Rydberg Molecules*, New J. Phys. **17** 013021 (2015).

[78] E. Fermi and E. Teller, *The Capture of Negative Mesotrons in Matter*, Phys. Rev. **72**, 399 (1947).

[79] J. E. Turner, *Minimum Dipole Moment Required to bind an Electron—Molecular Theorists Rediscover Phenomenon Mentioned in Fermi-Teller Paper Twenty Years Earlier*, Am. J. Phys. **45**, 758 (1977).

[80] C. W. Clark, *Electron Scattering from Diatomic Polar Molecules. II. Treatment by Frame Transformations*, Phys. Rev. A **20**, 1875 (1979).

[81] H. Hotop, M. W. Rul, and I. I. Fabrikant, *Resonance and Threshold Phenomena in Low-Energy Electron Collisions with Molecules and Clusters*, Physica Scripta **2004**, 22 (2004).

[82] M. Gärttner, J. J. Omiste, P. Schmelcher, and R. González-Férez, *Fine structure of open-shell diatomic molecules in combined electric and magnetic fields*, Mol. Phys. **111**, 1865 (2013).

[83] M. Lara, B. L. Lev, and J. L. Bohn, *Loss of Molecules in Magneto-Electrostatic Traps due to Non Adiabatic Transitions*, Phys. Rev. A **78**, 033433 (2008).

[84] B. K. Stuhl, M. Yeo, B. C. Sawyer, M. T. Hummon, and J. Ye, *Microwave State Transfer and Adiabatic Dynamics of Magnetically Trapped Polar Molecules*, Phys. Rev. A **85**, 033427 (2012).

[85] E. Kuznetsova, R. Côté, K. Kirby, and S. F. Yelin, *Analysis of Experimental Feasibility of Polar-Molecule-Based Phase Gates*, Phys. Rev. A **78**, 012313 (2008).

[86] E. Kuznetsova, S. T. Rittenhouse, H. R. Sadeghpour, and S. F. Yelin, *Rydberg-Atom-Mediated Nondestructive Readout of Collective Rotational States in Polar-Molecule Arrays*, Phys. Rev. A **94**, 032325 (2016).

[87] M. Zeppenfeld, *Nondestructive Detection of Polar Molecules via Rydberg Atoms*, Europhys. Lett. **118**, 13002 (2017).

[88] J. Aguilera-Fernández, P. Schmelcher, and R. González-Férez, *Ultralong-Range Triatomic Rydberg Molecules in an Electric Field*, J. Phys. B **49**, (2016).

[89] K.-K. Ni, S. Ospelkaus, M. H. G. de Miranda, A. Pe'er, B. Neyenhuis, J. J. Zirbel, S. Kotochigova, P. S. Julienne, D. S. Jin and J. Ye, *A High Phase-Space-Density Gas of Polar Molecules*, Science **322**, 231 (2008).

[90] K.-K. Ni, S. Ospelkaus, D. J. Nesbitt, J. Ye and D. S. Jin, *A Dipolar Gas of Ultracold Molecules*, Phys. Chem. Chem. Phys. **11**, 9626 (2009).

[91] J. Aguilera-Fernández, H. R. Sadeghpour, P. Schmelcher, and R. González-Férez, *Ultralong-Range Rb-KRb Rydberg Molecules: Selected Aspects of Electronic Structure, Orientation and Alignment*, J. of Phys. Conf. Ser. **635**, 012023 (2015).

[92] J. Aguilera-Fernández, H. R. Sadeghpour, P. Schmelcher, and R. González-Férez, *Electronic Structure of Ultralong-Range Rydberg Pentaatomic Molecules with Two Polar Diatomic Molecules*, arXiv:1710.01393, accepted for publication in Physical Review A (2017).

[93] D. C. Sorensen, *Implicit Application of Polynomial Filters in a K-Step Arnoldi Method*, SIAM J. Matrix Anal. and Appl. **13**, 357 (1992).

[94] R. B. Lehoucq, D. C. Sorensen, and C. Yang, *Arpack Users' Guide*, Siam, (1998).

[95] R. B. Lehoucq, K. Maschhoff, D. C. Sorensen, and C. Yang, *ARPACK Software Package*, http://www.caam.rice.edu/software/ARPACK, (1996).

[96] C. Bahrim and U. Thumm, *Low-lying* $^3P^o$ *and* $^3S^e$ *States of* Rb^-, Cs^-, *and* Fr^-, Phys. Rev. A **61**, 022722 (2000).

[97] M. Marinescu, H. R. Sadeghpour, and A. Dalgarno, *Dispersion Coefficients for Alkali-Metal Dimers*, Phys. Rev. A **49**, 982 (1994).

[98] C. J. Lorenzen and K. Niemax, *Quantum Defects of the* $n^2P_{1/2,3/2}$ *Levels in* ^{39}K *I and* ^{85}Rb *I*, Phys. Scr. **27**, 300 (1983).

[99] W. Li, I. Mourachko, M. W. Noel, and T. F. Gallagher, *Millimeter-Wave Spectroscopy of Cold Rb Rydberg Atoms in a Magneto-Optical Trap: Quantum Defects of the ns, np, and nd Series*, Phys. Rev. A **67**, 052502 (2003).

[100] A. A. Khuskivadze, M. I. Chibisov, and I. I. Fabrikant, *Adiabatic Energy Levels and Electric Dipole Moments of Rydberg States of* Rb_2 *and* Cs_2 *dimers*, Phys. Rev. A **66**, 042709 (2002).

[101] K. Ayuel and P. de Châtel, *Multipole Expansions: Magnetic and Electric Fields Generated by Electrons bound in Spin-Orbit Eigenstates*, Physica B **404**, 1209 (2009).

[102] R. González-Férez, and P. Schmelcher, *Rovibrational Spectra of Diatomic Molecules in Strong Electric Fields: The Adiabatic Regime*, Phys. Rev. A **69**, 023402 (2004).

[103] R. González-Férez, and P. Schmelcher, *Electric-Field-Induced Adiabaticity in the Rovibrational Motion of Heteronuclear Diatomic Molecules*, Phys. Rev. A **71**, 033416 (2005).

[104] R. González-Férez, M. Mayle, P. Sánchez-Moreno, and P. Schmelcher, *Comparative Study of the Rovibrational Properties of Heteronuclear Alkali Dimers in Electric Fields*, Eur. Phys. Lett. **83**, 43001 (2008).

[105] T. M. Weber, M. Höning, T. Niederprüm, T. Manthey, O. Thomas, V. Guarrera, M. Fleischhauer, G. Barontini and H. Ott, *Mesoscopic Rydberg-Blockaded Ensembles in the Superatom Regime and Beyond*, Nat. Phys. **11**, 157 (2015).

[106] J. Zeiher, R. van Bijnen,P. Schauß, S. Hild, J.-y. Choi, T. Pohl, I Bloch, and C. Gross, *Many-Body Interferometry of a Rydberg-Dressed Spin Lattice*, Nat. Phys. **12**, 1095 (2016).

[107] Y.-Y. Jau, A. M. Hankin, T. Keating, I. H. Deutsch, and G. W. Biedermann. *Entangling Atomic Spins with a Rydberg-Dressed Spin-Flip Blockade*, Nat. Phys. **12**, 71 (2016).

[108] D. Booth, J. Isaacs, M. Saffman, *Reducing the Sensitivity of Rydberg Atoms to DC Electric Fields Using AC Field Dressing*, arXiv:1709.03437 (2017).

[109] T. Takekoshi, L. Reichsöllner, A. Schindewolf, J. M. Hutson, C. R. Le Sueur, O. Dulieu, F. Ferlaino, R. Grimm, H.-C. Nägerl, *Ultracold Dense Samples of Dipolar RbCs Molecules in the Rovibrational and Hyperfine Ground State*, Phys. Rev. Lett. **113**, 205301 (2014).

[110] P. K. Molony, P. D. Gregory, Z. Ji, B. Lu, M. P. Koeppinger, C. R. Le Sueur, C. L. Blackley, J. M. Hutson, and S. L. Cornish, *Creation of Ultracold* $^{87}Rb^{133}Cs$ *Molecules in the Rovibrational Ground State*, Phys. Rev. Lett. **113**, 255301 (2014).

[111] M. Gröbner, P. Weinmann, F. Meinert, K. Lauber, E. Kirilov, and H. C. Nägerl *A New Quantum Gas Apparatus for Ultracold Mixtures of K and Cs and KCs Ground-State Molecules*, Journal of Modern Optics **63**, 1829 (2016).

[112] S. Ospelkaus, K. K. Ni, G. Quéméner, B. Neyenhuis, D. Wang, M. H. G. de Miranda, J. L. Bohn, J. Ye, and D. S. Jin, *Controlling the Hyperfine State of Rovibronic Ground-State Polar Molecules*, Phys. Rev. Lett. **104**, 030402 (2010).

[113] S. A. Will, J. Woo Park, Z. Z. Yan, H. Loh, and M. W. Zwierlein *Coherent Microwave Control of Ultracold* $^{23}Na^{40}K$ *Molecules*, Phys. Rev. Lett. **116**, 225306 (2016).

[114] M. S. Heo, T. T. Wang, C. A. Christensen, T. M. Rvachov, D. A. Cotta, J. H. Choi, Y. R. Lee, and W. Ketterle, *Formation of Ultracold Fermionic NaLi Feshbach Molecules*, Phys. Rev. A **86**, 021602 (2012).

[115] C. Haimberger, J. Kleinert, M. Bhattacharya, and N. P. Bigelow, *Formation and Detection of Ultracold Ground-State Polar Molecules*, Phys. Rev. A **70**, 021402(R) (2004).

[116] P. Zabawa, A. Wakim M. Haruza and N. P. Bigelow, *Formation of Ultracold* $X^1\Sigma^+(\nu'' = 0)$ *NaCs Molecules via Coupled Photoassociation Channels*, Phys. Rev. A **84** 061401 (2011).

[117] L. R. Liu, J. T. Zhang, Y. Yu, N. R. Hutzler, Y. Liu, T. Rosenband, K. K. Ni, *Ultracold Molecular Assembly*, arXiv:1701.03121 (2017).

[118] C. Bruni, A. Görlitz, *Observation of Hyperfine Interaction in Photoassociation Spectra of Ultracold RbYb*, Phys. Rev. A **94**, 022503 (2016).

[119] B. K. Stuhl, M. T. Hummon, M. Yeo, G. Quéméner, J. L. Bohn, and J. Ye, *Evaporative Cooling of the Dipolar Hydroxyl Radical*, Nature **492**, 396 (2012).

[120] E. S. Shuman, J. F. Barry, and D. DeMille, *Laser Cooling of a Diatomic Molecule*, Nature **467**, 820 (2010).

[121] M. Aymar, and O. Dulieu, *Calculation of Accurate Permanent Dipole Moments of the Lowest States of Heteronuclear Alkali Dimers Using Extended Basis Sets*, J. Chem. Phys. **122**, 204302 (2005).

[122] L. K. Sørensen, S. Knecht, T. Fleig, and C. M. Marian, *Four-Component Relativistic Coupled Cluster and Configuration Interaction Calculations on the Ground and Excited States of the RbYb Molecule*, J. Phys. Chem. A **113**, 12607 (2009).

[123] R. N. Zare, *Angular Momentum. Understanding Spatial Aspects in Chemistry and Physics*, Jonh Wiley and Sons, (1988).

[124] W. Ritz, *Über eine neue methode zur lösung gewisser Variationsprobleme der mathematischen physik*, J. f. Reine u. Angew. Math. **135**, 1 (1909).

[125] J. K. L. MacDonald, *Successive approximations by the Rayleigh-Ritz Variation method*, Phys. Rev. **43**, 830 (1933).

[126] M. Beck, A. Jäckle, G. Worth, and H.-D. Meyer, *The multiconfiguration time-dependent Hartree (MCTDH) method: a highly efficient algorithm for propagating wavepackets*, Physics Reports **324**, 1 (2000).